CCMS-91-08
P-194 VPI-E-91-07

VIRGINIA TECH

CENTER FOR COMPOSITE MATERIALS AND STRUCTURES

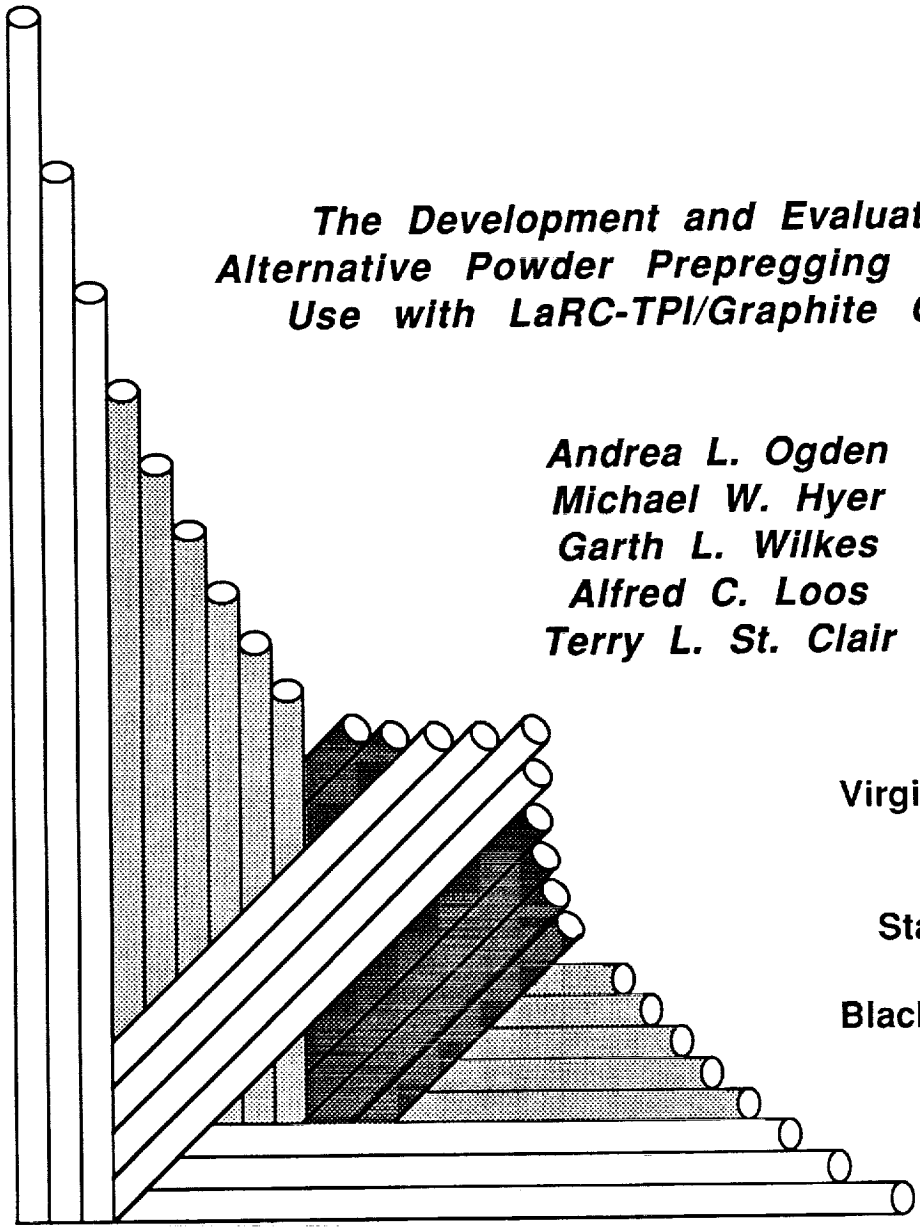

The Development and Evaluation of an Alternative Powder Prepregging Technique for Use with LaRC-TPI/Graphite Composites

Andrea L. Ogden
Michael W. Hyer
Garth L. Wilkes
Alfred C. Loos
Terry L. St. Clair

Virginia Polytechnic Institute and State University

Blacksburg, Virginia 24061

April 1991

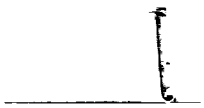

College of Engineering
Virginia Polytechnic Institute and State University
Blacksburg, Virginia 24061

April 1991

CCMS-91-08
VPI-E-91-07

The Development and Evaluation of an Alternative Powder Prepregging Technique for Use with LaRC-TPI/Graphite Composites

Andrea L. Ogden[1]
Michael W. Hyer[2]
Garth L. Wilkes[3]
Alfred C. Loos[4]
Terry L. St. Clair[5]

Department of Engineering Science and Mechanics

NASA Grant NAG-1-343

Interim Report 85

The NASA-Virginia Tech Composites Program

Prepared for: Polymeric Materials Branch
National Aeronautics and Space Administration
Langley Research Center
Hampton, Virginia 23665-5225

---

1 Graduate Student, Department of Engineering Science and Mechanics, Virginia Polytechnic Institute and State University

2 Professor, Department of Engineering Science and Mechanics, Virginia Polytechnic Institute and State University

3 Professor, Department of Chemical Engineering, Virginia Polytechnic Institute and State University

4 Associate Professor, Department of Engineering Science and Mechanics, Virginia Polytechnic Institute and State University

5 Branch Head, Polymeric Materials Branch, NASA Langley Research Center

Abstract

This study investigates an alternative powder prepregging method for use with LaRC-TPI/graphite composites. The alternative method incorporates the idea of moistening the fiber prior to powder coating. Details of the processing parameters are given and discussed. Processing efforts initially concentrated on producing amorphous LaRC-TPI/AS-4 prepreg. The material was subsequently laminated into small coupons which were evaluated for processing defects using electron microscopy. After the initial evaluation of the material, no major processing defects were encountered but there appeared to be an interfacial adhesion problem. As a result, prepregging efforts were extended to include an additional fiber system, XAS, and an semicrystalline form of the matrix. The semicrystalline form of the matrix was the result of a complex heat treating cycle. Using SEM, the fiber/matrix adhesion was evaluated in these systems relative to the amorphous/AS-4 coupons. Of the samples evaluated, the semicrystalline/AS-4 and amorphous/XAS showed improvements relative to the amorphous/AS-4 coupons. Based on these results, amorphous and semicrystalline/AS-4 and XAS materials were prepregged and laminated for transverse tensile testing. Of the samples tested, the amorphous/AS-4 and XAS coupons had average transverse tensile strengths around 33 MPa, and average transverse tensile moduli around 9.3 GPa. The semicrystalline/AS-4 and XAS had a poorer mechanical performance. The average transverse strengths for these samples was approximately 11 MPa. There was a slight improvement in the transverse modulus for the semicrystalline/AS-4 sample but there was no improvement in the modulus for the XAS counterpart. In terms of adhesion, the interfacial adhesion was comparable with previous results. The notable exception was the semicrystalline/XAS coupons. These coupons exhibited extremely poor interfacial adhesion.

Optical micrographs revealed that both semicrystalline samples showed poorer infiltration than the amorphous counterparts, thus offering a partial explanation for the poor mechanical and interfacial response. In an effort to obtain more information on the effect of the matrix, remaining semicrystalline transverse tensile coupons were transformed back to the amorphous state and tested. The mechanical properties of the transformed coupons returned to the values observed for the original amorphous coupons and the interfacial adhesion, as observed by scanning electron microscopy, was better than in any previous sample.

Acknowledgements

This study was supported by the NASA-Virginia Tech Composites Program under NASA Grant NAG-1-343. Thanks are due to the engineers, technicians, and the staff of the Polymeric Materials Branch at NASA Langley Research Center. In addition, the authors would like to acknowledge Joan Muellerleile, Robert Simonds, Tamara Knott, and Charles Chandler for assistance with various experiments while at Virginia Tech.

Table of Contents

List of Illustrations

List of Tables

1.0 Introduction

Though polymer matrix fiber-reinforced composite materials have been applied in a variety of situations in the aerospace community, demands for even more widespread use of these materials continue. This is particularly true in the area of high temperature applications. Wholesale usage in the airframe of the planned high speed civil transport and selected usage in jet engine components are but two areas where the application of fiber-reinforced materials in an elevated temperature environment results in performance gains. Unfortunately, there are not that many candidate matrix materials for these applications. One very promising material is LaRC-TPI (Langley Research Center Thermoplastic Polyimide), a thermoplastic polyimide developed by NASA-Langley Research Center. The high temperature capability of this material is such that it could be considered a leading candidate. The problem is that LaRC-TPI can be difficult to process. A number of methods do exist, however, but not all of them are applicable when processing high performance resins. High performance resin systems tend to be insoluble in most liquid media. The few solvents that are effective with these resin systems can be dangerous to the workers and the environment. As an alternative, fugitive agents can be combined with the resin to suspend the resin in the liquid. The addition of outside agents introduces sources of impurities which could ultimately reduce the potential of the material. Hence alternative methods of prepregging are necessary if the material is to

be used on a wider scale. The work discussed here began as an effort to make LaRC-TPI/graphite fiber prepreg by directly using dry powder and avoiding the use of strong solvents. During the course of this study a variety of problems occurred, some of which had nothing to do with the powder process itself, which caused deviations from the original thrust of the study. The most serious problem encountered was the almost complete lack of adhesion between LaRC-TPI and the fiber chosen for the study, AS-4. The lack of adhesion resulted in very poor quality laminates. This made it impossible to draw any conclusions regarding the relationship between powder processing and the properties of the final laminates. The other significant problem which was encountered early in the study was the fact that the supplier of the LaRC-TPI powder had little control of the particle size from one lot of powder to the next. Hence a process which used 10μm particles from one lot quite effectively became less effective when the particle diameter from the next lot was 40μm This lack of control can lead to an interesting area of research, namely the influence of particle size on the steps used in the powder prepregging process and the quality of the finished laminates. However, studies such as this can not be conducted in the face of serious fiber/matrix adhesion problems. Poor fiber/matrix adhesion can mask any influence of particle size. As a result of the problems encountered, particularly the fiber/matrix adhesion problem, the study had to focus on more than the issue surrounding the use of dry powder to make prepreg. To be sure, issues germane to powder prepregging were addressed. In addition, fiber/matrix adhesion in LaRC-TPI composites was studied by switching to XAS fibers and comparing the adhesion with that fiber to the adhesion observed for the AS-4 fibers. Since the surface features of the AS-4 and XAS were so different, this comparison was of value. An additional and perhaps more important comparison was made. In another study on LaRC-TPI being performed concurrently by another investigator, it was observed that the structure of LaRC-TPI could be altered using various heat treatments. Although the concurrent study was not originally directed at composites, it was felt that the results of that study might lead to better laminates made using the alternative powder process. This concurrent study was being conducted to determine if a thermal cycle could be devised so that it would be possible to recrystallize LaRC-TPI. Thus

using the results of that work in the present study, the prepregging and consolidation steps consisted of two heat treatments. One heat treatment resulted in a semicrystalline matrix and the other resulted in an amorphous matrix. The intention of using a semicrystalline matrix was to improve the adhesion at the fiber/matrix interface in comparison to the adhesion observed in the amorphous matrix laminates. Thus two forms of the matrix and two fibers were considered in this study, along with the notion of dry powder prepregging.

This thesis discusses all aspects of this study. Chapter 2 is devoted to an overview of the current thermoplastic prepregging techniques. The primary steps of each method and their advantages and disadvantages are discussed. In ch. 3, the development of the dry powder process is presented. As an alternative to current powder prepregging techniques, this study considers the idea of depositing dry powder onto moistened filaments. The moisture acts as a temporary binding agent until the powder can be melted onto the fibers. The method of moistening the fibers and the quantity and the quality of the moisture droplets are discussed. In addition, the method of powder deposition and the melt-tacking of the powder to the fibers are also discussed. Chapter 4 focuses on the characterization of the raw materials used in powder prepregging. This chapter provides information on the characteristics of LaRC-TPI, namely its structural, physical and thermal properties. A general description of the fiber characteristics and properties are also given in this chapter. Chapter 5 examines the fabrication and subsequent characterization of preliminary test specimens made using this moistened fiber approach. These preliminary specimens are used to evaluate the quality of the material produced using the new process. From these specimens, it was observed that there was an adhesion problem using the amorphous form of LaRC-TPI with AS-4 fibers. In an attempt to find solutions to the problem, several avenues are pursued, namely using another fiber system, and using a semicrystalline form of the matrix. The early investigation of these solutions is qualitative in nature and places a great deal of emphasis on photographs from the scanning electron microscope. In an effort to quantify the behavior, laminates are fabricated to be used as transverse tensile strength coupons. The transverse tensile strength

is used as a measure of the strength of the fiber/matrix interface. Chapter 6 discusses fabrication and testing of these coupons, and presents the stress-strain relations and the transverse mechanical properties for the amorphous and semicrystalline laminates made with both fiber systems. Chapter 7 evaluates the microstructural behavior of the laminates used in mechanical testing. This chapter discusses the results of optical and electron microscopy and the relationship of the results with the mechanical properties given in ch. 6. As will be seen, the strengths of the semicrystalline coupons are rather low in comparison with the strengths of the amorphous coupons, for both fibers. To study the poor strength of the semicrystalline material further, several untested coupons are heat treated to transform the semicrystalline coupons back to the amorphous state. These transformed coupons are then tested for transverse tensile strength, and the strengths compared with the original amorphous and semicrystalline coupons. The details of this transformation study constitute ch. 8. Chapter 9 summarizes the study, provides conclusions, and makes recommendations for future work.

2.0 Background

2.1 Traditional Thermoplastic Prepregging Techniques

In comparison to thermoset polymer prepregging techniques, thermoplastic polymer prepregging has proven to be a challenge. Thermoplastic polymers are more challenging to prepreg because they are significantly more viscous than their thermosetting counterparts. Generally, ease of impregnation varies inversely with the viscosity. However, many of these highly viscous thermoplastics have excellent mechanical and thermal properties, thus it is important to have them in prepreg form for use in fabrication of structural components. To date, thermoplastic prepreg has been produced by hot melt coating, solvent coating, and slurry coating. The following sections will review the basics of these processes.

2.1.1 Hot Melt Coating

Hot melt coating is a technique in which a fiber tow is impregnated with molten polymer. Even in the molten state thermoplastics are highly viscous, e.g., viscosities greater than 10^4 Pa-s,

making impregnation difficult. Impregnation may be achieved either by passing a fiber tow through a molten resin bath, or by sandwiching sheets of polymer and fiber between heated rollers. In the former case, resin content is controlled primarily by the degree that the tow is spread and the degree the resin is removed after impregnation. Fibers are spread by traversing the tow through a a series of pins. Spreading the fibers permits a greater amount of polymer to impregnate the tow. Resin can be removed from the tow either by using rollers to extract excess resin or by scraping resin from the surface of the fibers using a blade. In the sandwiching approach, the resin content is determined by the thickness of the polymer sheet. Although impregnation is mechanically induced in either approach, chemical additives or plasticizers may be added to lower the viscosity of the polymer, making it easier for the polymer to penetrate the fiber tow. Once the tow is impregnated with polymer, the tows are typically wound onto a drum to form a continuous sheet of material, e.g., prepreg.

Unfortunately, hot melt coating is plagued by problems. The major problem is the high viscosities of the polymers being used. The introduction of additives alleviates that problem but additives can adversely influence the properties of the polymer. In addition, the material made by hot melt coating tends to lack "tack," or the ability to have interply and intraply adhesion. The material also tends to be stiff, lacking the ability to conform to contoured surfaces without the application of heat or pressure, i.e., the material lacks "drape." Both of these characteristics make handling of the prepreg more difficult during laminate fabrication (1).

2.1.2 Solvent Coating

Solvent coating impregnates a fiber tow using a solution of a polymer and a volatile, organic solvent. Solvents are added to lower the viscosity of the polymer and thus ease impregnation of the fiber tow. Although solvents make impregnation easier, many of the organic solvents used are considered to be hazardous materials, creating an undesirable environment for the

worker. On the other hand, the solvents give the prepreg tack and drape. Tack and drape permit complex composite structures to be fabricated with ease, i.e., with minimal interply slippage. The gains realized in the fabrication steps are countered by the need to remove the solvents during consolidation. Solvent removal is essential because residual traces promote void formation within the finished laminate. Voids ultimately lower the properties of the composite. With the trend toward larger and thicker laminates, solvent removal can be a key issue (2,3).

The equipment used in solution coating is similar to the setup used for hot melt coating. Here the tow enters a resin bath containing a polymer solution. In the resin bath, impregnation is aided by a series of spreader pins. Resin content is controlled by the amount of polymer in the solution and by the amount of the polymer extracted from the fibers after impregnation. The impregnated tow is wound onto a drum where a heat source is used to drive off the solvent (1).

As might be expected, the selection of the solvent in this process is a key step, mainly because the structure of a polymer influences it solubility, and thus its processability. Structurally, thermoplastic polymers exist in two basic forms: amorphous and semicrystalline. Amorphous thermoplastics exist as polymer chains with no ordered structure, e.g., the polymer chains are randomly oriented in the bulk material. On the other hand, semicrystalline polymers have ordered and random regions. The ordered regions, or crystals, can exist in many forms but all forms consist of closely packed polymer chains. In these crystalline regions, the forces between the polymer chains are very strong. For these polymers to go into solution, a solvent with similar strength must be chosen. Finding such a solvent can be difficult if not impossible. On the other hand, amorphous polymers generally have much weaker intermolecular forces, creating a greater number of solvent possibilities (4). Because of polymer structure, solvent coating is effective only for amorphous polymers. Unfortunately, amorphous thermoplastics tend to have lower thermal and mechanical properties than their semicrystalline counterparts. These lower overall properties make amorphous thermoplastics

less desirable for advanced applications. Thus, it can be seen that the structure of a polymer influences the selection of the solvents that can be used, and it influences the properties of the final laminate. The need for easy fabrication and consolidation, and the desire for higher performance laminates present competing demands on polymers.

2.1.3 Slurry Coating

Slurry coating involves suspending polymer particles in a medium such as water. Surfactants are usually added to stabilize the suspension and binding agents are used to promote adhesion to the fibers. A slurry coating process uses essentially the same setup as solvent coating process, the difference being in the contents of the resin bath.

There are two drawbacks to slurry coating. First, producing a uniform distribution of polymer on the fibers is difficult. Second, this technique also uses chemical additives to improve processibility, i.e., the surfactants. Removal of the additives from the prepreg is necessary, and is difficult. Residual binders and surfactants on the fibers may weaken the fiber/matrix interface, thus lowering the overall performance of the material.

2.1.4 Summary

To date, all traditional thermoplastic prepregging techniques have major drawbacks. Since high performance thermoplastic polymers are targeted for aerospace applications, a reliable, economical manufacturing technique is required. Rising to the challenge presented by thermoplastics, researchers have directed their attention to powder coating, better known as powder prepregging. Powder coating is an attractive alternative to hot melt, solvent, or slurry coating methods because the resin can contact the fibers without concern over the viscosities

of the materials, or introducing residual materials, such as solvents, surfactants, or binders, into the system. The next section introduces the basic concepts of the powder coating process, both in general terms and in terms of specific approaches being used.

2.2 *Thermoplastic Powder Prepregging*

Currently, several variations on powder prepregging have been developed. Among the different techniques, there appears to be a commonly shared processing schematic. This generic processing schematic is shown in fig. 1 (5). As can be seen, the generic powder prepregging line has several essential steps. The steps are: fiber spreading; powder deposition; powder tacking; and appropriate take-off and take-up spooling of the material. Each of these steps will be briefly discussed.

2.2.1 Fiber Spreading

Fiber spreading is a key part of powder prepregging. The purpose of spreading the fibers is to expose the maximum amount of fiber surface area available for coating. The increased amount of surface area promotes greater contact between the fibers and the powdered matrix. In previous powder prepregging work, fiber spreading occurs either by using a series of rollers (6) or a pneumatic spreading device (5,7,8,9,10). Because of friction from the rollers, the roller spreading system puts undue stress on the tow. This makes spreading more difficult and causes fiber breakage. Of the two systems, the pneumatic spreading device is better because it minimizes tow tension and fiber breakage (6). The concept for the original pneumatic spreader was developed by Kim and Gray for use with metal matrix composites (11). The fiber spreader operates on the principle of laminar flow. The fibers are spread using a

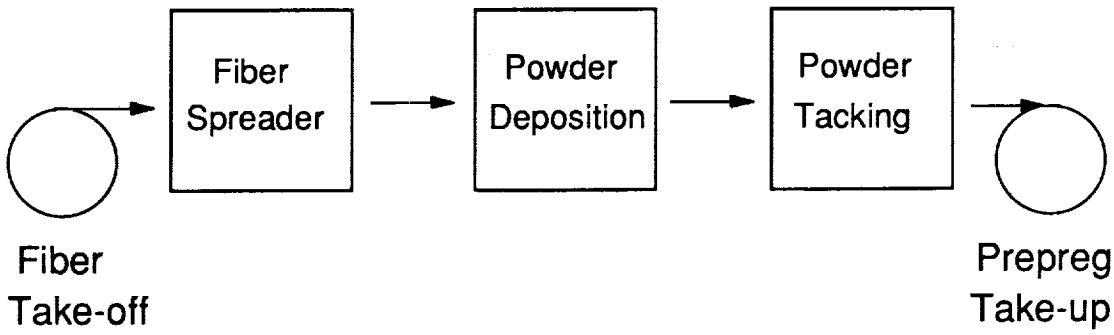

fig. 1. Schematic of Generic Continuous Powder Prepregging Process (5)

combination of concurrent and countercurrent air flow, with concurrent flow being in the direction that the fibers are moving and countercurrent flow being in the direction opposite to the fiber movement. Concurrent air flow separates the filaments in the tow, while the countercurrent air flow spreads the filaments in the tow. Most research efforts have chosen a spreading unit based on the concept originated by Kim and Gray. The most notable modification of the Kim-Gray spreading unit is the work done by Baucom and Marchello (8). A schematic of their pneumatic fiber spreader can be seen in fig. 2. In their fiber spreading unit, air enters through the tow outlet end of the spreading unit. The air is drawn into the spreading unit and through the porous walls in the fiber channel. Finally, the air exits through vacuum ports on the side of the spreading unit. This method simultaneously separates and spreads the fibers using only countercurrent air flow. This pneumatic device is also attractive since the tow width is adjustable. The width of the spread tow is controlled by the size of the tow outlet.

2.2.2 Powder Deposition

In the generic processing schematic, the powder deposition chamber is the next step in the prepregging line. This is the step where variations appear in powder prepregging, illustrating that there are several potential solutions to this problem. Although there are several powder prepregging methods, there are only a few mechanisms that control how the powder and the fiber remain in contact. These mechanisms are: mechanical entrapment, or netting; electrostatic attraction; or, a combination of the two mechanisms. To effect these mechanisms, powder deposition has been achieved by electrostatic coating, fluidized bed coating, and electrostatic fluidized bed coating. Besides these techniques, there are also two commercialized powder prepregging techniques in existence. All efforts have shown that the individual filaments can be coated effectively. Since all the methods are viable, it is important

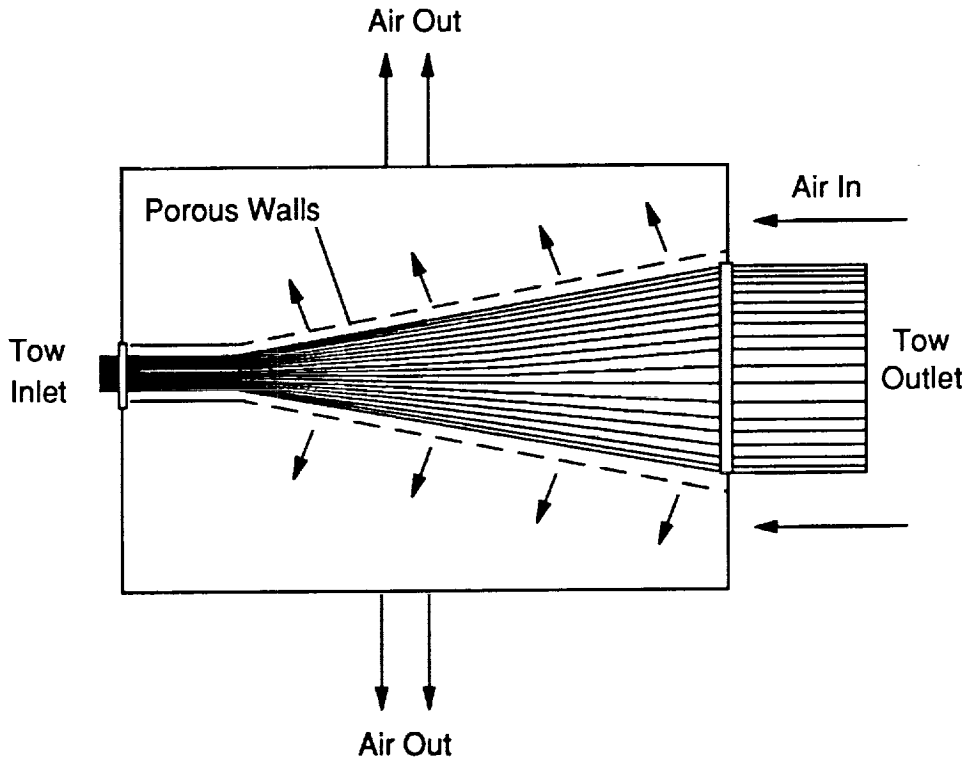

fig. 2. Layout of Pneumatic Fiber Spreader (8,9)

to understand the means by which each method produces prepreg. A discussion of these methods follows.

2.2.2.1 *Electrostatic Powder Prepregging*

Electrostatic powder prepregging has been achieved by two methods: electrostatic spraying (5) and electrostatic fluidized bed deposition (6). A schematic of the electrostatic spraying device is given in fig. 3 and a schematic of the electrostatic fluidized bed is given in fig. 4. The electrostatic spraying approach aspirates an air-powder mixture through a gun. At the tip of the electrostatic gun, the carrier gas is ionized. The charge is transferred from the carrier gas to the powder. The spread tow, which is grounded, moves past the nozzle of the gun and attracts the charged powder. In the electrostatic fluidized bed approach, air is drawn in through the bottom of the chamber. The air ionizes as it passes through a charging medium. The ionized air enters the chamber through a porous plate. At the porous plate, the powder is charged and fluidized simultaneously. The grounded tow, passing through the charged, fluidized powder, attracts the powder, thus coating the fibers. The powder is not continuously cycled in the chamber, rather the unused powder is drawn through the the top of the chamber into a vacuum bag for future use. The essential parameters for electrostatic powder coating include degree of fiber spreading, charging voltage, velocity of powder-carrying medium, particle size of the powder, and residence time in the bed. All of these parameters influence tow velocity and the volume fraction of resin deposited onto the fibers. Muzzy at Georgia Tech extensively studied the effects of these parameters using the electrostatic fluidized bed approach (6).

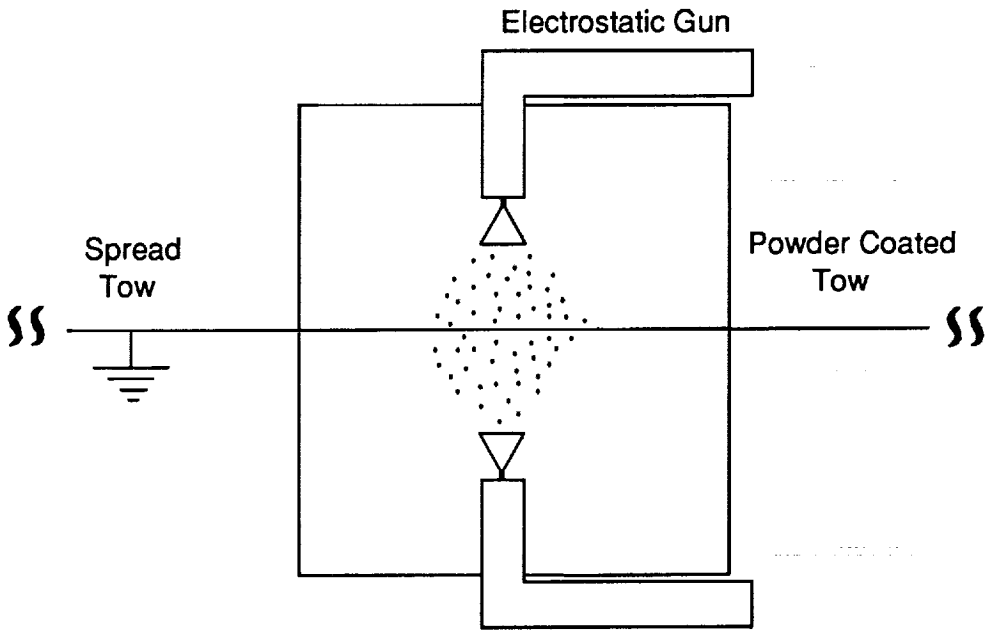

fig. 3. Schematic of Electrostatic Spraying Device (5,9)

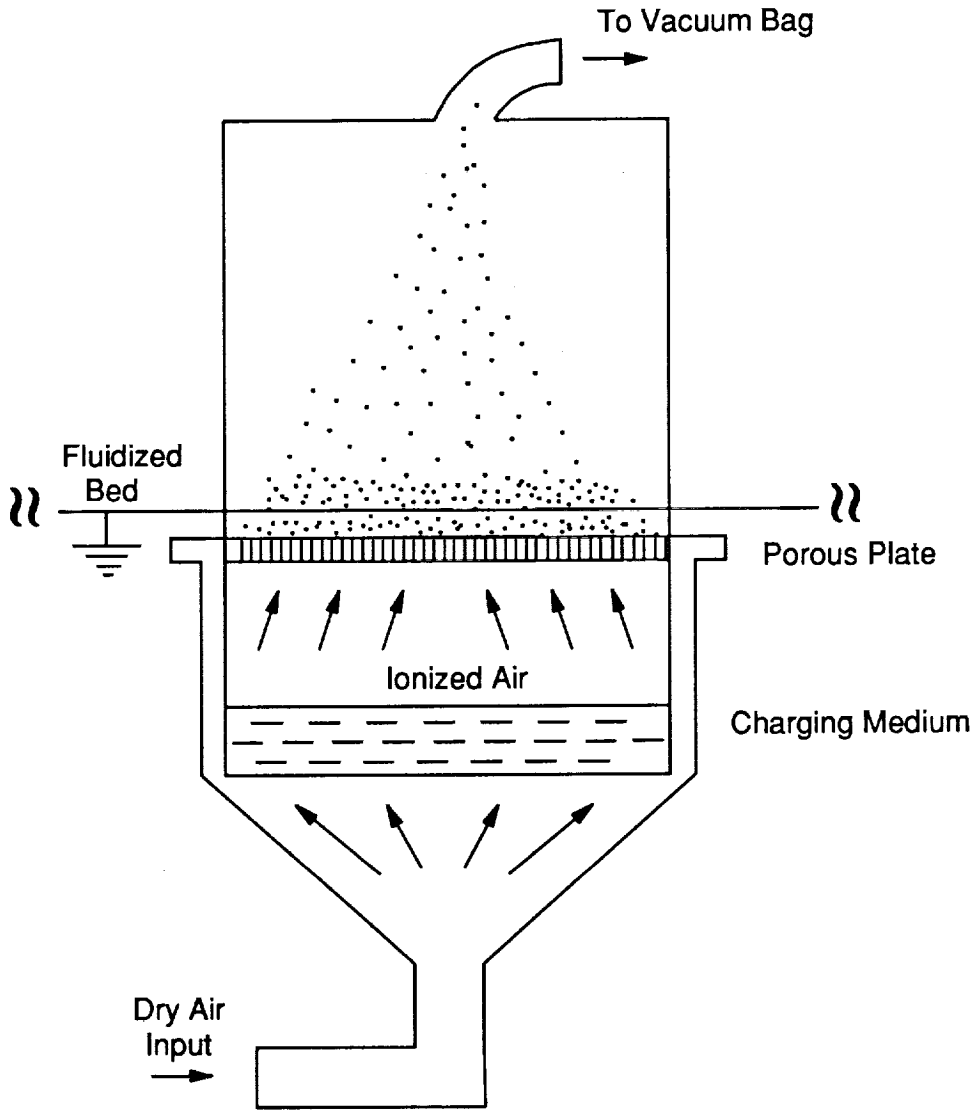

fig. 4. Schematic of Electrostatic Fluidized Bed (6,9)

2.2.2.2 *Fluidized Bed Coating*

The fluidized bed approach coats the fibers by generating a suspension of powder in an inert carrying gas, generally nitrogen (7,8). The fibers are coated when the terminal velocity of the powder exceeds the velocity of the carrier gas, e.g., the powder settles out of suspension and onto the tow. Powder coating using the fluidized bed approach is dependent on the particle size of the polymer. The relationship between particle size and terminal velocity for spherical particles of varying specific gravity is given in fig. 5 (5). Typically, the specific gravity of the polymeric materials is generally between 1.00 to 1.50. As one can see, fine particles, e.g., under 10 μm, with a specific gravity in that range have terminal velocities under 10 in./min. Since the terminal velocities rapidly decrease in this range with decreasing particle size, it is difficult to find a carrier velocity that will fluidize the material and allow the powder to settle out of the suspension. If the carrier velocity is too fast, the fine powder is carried off with the fluidizing medium or it will remain suspended, leaving the tow uncoated or poorly coated. Fluidized bed coating lends itself well to materials that have coarser particle sizes. Coarser particles have higher terminal velocities, thus the powder can settle out of suspension and coat the fibers.

The fluidized bed approach has been studied by researchers at Clemson University and at NASA-Langley. Their approaches are similar. A schematic of the Clemson fluidized bed can be seen in fig. 6. A nitrogen-powder mixture is continuously supplied to the chamber to maintain the proper concentration of polymer powder needed for coating. In addition, powder is continually circulated throughout the chamber, thus minimizing the amount of powder added.

The Polymeric Materials Branch at NASA-Langley's has essentially the same system with a few notable differences. Langley uses a "bubbling bed" to feed the powder chamber. The "bubbling bed" feeds the chamber by fluidizing the powder in a long, vertical column using

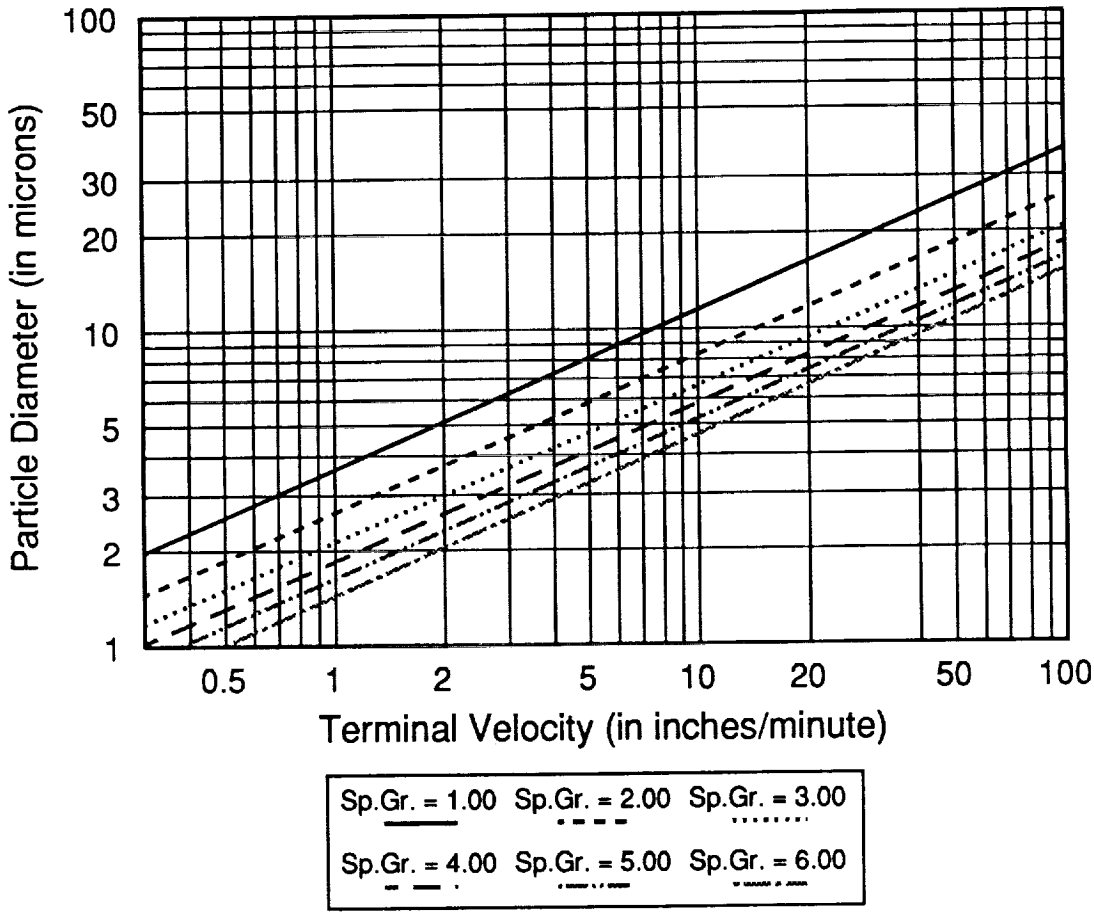

fig. 5. Graph of Terminal Velocity vs. Particle Size for Spherical Particles (5)

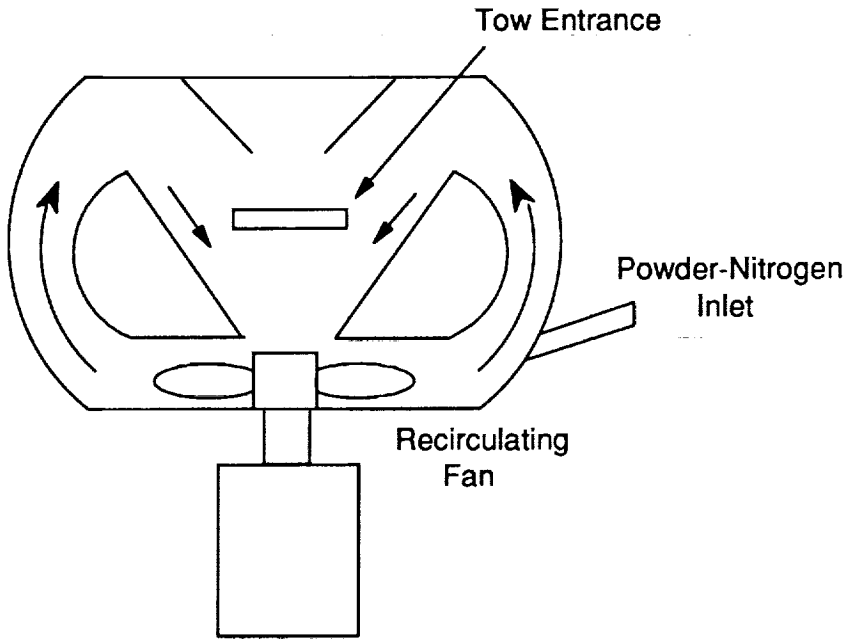

fig. 6. Schematic of Clemson Fluidized Bed System (7,9)

nitrogen as the carrier gas. A schematic of the NASA-Langley system can be seen in fig. 7. The nitrogen/powder stream enters the powder deposition chamber in the sloped region directly above the fan. The powder is drawn through the fan and is circulated into the top of the deposition chamber via a duct. This circulating system ensures that the tow is evenly coated on both sides. Langley also added a set of three baffles on either side of the chamber to prevent powder from escaping out the tow entrance and exit. This reduces the potential breathing hazards that these materials present. Baucom and Marchello have extensively characterized this system. Characterization has made it possible for them to effectively coat using fine materials. They reported being able to successfully coat graphite fibers with powders under 20 μm.

For both the Clemson and the NASA-Langley system, the mechanisms that control powder deposition are both mechanical and electrostatic. Mechanically, the spread fiber tow acts as a net and entraps the polymer particles. Besides entrapment, the powders, especially the fine materials, tend to have an inherent electrostatic nature, thus obtaining a more efficient coat without additional charging.

2.2.2.3 Commercial Processes

ATOCHEM has developed a powder process known as "FIT" or "Fibers Impregnated with Thermoplastic." The "FIT" process commingles dry thermoplastic powder with dry fibers and encapsulates the impregnated fiber tow with a sheath of thermoplastic. A view of the material system is given in fig. 8. To produce the sheathed mixture of powder and fibers, the dry fibers are first spread using a set of staggered cylinders. The spread fibers then enter a fluidized bed where polymer is deposited onto the fibers. Once the tow is coated with powder, it enters a cooling injector where the tow is centered along the axis of the extrusion die. As the tow enters the heated die, a sheath of thermoplastic polymer is extruded around the fibers, thus

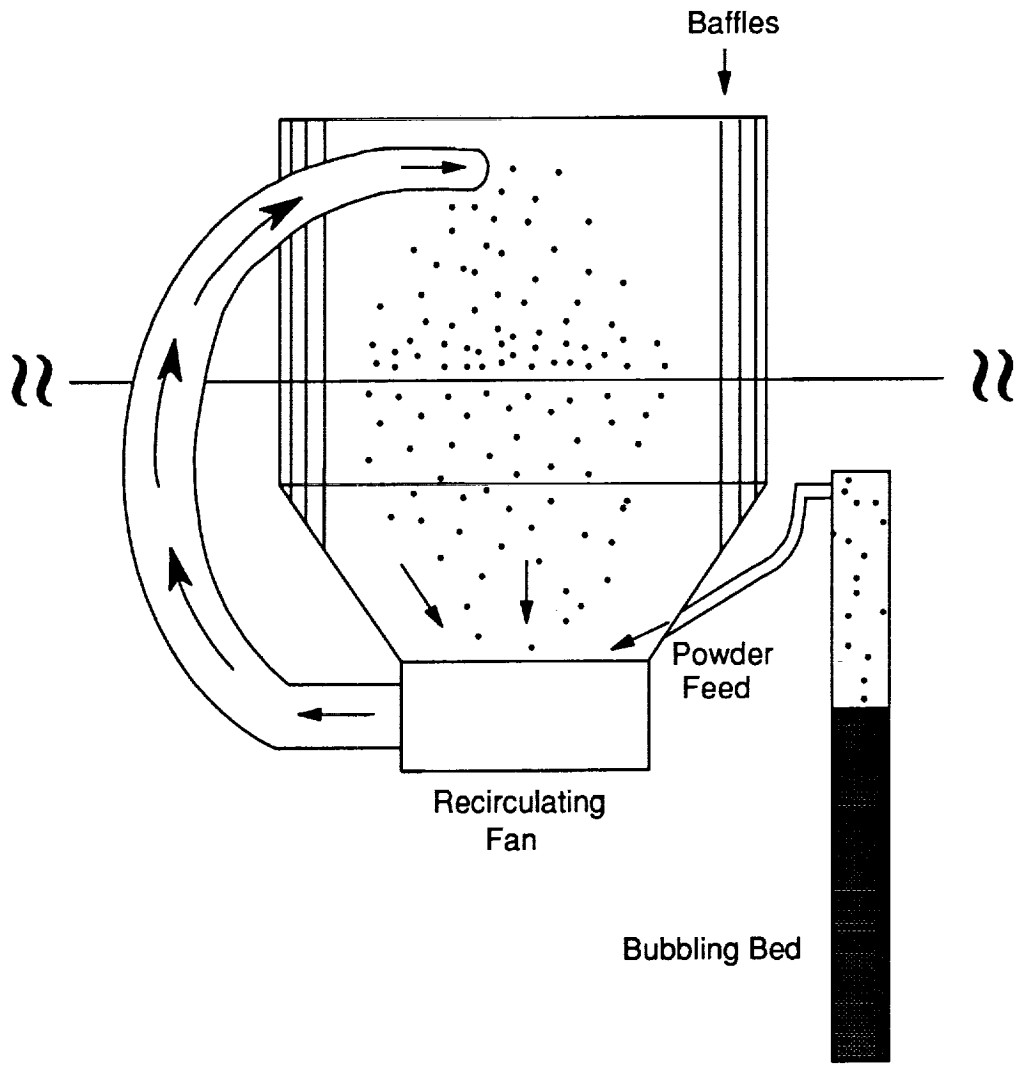

fig. 7. Schematic of NASA-Langley Fluidized Bed (8,9)

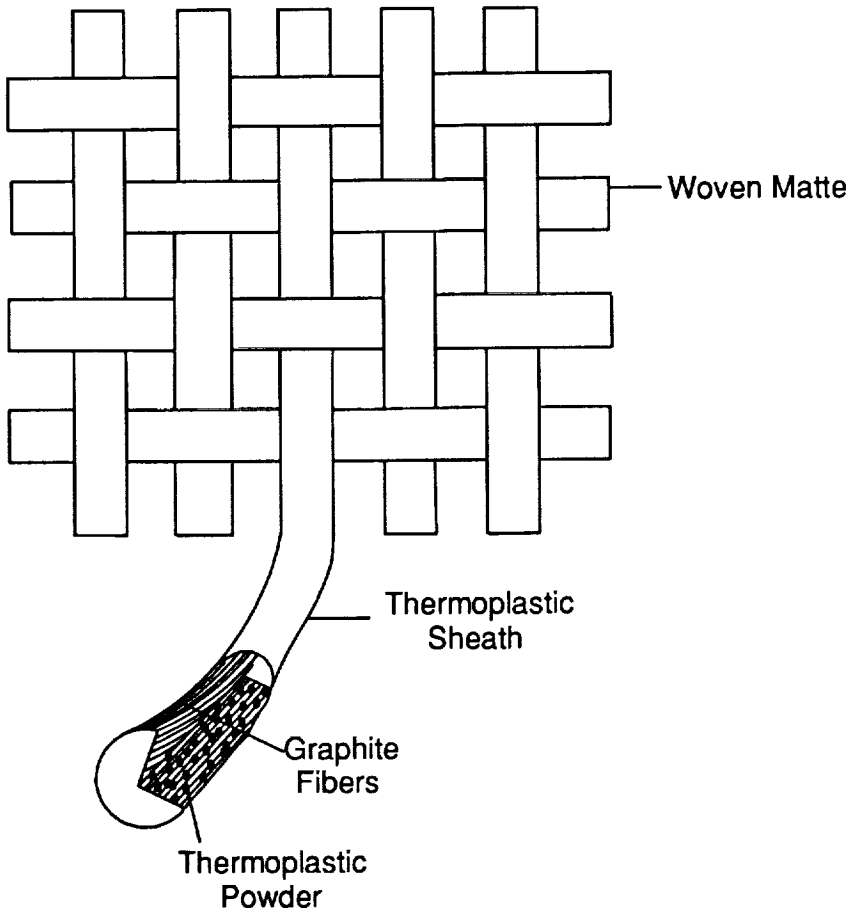

fig. 8. Cross Section of "FIT" Tow (12)

completing the process. The "FIT" material is suitable for almost any manufacturing method, e.g., filament winding, weaving or braiding. At this time, the "FIT" material is targeted primarily for use in woven structures (12).

BASF Thermoplastic Materials has a proprietary powder prepregging process. Apparently in their process, the fibers are sprayed with a binding medium to tack the dry powder to the fiber (5).

2.2.3 Polymer Tacking

From the generic processing scheme in fig. 1, a heating step follows the powder deposition phase. In this step, the powder is tacked onto the fibers to eliminate powder loss due to handling prior to consolidation. To date, most researchers (5,6,8,9) have used radiant heating, either in the form of a tube furnace or quartz heaters. The notable exception to this is the BASF process. The BASF process does not use heat to tack the powder to the fibers prior to consolidation, making powder drop-off a problem with this process. Researchers at Clemson University are using a combination of electric resistance heating with convective heating. (13) Convective heating is used to attach the powder to the fibers to prevent drop-off. Electric resistance heating is used to improve wet-out between the polymer and the fiber.

2.2.4 Spooling

Typically, the material is simply unspooled from the fiber creel prior to spreading. The differences arise when the impregnated tow is taken up. Many approaches can be taken. The most notable approaches include: a traversing take-up system used by Clemson researchers (7); or, an elongated mandrel used by Georgia Tech researchers (14). The Clemson system

uses a traversing take-up system which apparently minimizes fiber breakage and prevents additional tension from being put on the tow. A schematic of this can be seen in fig. 9. The elongated mandrel Georgia Tech uses looks like a rectangular box with hemispherical caps at the ends, as can be seen in fig. 10. The purpose for their design was to produce long flat sections for unidirectional preform construction.

2.2.5 Cost Effectiveness

Cost effectiveness is an important issue in thermoplastic processing. It is an issue because the raw materials can be as expensive as the manufacturing costs. Since most of the powder processing work discussed has been investigated at a laboratory or pilot line level, it is difficult to project the actual cost of powder prepreg material. Muzzy (14) at Georgia Tech estimates that prepreg made using the electrostatic fluidized bed approach would cost $ 20.00 per pound. This figure includes all manufacturing expenses except for the price of the raw materials. In this price range, powder coating appears to be competitive with almost any prepregging process. No specific cost analysis has been given for the electrostatic spraying or fluidized bed approach. The electrostatic spraying approach appears limited by equipment costs. Electrostatic equipment tends to be costly, making scale-up less attractive. The fluidized bed approach uses simple, affordable technology. Of all current approaches, it seems more viable.

2.3 Summary

As can be seen, all currently developed techniques are capable of producing adequate prepreg. Certain processes, namely the fluidized bed approaches, seem better suited for

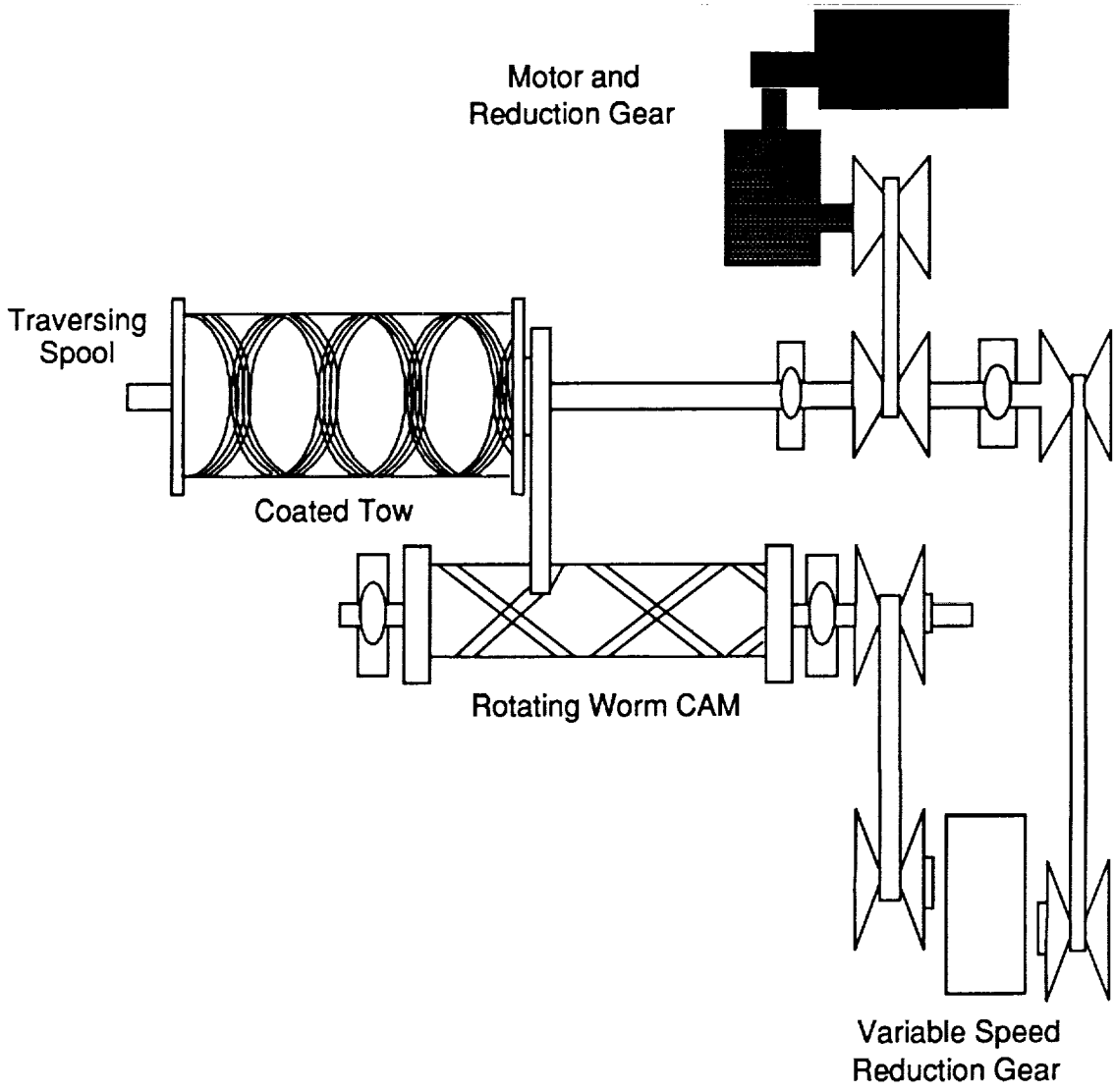

fig. 9. Schematic of Clemson's Traversing Take-up System (7)

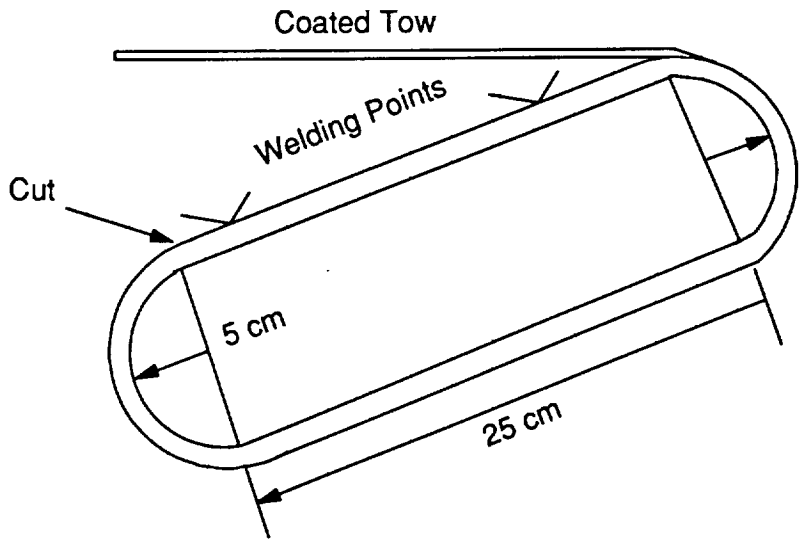

fig. 10. Schematic of Georgia Tech's Mandrel used in Prepreg Take-up (14)

specific particle size ranges. As noted previously, the fluidized bed approach is most effective with larger particle sizes. NASA-Langley's "bubbling bed" approach appears to have overcome this problem. They effectively coated a tow using particles under 20 μm. Looking at the various processes, it appears that NASA-Langley's approach is the most viable. Their approach effectively coats a tow using modest equipment. This makes scale up more attractive.

3.0 Process Development

As was discussed in ch. 2, dry powder prepregging is accomplished currently using a number of techniques. Those techniques coat the fibers by entrapping the powder in the tow or by attracting electrostatically charged powder to the tow. As an alternative in the present study, the use of a light coating of moisture on the fibers, to temporarily hold the dry powder to the fiber, is investigated. As the fiber-powder system is heated, the moisture disappears and the powder tacks to the fiber free of residual materials. Also, this method can be accomplished by using inexpensive, off-the-shelf equipment. As a result, this approach may be cost effective compared with the other methods.

The process development was carried out using LaRC-TPI powder, and two fibers, AS-4 and XAS. The LaRC-TPI powder used was manufactured by Mitsui Toatsu Company. The AS-4 fibers were manufactured by Hercules, and the XAS fibers were manufactured by Hysol-Grafil. These materials will be discussed in detail in the next chapter, but first the steps in the alternative prepregging process are discussed.

3.1 Process Concept

The concept for powder deposition onto moistened filaments evolved from a study on LaRC-TPI paste prepregging (15). Paste prepregging was a technique that extrudes a paste onto spread fibers. While working with this technique, it was observed that the fibers had the tendency to extract liquid from the paste, making the paste too dry to spread on the spread fibers. In an attempt to keep the paste from drying out, water was applied to the fibers before the paste was added. Adding moisture improved the ability to spread the paste onto the fibers. Although the ability to spread the paste improved, the paste approach seemed less viable because the resin content and distribution were difficult to control. Despite the dismissal of paste prepregging as a viable technique, the idea of moistening fibers followed by powder coating merited investigation. Much of the information obtained in the paste prepregging study was incorporated into the moistened-fiber prepregging approach. In the moistened-fiber approach, the purpose of moistening the fibers prior to powder deposition was to provide a temporary binding medium. The moisture kept the powder on the fibers, especially at ambient temperature, until the powder could be tacked to the fibers using heat. Rapid convective heating was used to tack the powder to the fibers. As a result, it is believed that an additional mechanism played a part at elevated temperature since the moisture appeared to be quickly dissipated. Electrostatic attraction may have kept the small powder particles attached to the fibers. The powder employed in processing has been observed to have a slight, inherent electrostatic attraction. From the early studies, there was ample evidence that this approach would lead to uniformly coated fibers with a sufficient amount of powder.

3.2 Process Schematic

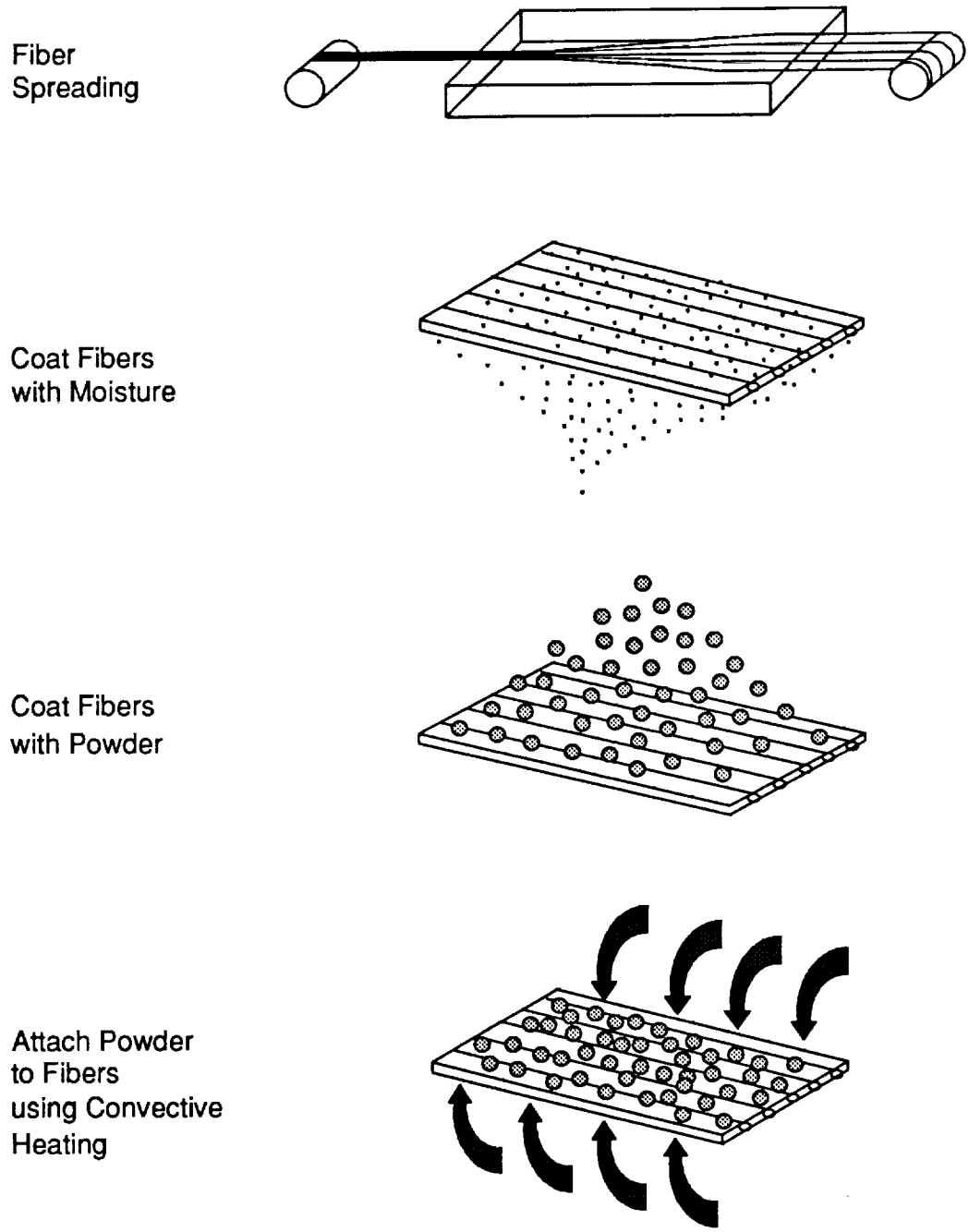

fig. 11. Schematic of Powder Deposition onto Moistened Filaments

Powder deposition onto moistened filaments uses four basic steps (16). These steps are outlined in fig. 11. The basic steps include fiber spreading, moisture deposition, powder deposition, and powder tacking. As may be noted, this processing scheme closely follows the generic processing scheme seen in fig. 1. The major difference is that all the powder prepregging methods mentioned in ch. 2 are continuous processes. In the present case, the batch approach is used for all powder process development and prepreg production. Batch processing is employed specifically to isolate the importance of process parameters such as amount of moisture, level of heating needed to tack the powder to the fiber, etc. By isolating the parameters, it is possible to characterize each step and to understand how these parameters influence this and subsequent steps. Other powder processing studies have concentrated on assembling a continuous process without significant study at the modular level. By having an adequate knowledge of the individual components, it is felt that a more effective continuous process can be constructed.

3.3 Determination of Process Parameters

3.3.1 Fiber Spreading

All fibers used in process development were spread using a pneumatic fiber spreader, specifically the spreader in the Polymeric Materials Branch (PMB) at NASA-Langley Research Center. An overview of the pneumatic spreader was given in ch. 2. Details of the operating parameters of the NASA-Langley unit were described elsewhere (8,9). All fibers were spread to be approximately 2.5 cm wide. The distribution of fibers was uniform across the width of the tow. After the fibers were spread, they were spooled between layers of release paper for future use.

3.3.2 Moisture Deposition

Water vapor is deposited onto the tow to temporarily bind the powder to the fibers. Ideally, the moisture droplets should be fine and uniformly coat the tow. Like powders, the droplet size should be close to the fiber diameter so that the maximum surface area is covered.

3.3.2.1 Procedure

A section of spread fiber, approximately 2.5 cm wide by 20.3 cm long, was cut and clamped into a steel frame. The frame was designed to keep the fibers under tension to prevent the tow from wicking, or being drawn together, once the moisture was added. A schematic of the setup can be seen in fig. 12. Once the fibers were clamped, the sample traversed through a plume of water vapor just above the nozzle of the ultrasonic humidifier. After coating the entire length, the sample was turned over and the other side was moistened.

3.3.2.2 Moisture Characterization

The ultrasonic humidifier employed in processing had variable humidity and variable volume flow controls. Humidity level was controlled by a knob. There was no indication on the knob or in the humidifier operating instructions that quantified what the actual humidity level was. As a result, an initial study was performed to determine how moisture deposition onto the fibers varied with increasing volume flow and constant humidity level. In all stages of characterization, the highest humidity level of the humidifier was used. Volume flow was controlled by another knob. Like the humidity level control, no quantitative information was given for this parameter. In this study, a broad spectrum of volume flow settings was initially investigated. At a high volume flow, moisture deposition was copious. The tow was laden with large drop-

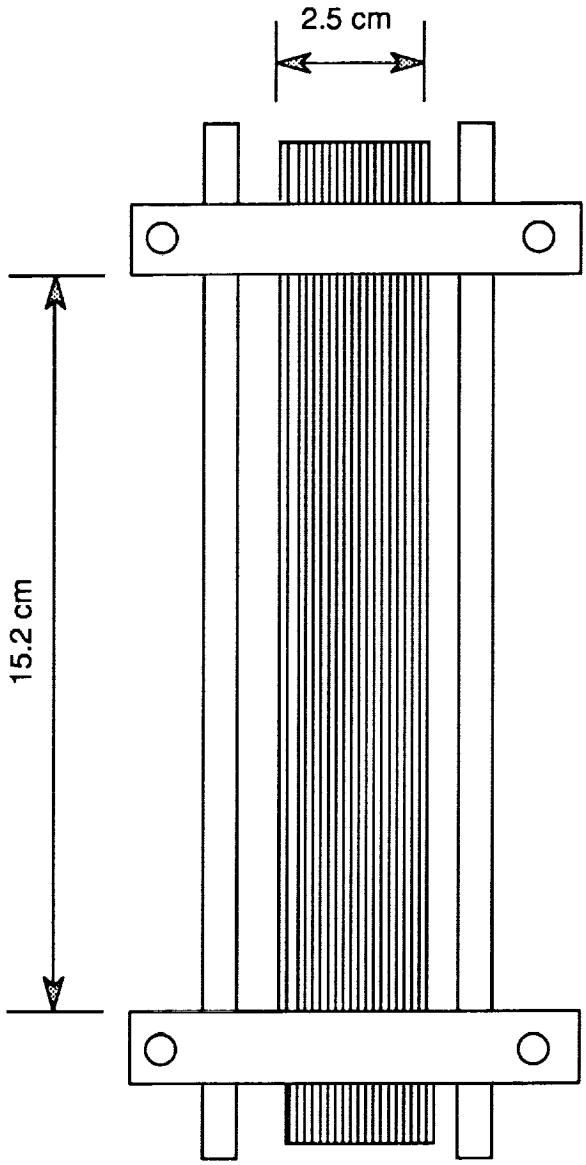

fig. 12. Schematic of Spread Fiber Clamped in Frame

lets, e.g., 100 to 400μm in diameter. When the tow was this wet, the fibers started to wick together, counteracting the initial fiber spreading. At low volume flow, the moisture deposition onto the tow was negligible. Too little moisture on the fibers was unacceptable for processing. A moderate volume flow appeared to be more suitable. After the initial study, the moisture deposition behavior in this region was studied in greater detail.

Moisture deposition was investigated originally for AS-4 fibers. The moisture deposition for the XAS fibers was studied at a later time. The AS-4 fibers were moistened using the procedure described previously. The effective moistened length, or the length between the clamps, was 15.2 cm. Each side of the tow was moistened five times by passing it through the water vapor plume. For characterization purposes, four moisture deposition rates and two volume flow were studied. The volume flow settings chosen were a subset of the moderate volume flow region. From this point forward, moderate volume flow will refer to the lower value in the subset and high volume flow will refer to the higher value in the subset. Moisture deposition rate was determined by the length of carbon fiber exposed to moisture per unit time, and thus has the units of cm/s. In this study, the total length of carbon fiber exposed to moisture was 152.4 cm. The total length of the fiber was determined by multiplying the number of sides, the number of passes used to coat a side, and the length of a side. Moisture deposition rate varied as the exposure time changed. The moisture deposition behavior for AS-4 in the moderate volume flow region at an ambient relative humidity of 55% and an ambient temperature of 23°C can be seen in fig. 13. Moisture accumulation is expressed as a percentage of the weight increase relative to the dry fiber. Specifically, the percent increase in moisture deposition is determined by:

$$\text{percent moisture accumulation} = \frac{m_{WF} - m_{DF}}{m_{DF}} X100,$$

where m_{WF} is the mass of fiber after moisture deposition and m_{DF} is the mass of the dry fiber. For the moderate volume flow, moisture accumulation varied from 60-290%. At the higher volume flow rate, moisture accumulation varied from 60-450%. In both cases, moisture ac-

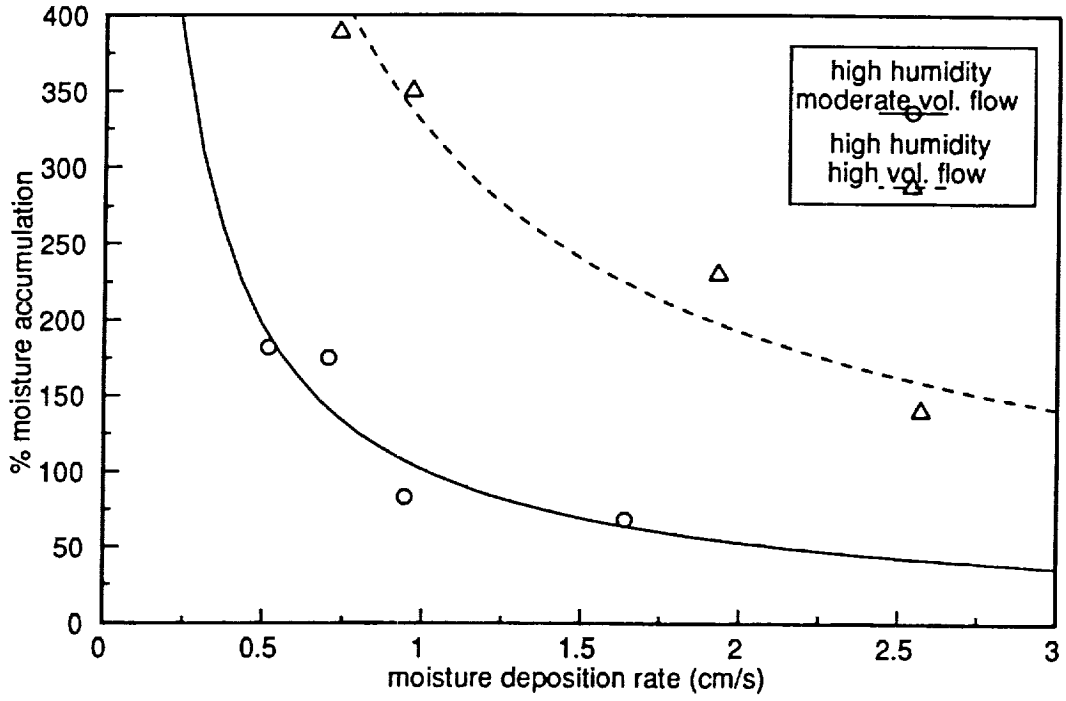

fig. 13. Plot of Moisture Accumulation vs. Moisture Deposition Rate for AS-4 Fibers at an Ambient RH=55% and Ambient T=23.3°C (16)

cumulation varied dramatically at slower moisture deposition rates and varied very little at faster moisture deposition rates.

Moisture deposition parameters were based on the amount and size of the droplets generated. When the higher volume flow was used, the amount of moisture accumulated and the drop size increased rapidly as moisture deposition rate decreased. At lower volume flow, the amount of moisture accumulated onto the fibers did not increase as rapidly and the droplets were smaller, e.g., around 40μm. One objective of process development was to introduce the minimum amount of moisture needed to bind the powder to the fiber. The amount of moisture accumulated on the fibers was minimized to suppress potential problems during subsequent composite manufacturing steps, namely void formation. As a result, the moderate volume flow was chosen in the high moisture deposition rate region. Specifically, moisture deposition rates around 1.5 cm/s were used. A micrograph of a moisture coated AS-4 tow using these specified process parameters can be seen in fig. 14. The tow was evenly coated with small moisture droplets and the drop size distribution appeared to be narrow.

3.3.3 Powder Deposition

Powder deposition was accomplished by filtering the powder onto the fibers. The powder was dispensed using a 105μm polyester mesh bag. The polymer powder was distributed onto the fibers by manually moving the mesh bag in an oscillatory pattern back and forth across the width of the tow. Each side of the tow was individually coated in this fashion. During coating, some powder fell through the fiber tow. Powder loss was minimized by placing a sheet of paper under the tow. The lost material replenished the powder in the mesh bag which was used to touch up weakly coated areas of the tow. An example of an unheated powder coated tow can be seen in fig. 15. In the micrograph, it can be seen that the tow is uniformly coated with powder.

fig. 14. Micrograph of Moisture Coated AS-4 Fibers (16)

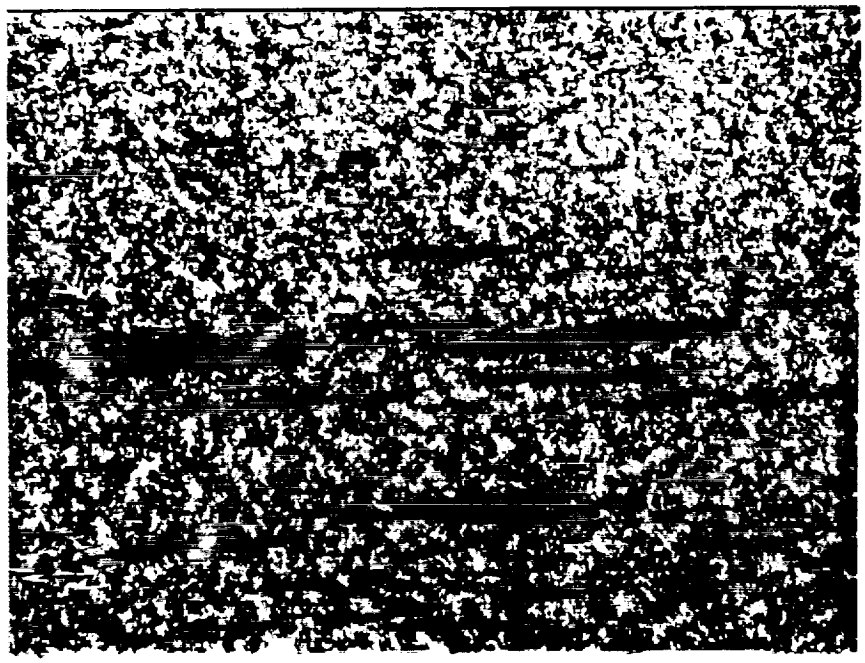

fig. 15. Micrograph of AS-4 Tow Coated with LaRC-TPI Powder (16)

The particle size used predominantly in this study was the 20-30μm material. As will be discussed in the next chapter, the powder received from Mitsui Toatsu was ball-milled and separated into seven particle size ranges. From the seven particle size ranges, four particle size ranges were chosen for initial prepregging. Those particle size ranges were: 20-30μm, 48-58μm, 74-83μm, and greater than 83μm. In this initial prepregging phase, it was observed that powder loss increased as particle size increased. Some of the powder loss occurred during powder deposition but, as it will be seen in the next section, a greater amount of powder was lost during the powder tacking step. Based on this information, all remaining samples were prepregged with the 20-30μm material.

The amount of powder needed to coat a section of carbon fiber was based on a series of calculations which started by determining the mass of the carbon fiber to be coated. The average mass of a section of carbon fiber, m_F, was determined by using the average mass of a centimeter of fiber and the length of the carbon fiber section, i.e.,

$$m_F = m_f L, \tag{1}$$

where m_f was the fiber mass per centimeter and L was the length of fiber be coated. The average mass of a centimeter of AS-4 and XAS fiber were 0.0081 g and 0.0080 g, respectively. Fiber volume fraction is defined as

$$v_F = \frac{V_F}{V_T} \tag{2}$$

where V_F = the volume of fiber and V_T = the volume of the fiber and the matrix, i.e., the total volume. The density of the fiber is given by

$$\rho_F = \frac{m_F}{V_F}. \tag{3}$$

Substituting equation (2) into (3) yields an expression for the total volume in terms of fiber variables, namely

$$V_T = \frac{m_F}{\rho_F \nu_F}. \tag{4}$$

A similar expression can be written in terms of the matrix variables

$$V_T = \frac{m_M}{\rho_M \nu_M} \tag{5}$$

or

$$m_M = \nu_M \rho_M V_T. \tag{6}$$

By substituting equation (4) into (6), the mass of the matrix, m_M, can be expressed in terms of known quantities, i.e.,

$$m_M = \frac{\nu_M m_F \rho_M}{\rho_F \nu_F}. \tag{7}$$

The densities of the AS-4 and XAS fibers were 1.76 and 1.80 g/cm^3, respectively. The density of amorphous LaRC-TPI was 1.324 g/cm^3, as determined using a density gradient column. This value was used in all prepregging calculations. Although this value was for the amorphous form, it was a good approximation for the semicrystalline form. In actuality, the density of the semicrystalline LaRC-TPI should be higher than the amorphous LaRC-TPI because chain folding allows an equivalent amount of material to fit into a smaller volume. By using ρ_M (amorphous) as an approximation for ρ_M (semicrystalline), the amount of matrix determined by eq. (7) overestimated the amount actually needed.

Generally, commercial prepreg has a fiber volume fraction around 0.6. This was the target fiber volume fraction in the resultant powder prepreg produced in this study. Due to various sources of powder loss, a lower fiber volume fraction, namely $\nu_F = 0.5$, was used in the calculations to determine the mass of the matrix needed. This correction factor compensated for

powder losses. As a result, the matrix volume fraction of the prepreg was approximately 0.4 and the fiber volume fraction was approximately 0.6.

3.3.4 Powder Tacking

Powder tacking was accomplished using convective heating in an Instron 3116 Environmental Chamber. Once the moistened tow was coated with powder, the frame was placed into the chamber. The samples were heated at approximately 330°C and the residence time in the chamber depended on whether a semicrystalline or an amorphous sample was produced.

A brief study was conducted to determine the minimum residence time needed to attach the powder to the fibers. This study examined the variations in melting phenomena for equivalently coated tows as a function of different residence times in the convection oven. In this study, the frame was suspended vertically from the top of the oven. It was observed that the powder melted completely in about 15 seconds. The powder retained its basic form, e.g., spherical, for up to 120 seconds in the oven. At times greater than 120 seconds, significant amounts of polymer bridging occurred. Although the powder melted in less than 60 seconds, a residence time of 60 seconds was chosen. This was done to allow the oven to equilibrate after sample exchange and to facilitate easier sample exchange. An example of the powder melted to the AS-4 fibers under the given conditions can be seen in fig. 16. Comparing fig. 15 to fig. 16, it can be seen that the distribution of the melted powder on the fibers is less uniform than its premelted counterpart. The loss of powder and the non-uniformities in the powder distribution can be attributed to the use of convective heating. Specifically, the fan in the convective oven caused the powder coated fibers to vibrate which initiated powder removal.

fig. 16. Micrograph of LaRC-TPI Melted onto AS-4 Fibers (16)

3.3.5 Summary

After characterizing the basic processing elements, the parameters used in depositing powder onto moistened filaments were:

- width of spread tow — 2.54 cm
- moisture deposition rate — 1.64 cm/s
- moisture volume flow — moderate
- humidity level — high
- ambient room temperature — 23°C
- ambient relative humidity — 55%
- oven temperature — 330°C
- residence time — 60 seconds
- matrix volume fraction — 38-40%.

4.0 Material System

Before discussing efforts to evaluate the prepreg that resulted from the moistened-fiber process, the characteristics of the constituents in the material system, namely the LaRC-TPI powder and the two fibers, are briefly discussed. Understanding the constituents will aid in understanding the character of the prepreg and in fact, the laminates made from the prepreg.

4.1 LaRC-TPI

LaRC-TPI is a linear aromatic polyimide. Its structure can be seen in fig. 17. LaRC-TPI is available in many forms including films, molding powder, and fibers (17). The applications of LaRC-TPI have concentrated on its high temperature capabilities, namely it is being used as adhesive for metal and polymer bonding, and as a matrix material for composites. At this time, LaRC-TPI composites are made using powder, either in slurries or with dry powder coating as has been discussed previously (5,6,7,8,9,18).

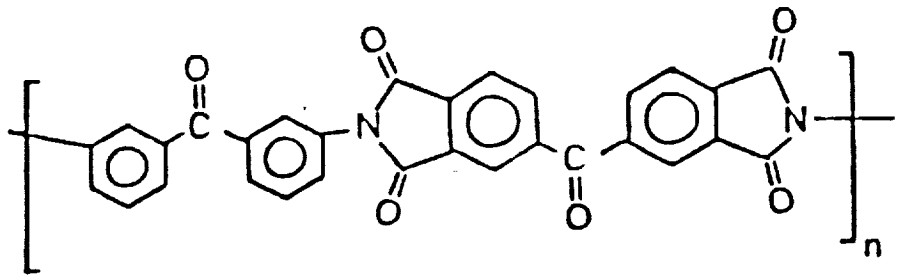

fig. 17. Structure of LaRC-TPI (17)

Since LaRC-TPI was first synthesized, several generations of the polymer powder have evolved. The original LaRC-TPI molding powder was only partially imidized. It was approximately 90% imidized in the as-received state (18). The early versions of LaRC-TPI were called the 1000 and 2000 series materials. Upon molding, these materials continued to imidize as they were heated. This was evidenced by increases in the glass transition temperature as the annealing temperature increased (19,20). The 1000 and 2000 series materials had poor melt flow characteristics. This led to difficulties in processing, particularly for composites. Since imidization was incomplete, by-products, or volatiles, evolved as the reaction progressed. By-product generation was undesirable since it promoted void formation.

The current series of LaRC-TPI, or the 1500 series material, is a fully imidized molding powder which is available in three melt flow forms from Mitsui Toatsu Company (21). The 1500 series materials have been end-capped to control the molecular weight (22). It is hoped that molecular weight control will improve its processability, e.g., its melt flow characteristics.

The matrix used in the current study was lot 58-702. This lot was a high flow, lower molecular weight version of the 1500 series material. In its as-received state, lot 58-702 had a initial melting point around 290°C, as seen in fig. 18A) and a glass transition temperature around 240°C, as seen in fig. 18B). This information was determined using a Perkin-Elmer DSC-4 at a rate of 20°C/min under a nitrogen atmosphere. The DSC scan for an as-received sample from lot 58-702 given in fig. 18A) was obtained upon the initial heating of the material and fig. 18B) was obtained by reheating the material after the initial heating followed by a quench. Originally, LaRC-TPI was a semicrystalline polymer in the as-received state. Previously, it had been observed that LaRC-TPI became amorphous after an initial heating through the melting point. If special care was taken to stay within specific thermal regimes, LaRC-TPI could remain semicrystalline. Hou (20,22) examined the effect of thermal treatment on the degree of crystallinity for both the 2000 and 1500 series materials. While studying the 2000 series material, Hou found that LaRC-TPI would remain semicrystalline if it was annealed below 320°C. The degree of crystallinity was a function of both time and temperature. If the material was

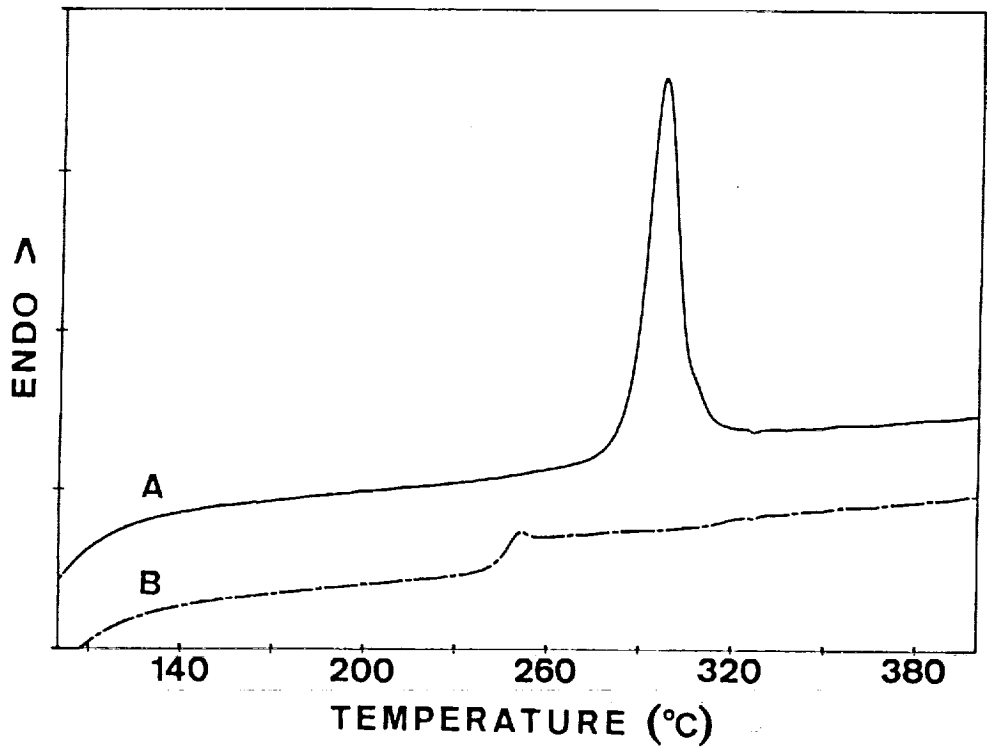

fig. 18. DSC Scan for As-received LaRC-TPI 58-702: A) upon initial heating and B) after initial heating and quench

annealed at temperatures above 330°C, the material was completely amorphous (23). The 1500 series material exhibited similar behavior (22).

In processing, the physical characteristics of the material could be as important as its thermal characteristics. With respect to powder processing, the physical attributes of primary interest were the mean particle size and the particle size distribution. For lot 58-702, the mean particle size was found to be approximately 40 μm. The particle size distribution of the as-received material, as seen in fig. 19, was quite broad, ranging from 3μm to 150μm. With regard to powder coating, a greater amount of the fiber surface area could be covered by smaller particle sizes, namely particles on the order of the diameter of graphite fibers, a diameter of 5-7μm. In addition, the particle size distribution should be narrow, as a narrow distribution makes coating more efficient. For lot 58-702, the mean particle size of the as-received material was roughly 7 to 8 times the fiber diameter and, as stated above, the particle size distribution was broad. In an attempt to obtain powder closer to the ideal conditions given above, the manufacturer was requested to produce another batch of LaRC-TPI with a mean particle size under 10 μm and a narrower particle size distribution. Unfortunately, the request could not be met satisfactorily within the time needed to continue with powder process development. In an effort to work with the given material, particle size reduction was accomplished by ball-milling the material. The material was milled for an hour in a either a 8.6 cm or a 14 cm alumina milling jar using 1.3 cm alumina balls as the grinding media. Although two jar sizes were used, the milling rates of the jars were equivalent since milling rate varies primarily with the inverse of the ball diameter. The jars were filled with proportional amounts of balls and powder. Samples of the ball milled material were examined using Shimadzu SALD-1100 Particle Size Analyzer (PSA). Ball milling narrowed the particle size distribution, as shown in fig. 20. After the powder was milled, it was separated into different particle size ranges using sieves. As a result, seven particle size ranges were produced. These ranges were: material less than 20μm, 20-30μm, 30-48μm, 48-58μm, 58-74μm, 74-83μm, and material greater than 83μm. Each separated particle size distribution was confirmed using the Shimadzu SALD-1100

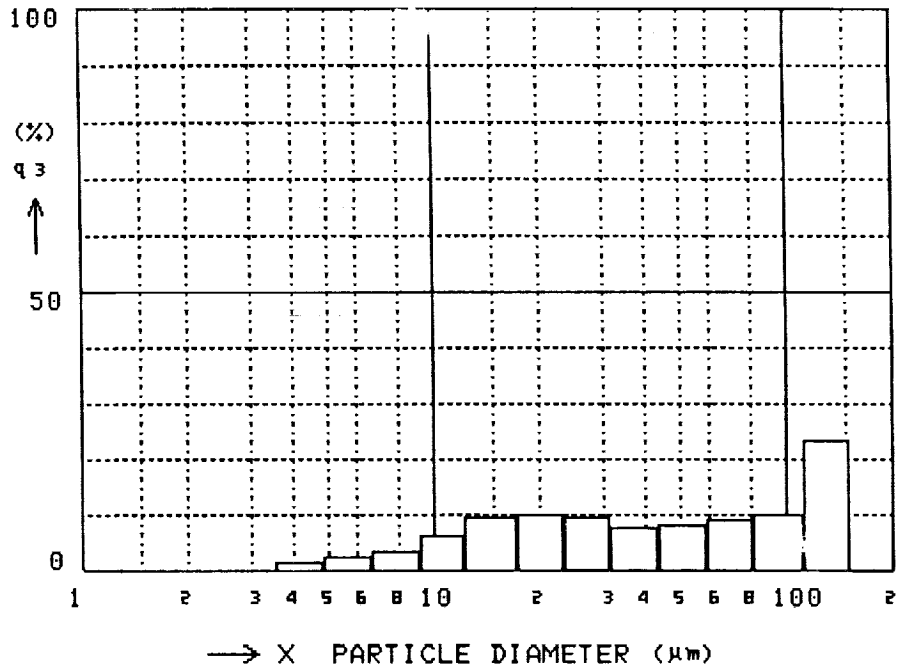

fig. 19. Particle Size Distribution for As-received LaRC-TPI Lot 58-702

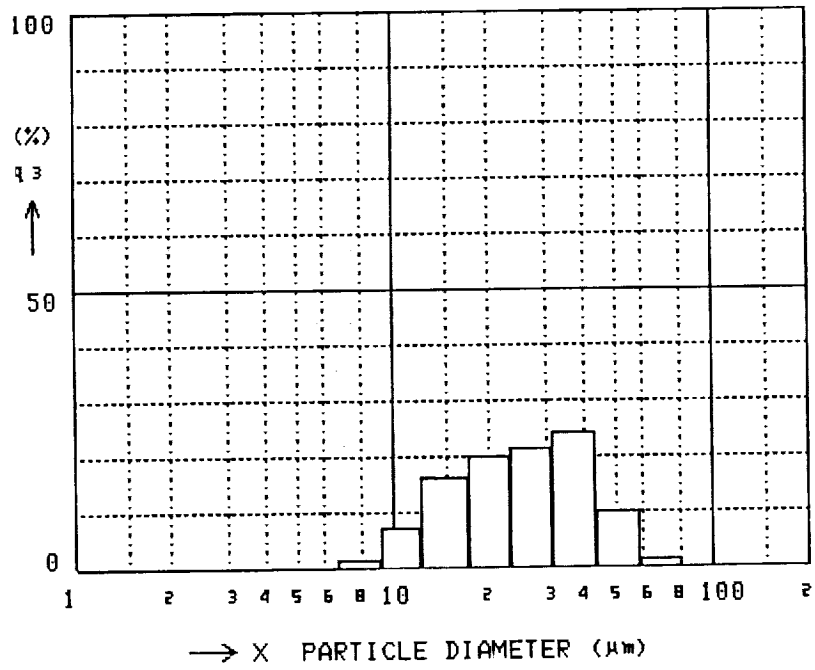

fig. 20. Particle Size Distribution for LaRC-TPI Lot 58-702 Ball Milled for One Hour

PSA. The fact that manufacturer was unable to control particle size raised several important issues, namely, would the diameter of the powdered particles strongly influence the manner in which the powder was handled in the prepregging step and would particle size influence the quality of the resultant prepreg. To some degree, this issue was addressed in this study.

4.2 Fibers

Two graphite fibers were used in process development, specifically, Hercules AS-4 and Hysol-Grafil XAS fibers were used. Both of these fibers were PAN based fibers. Each tow consisted of 12,000 filaments, or fibers, and the mean filament diameter was approximately 7 μm for each fiber. The two fibers are described below.

4.2.1 AS-4

The AS-4 fibers used in process development came from Lot 751-4E. These fibers were un-sized but were surface treated using a proprietary electrolytic etch. A scanning electron micrograph of an AS-4 fiber can be seen in fig. 21. As one can see, the fiber surface was extremely smooth. In terms of physical properties, AS-4 is designated as an intermediate modulus fiber. The modulus, tensile strength, and density of AS-4 Lot 751-4E are given in Table 1.

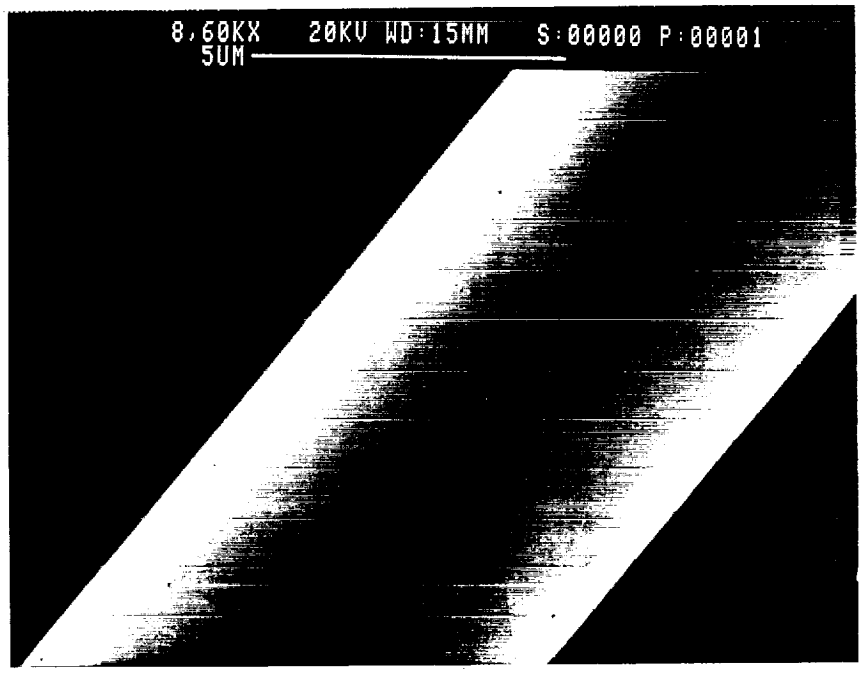

fig. 21. Scanning Electron Micrograph of AS-4 Fiber

4.2.2 XAS

Like AS-4, the XAS fibers used in process development were surface treated but unsized. The surface of the XAS fiber was drastically different than the surface of the AS-4 fibers. A scanning electron micrograph of a XAS fiber surface is given fig. 22. From the micrograph, it is evident that the fiber surface is contoured with many crevasses running along the axis of the fiber. The physical properties of XAS fibers are given in Table 1. The XAS and AS-4 fibers were similar in modulus and density but XAS had a slightly higher strength than its AS-4 counterpart.

Table 1. Physical Properties of AS-4 and XAS Graphite Fibers

Fiber	Density (g/cm^3)	Modulus (GPa)	Tensile Strength (GPa)
AS-4	1.76	228	3681
XAS	1.80	232	4170

With the properties of the constituents summarized, the next chapter is devoted to an evaluation of the prepreg made using the moistened-fiber process.

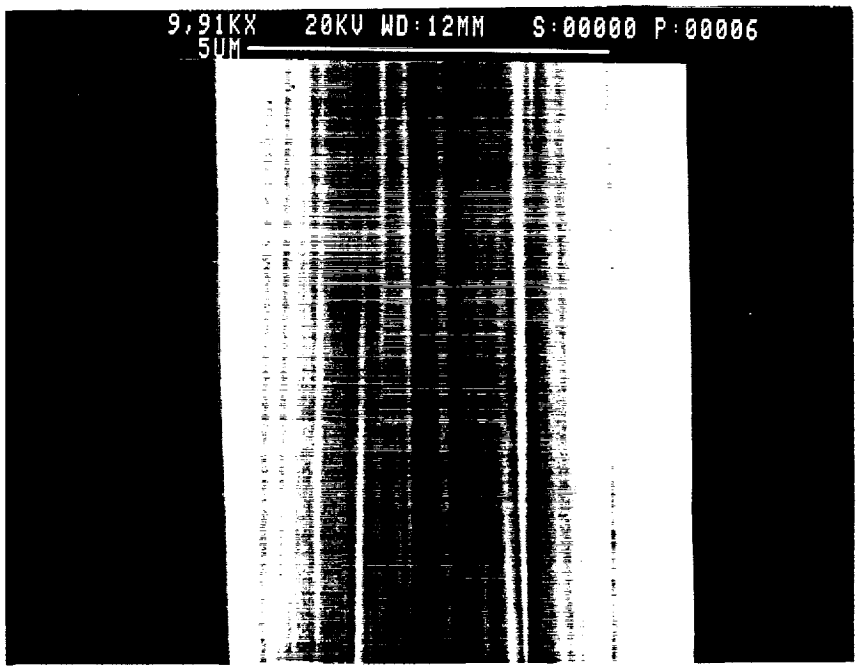

fig. 22. Scanning Electron Micrograph of XAS fiber

5.0 Prepreg Evaluation

5.1 Coupon Production

After producing LaRC-TPI/AS-4 prepreg with the method discussed in ch. 3, small unidirectional $0°_4$ coupons were produced so that the quality of the prepreg could be evaluated. The samples were evaluated primarily for processing defects such as voids, broken fibers, excessive resin, etc.

5.1.1 Fabrication

The small unidirectional test coupons were produced by using four 2.5 cm wide by 7.5 cm long strips of LaRC-TPI/AS-4 prepreg and a matched metal mold. The prepreg strips were arranged to produce a $0°_4$ laminate. Of the total sample size, only 6.3 cm of length was laminated. The remaining 1.2 cm consisted of dry fiber and unconsolidated prepreg. The dry region was separated from the consolidated region by keeping it outside the mold. For these samples, only the plunger and the well of a 7.5x7.5 cm matched metal mold were used. Since

the sample size was much smaller than the mold, a smaller mold was created in the larger mold by placing a layer of 0.1 mm Kapton tape along the length of the mold. The Kapton walls were centered on the plunger of the larger mold, The thickness of the tape was roughly the expected thickness of the final coupon. The cycle used to process the coupon consisted of:

- ramping the temperature from 22°C to 250°C at approximately 5°C/min
- applying a consolidation pressure of 2.1 MPa at 250°C
- continuing the temperature ramp from 250°C to 371°C at the previous rate
- holding the temperature at 371°C for an hour
- cooling sample under pressure and ambient conditions.

The resultant coupons were very thin. The four layer coupon was approximately 0.1 mm thick. The Kapton walled inner mold worked fairly well. The sample seemed to be well consolidated. A problem with this method was that the prepreg washed out of the mold area into the region between the Kapton walls and the plunger, causing these regions to be matrix poor.

5.1.2 Testing

Once the coupons were fabricated, they were tested in a double cantilever beam-like fashion. A schematic of the test specimen and testing mode are given in fig. 23. The samples were fractured by hand, using the unconsolidated regions as tabs. This method of testing was possible since the samples were so thin. As mentioned previously, these samples were produced and fractured in this manner to evaluate how well the prepreg was manufactured. For the early coupons, a qualitative rather than a quantitative evaluation was sufficient.

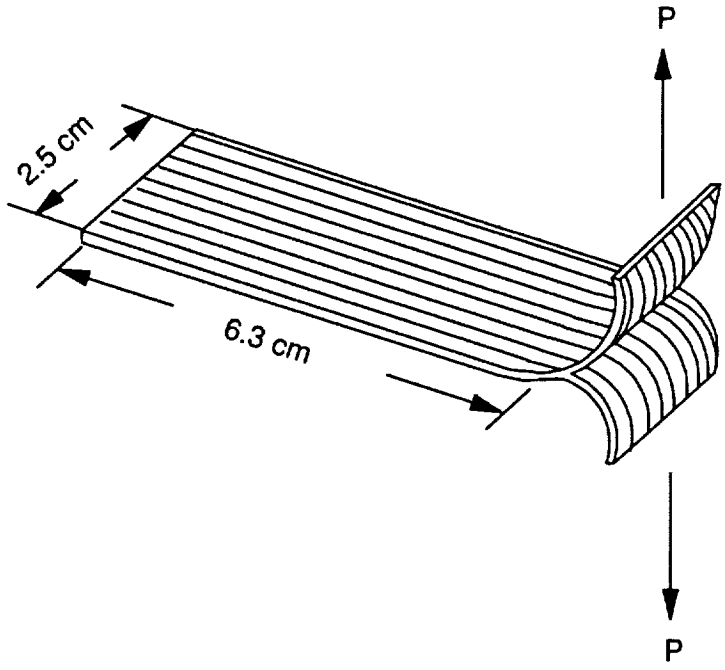

fig. 23. Schematic of Double Cantilever-like Test Coupon

During fracture, the coupons tended to split along the fibers rather than delaminate. When the sample did delaminate, it occurred in matrix poor areas. Matrix poor areas were identified by the surface characteristics of the sample. Such areas were generally associated with regions of dry fiber on the surface of the sample. The coupons were not evaluated using ultrasonics.

Small portions of the unidirectional coupons were used for thermal analysis using DSC. The composite samples were analyzed at a scan rate of 20°C/min on the DSC. From the thermal analysis, the matrix was observed to be amorphous, as illustrated by the presence of a glass transition temperature or T_g. The DSC scan for an amorphous LaRC-TPI/AS-4 coupon can be seen in fig. 24. From fig. 24, it can be seen that the glass transition temperature for the composite was around 235-240°C, which was comparable with the glass transition temperature of the neat resin, fig. 18.

Representative specimens were taken from the delaminated regions to evaluate the fracture surfaces. Several portions of the fractured surfaces were mounted onto Scanning Electron Microscope (SEM) stubs. The SEM stubs were sputter coated with a 140Å layer of gold and were then examined using a Cambridge Stereoscan 200 Scanning Electron Microscope.

The fractured amorphous LaRC-TPI/AS-4 coupons illustrated that the matrix adhered poorly to the AS-4 fibers, as seen in fig. 25. The poor adhesion was evidenced by extremely clean fiber tracks in the matrix and clean fiber surfaces. In terms of processing defects, no substantial void formation was noted. Any voids that were noted were sparsely distributed and were on the order of five to ten microns, as seen in fig. 26. This phenomena was observed in all the amorphous LaRC-TPI/AS-4 coupons that were produced.

The lack of void formation was a good sign. It demonstrated that the moisture initially introduced onto the fiber was successfully removed in the polymer tacking step. This was no great surprise considering the polymer powder was discretely deposited onto the fiber. Since the

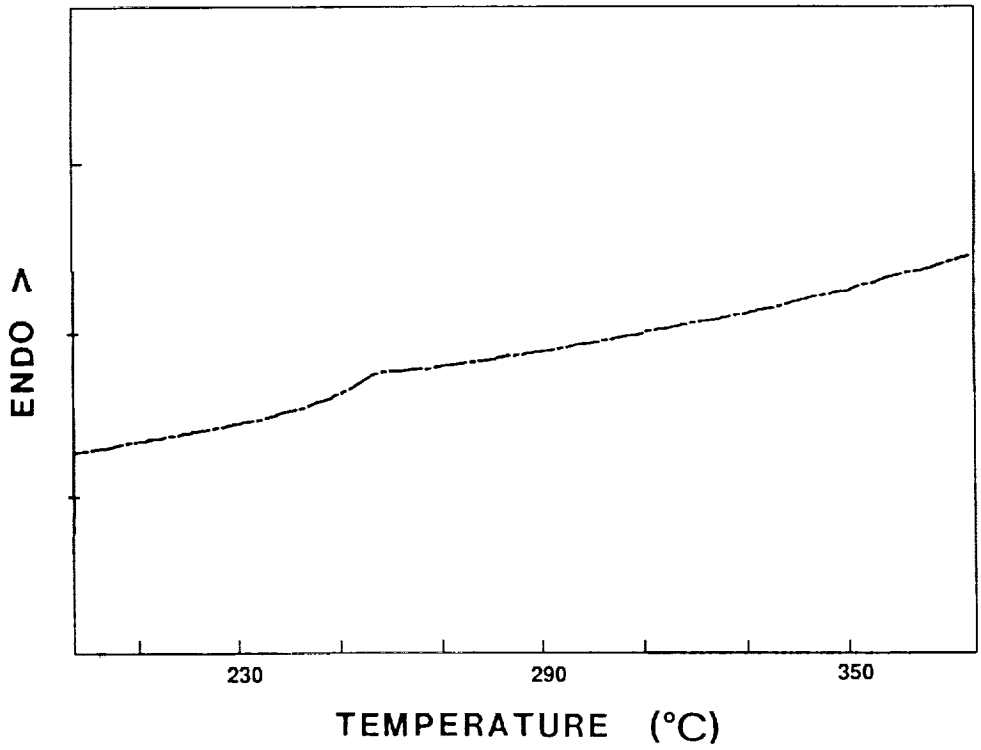

fig. 24. DSC Scan for Amorphous LaRC-TPI/AS-4 Composite

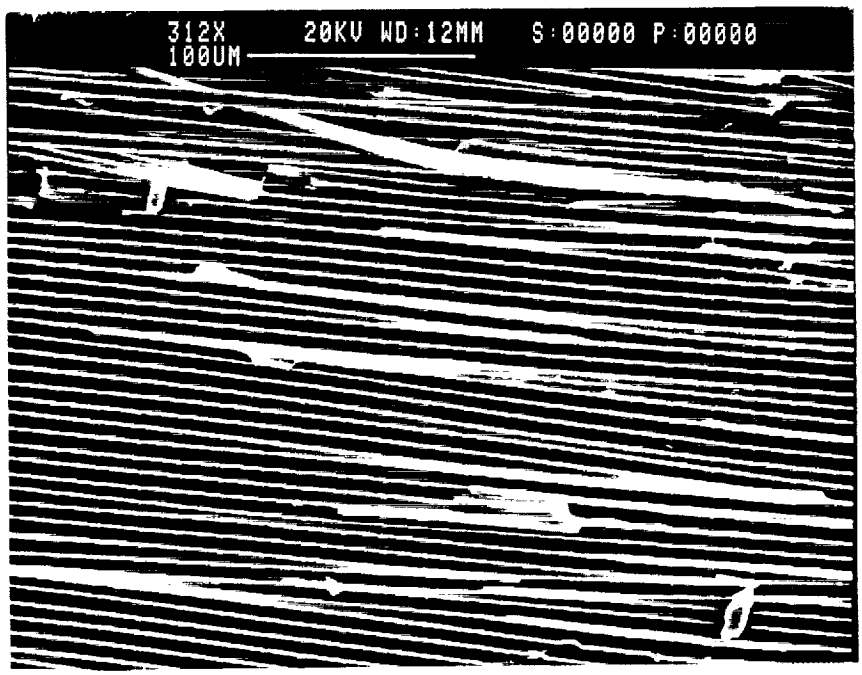

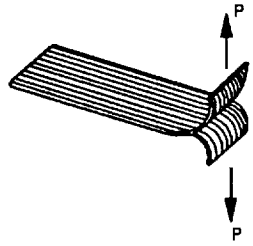

fig. 25. Micrograph of Amorphous LaRC-TPI/AS-4 Test Coupon Showing Poor Adhesion

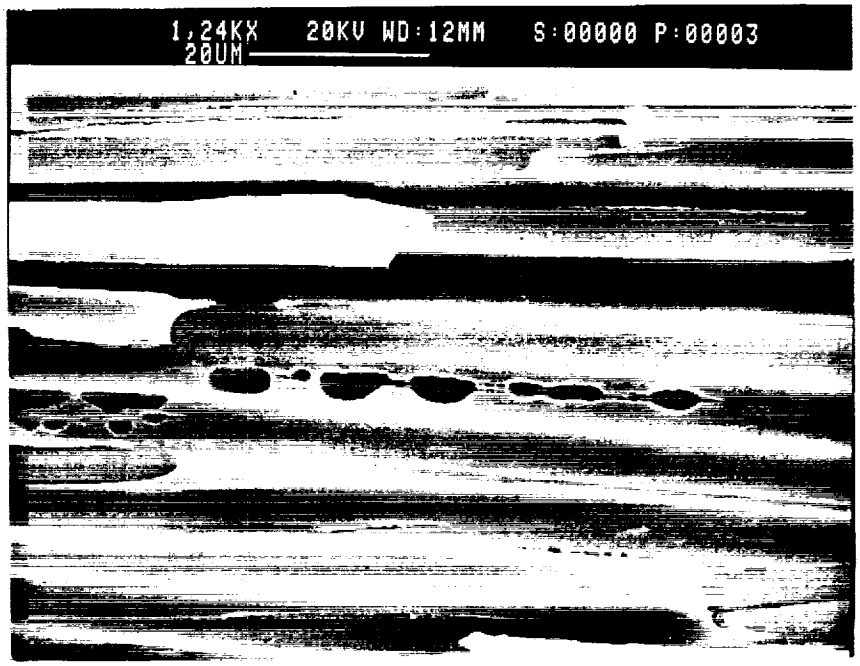

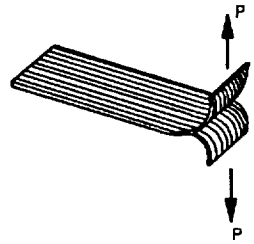

fig. 26. Micrograph of Amorphous LaRC-TPI/AS-4 Test Coupon Showing Little Void Formation

powder particles were not connected, the moisture vapor could easily percolate around the individual particles, leaving the powder in contact with the fiber.

5.2 *Adhesion Investigation*

An area of concern was the lack of adhesion observed between the fiber and the matrix. Concern arose as to the cause of the adhesion problem, namely whether was it process influenced or was it a material compatibility problem. To decipher this problem, a resin-rich amorphous LaRC-TPI/AS-4 sandwich was produced which consisted of layers of LaRC-TPI powder and AS-4 fiber. The layup of the sandwich was $(L/F/L/F/L)_T$, where L represents a layer of LaRC-TPI powder and F represents a layer of spread fiber. No moisture nor mold release agent contacted the surfaces of the raw materials of the sandwich, thus eliminating two potential processing agents that could affect adhesion. The sandwich was processed under the same thermal conditions used to produce the small unidirectional amorphous coupons. The only difference was that the consolidation pressure was 0.34 MPa. This was opposed to the 2.1 MPa used to process the composite coupons with higher fiber content. The lower pressure was used since the $(L/F/L/F/L)_T$ sandwich offered very little resistance to matrix flow. The matrix volume fraction of the sandwich was approximately 0.95.

From the processed sandwich, two, unidirectional 2.5x7.5 cm specimens were produced. Starting at the one end of the specimen, a 1.9 cm notch was cut along the centerline. The notch was sharpened using a razor blade. Initially, the specimens were to be fractured in mode I, using the notch, but it was impossible to fracture them by hand. As a result, the notch was sharpened further. The second time the specimens were fractured in Mode III. Like the unidirectional $0°_4$ coupons, the resin-rich sandwich was examined using SEM. A micrograph of the fracture surfaces can be seen in fig. 27. As can be seen, the fiber surfaces were very

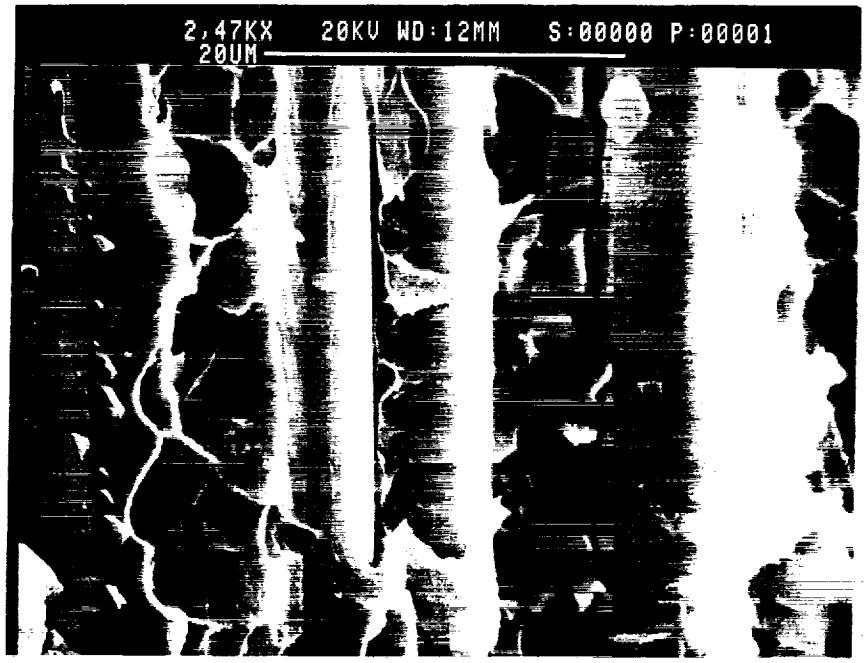

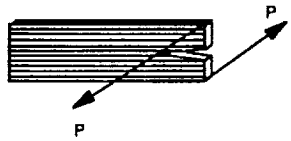

fig. 27. Micrograph of Amorphous LaRC-TPI/AS-4 Resin-rich Sandwich Showing Poor Adhesion

clean. This seemed to indicate that the adhesion problem was not process related, rather it appeared to be a problem associated with material incompatibility.

5.3 *Potential Solutions to the Adhesion Problem*

To determine the reasons for the interfacial adhesion problem observed in the LaRC-TPI/AS-4 laminates, two avenues were pursued. Interfacial adhesion could be improved by changing the fiber, or by changing the matrix. The fiber could be altered either by chemically treating the existing fiber, i.e., plasma treatment or sizing, or using a completely different fiber system. Of these two possibilities, an alternative fiber system was initially investigated. As mentioned in ch. 3, XAS graphite fibers were chosen as an alternative to the AS-4 fibers.

Pursuing the matrix aspect of improving adhesion, the structural duality of LaRC-TPI was exploited. As mentioned previously, LaRC-TPI can exist in both a semicrystalline or an amorphous form, depending on the thermal history of the material. The effect of altering the structure of the matrix was studied with regard to the AS-4 fibers. Eventually, the work was extended by altering the matrix with the XAS fiber system, providing an additional adhesion comparison for LaRC-TPI composites.

5.3.1 Alternative Fiber System

A study was not performed to find an alternative fiber system. The alternate fiber system, i.e., XAS, was chosen based on work by Bascom (24). In the study, Bascom investigated the adhesion of several thermoplastic/graphite systems. The fiber systems in the study included: AS-1, AS-4, and XAS. Of all these systems, the XAS fiber had the greatest adhesion and AS-1

had the poorest. The reasons for the improvement in adhesion with the XAS fiber were complex and could not be isolated to one parameter. Bascom felt that the subtle differences in the fiber surface chemistry may have accounted for the differences in adhesion. Since poor results were already observed in the present study with the AS-4 fiber system, XAS seemed to be a likely candidate.

5.3.1.1 Resin-Rich XAS Sandwich Investigation

As was done with the AS-4 fibers, a resin-rich $(L/F/L/F/L)_T$ sandwich was produced to gauge the potential of the amorphous LaRC-TPI/XAS system. The sandwich was processed similarly to the amorphous LaRC-TPI/AS-4 resin-rich sandwich. The resulting sandwich also had a matrix volume fraction around 0.95. The resin-rich sandwich was cut into 2.5x7.5 cm samples. Like the AS-4 samples, a 1.9 cm notch was placed in the center of each sample, at one end. The notch was sharpened using a razor blade and the samples were fractured by hand in Mode III. Sections along the fracture zone were removed and prepared for SEM analysis. The fractured surfaces were different from those observed in the resin-rich amorphous LaRC-TPI/AS-4 sandwich. In this case there appeared to be a greater amount of material retained on the fiber surface, as seen in fig. 28. In the micrograph, the matrix appeared to be caught in the crevasses on the surface, giving it a "dirtier" look. The LaRC-TPI/XAS resin rich sandwich appeared to be an improvement over what was observed with the amorphous LaRC-TPI/AS-4 sandwich but there still was room for improvement.

5.3.1.2 Prepreg Comparison

Based on the encouraging results of the resin-rich XAS sandwich, XAS prepreg was produced using the parameters developed for AS-4 fibers. The initial parameters were retained to maintain consistency in the samples so that material behavior difference would be detected.

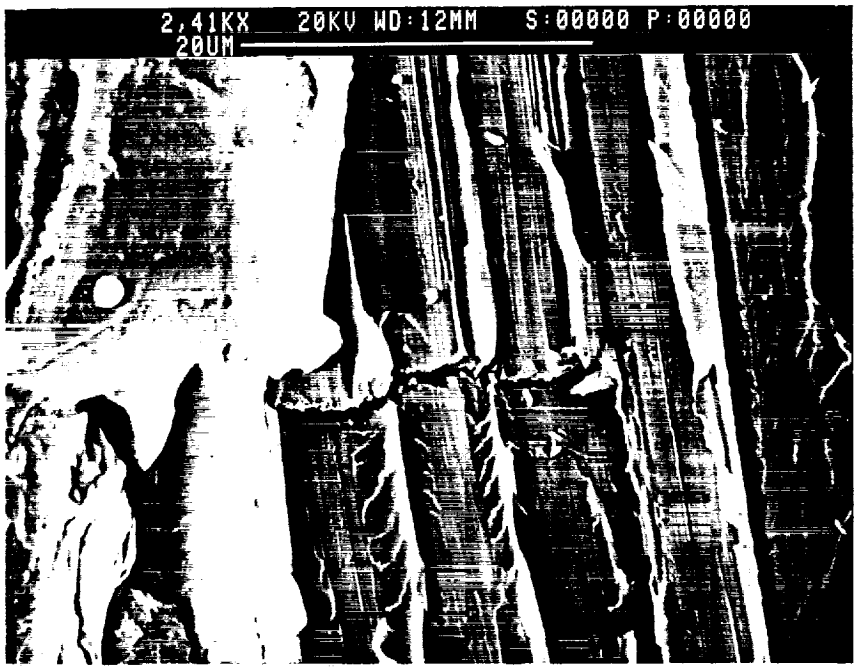

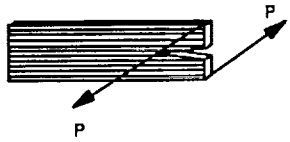

fig. 28. Micrograph of Fracture Surfaces in the LaRC-TPI/XAS Resin-rich Sandwich

A piece of amorphous LaRC-TPI/AS-4 and XAS prepreg were comparatively evaluated using the SEM. Micrographs of the respective pieces of prepreg are given in fig. 29 and fig. 30. In fig. 29, it can be seen that there are essentially perfect spheres of matrix on the AS-4 fibers. The existence of the perfect spheres indicates that the matrix poorly wet the fibers. If the wetting were ideal, there would be no droplets on the fiber surface, rather there would be a sheath of matrix around the fiber. This type of behavior demonstrates the case where the liquid has a zero or small contact angle with the surface of the fiber. Looking at the XAS prepreg in fig. 30, a greater degree of wetting is observed in comparison to the AS-4 prepreg. Generally, degree of adhesion varies inversely with the contact angle, namely the degree of adhesion increases as contact angle approaches zero. The decrease in contact angle for the XAS fibers correlates well with the increase in adhesion observed in the resin-rich LaRC-TPI/XAS sandwich.

A sample of each type of prepreg was abraded by scraping a razor blade along the length of the fibers. A section of the scraped prepreg was examined using the SEM. For the AS-4 prepreg, seen in fig. 31, very little matrix was retained on the fiber surface. This was no surprise, given the the degree of adhesion observed previously. The scraped XAS prepreg was consistent with degree of adhesion observed previously. In fig. 32, it can be seen that a significant amount of matrix remained on the fiber where the droplet was peeled away.

5.3.1.3 LaRC-TPI/XAS Coupon Evaluation

Amorphous LaRC-TPI/XAS $0°_4$ coupons were laminated and fractured as a double cantilever beam, similar in fashion to the lamination and fabrication of the amorphous LaRC-TPI/AS-4 $0°_4$ coupons. From SEM micrographs, greater amounts of the matrix appeared to remain on the fiber surface, as seen in fig. 33. Although there was a definite increase in the amount of material retained by the fiber, the overall fracture surfaces were not indicative of extremely good adhesion. Typically, good adhesion would be illustrated by a fiber with significant

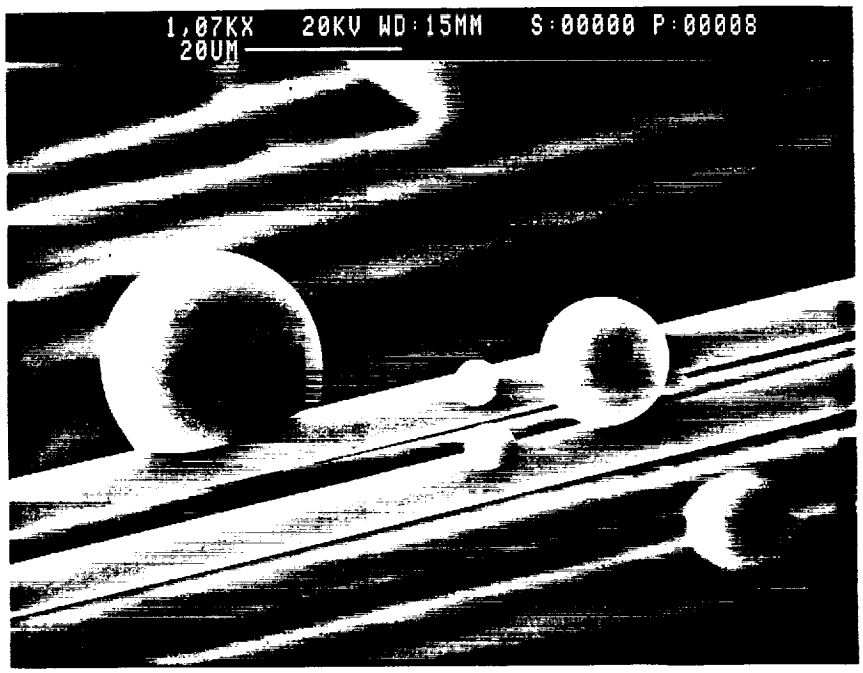

fig. 29. Micrograph of LaRC-TPI/AS-4 Prepreg

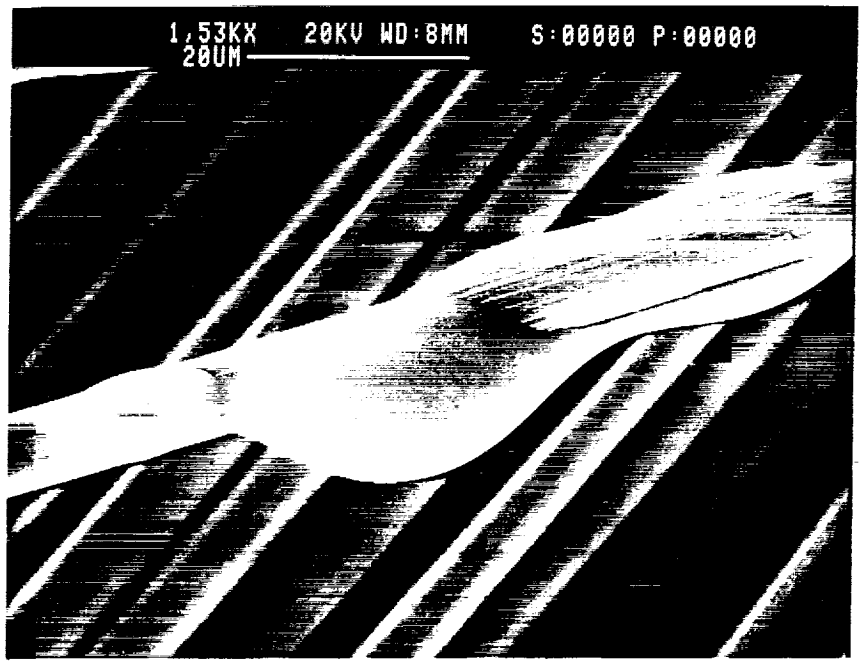

fig. 30. Micrograph of LaRC-TPI/XAS Prepreg

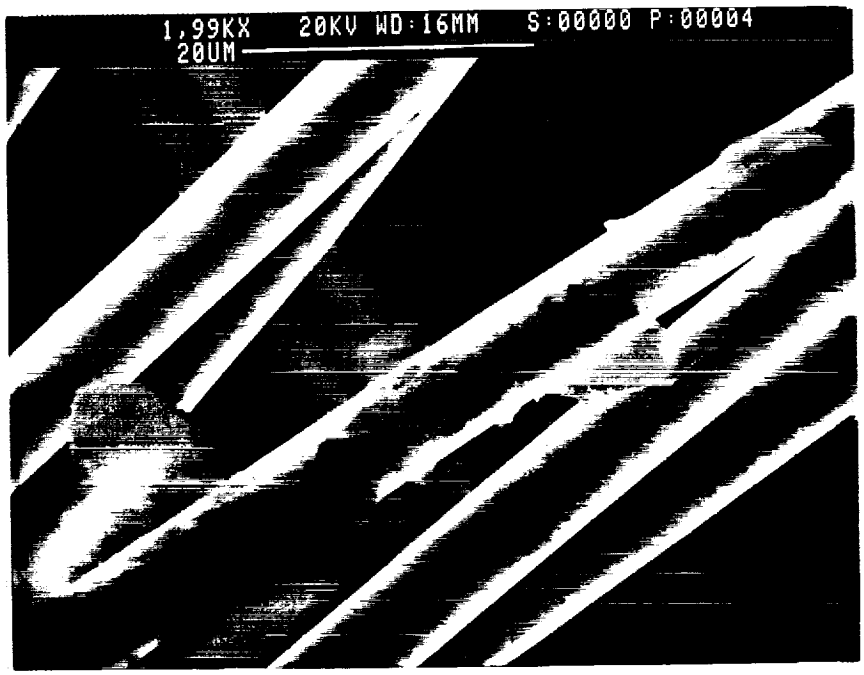

fig. 31. Micrograph of Scraped LaRC-TPI/AS-4 Prepreg

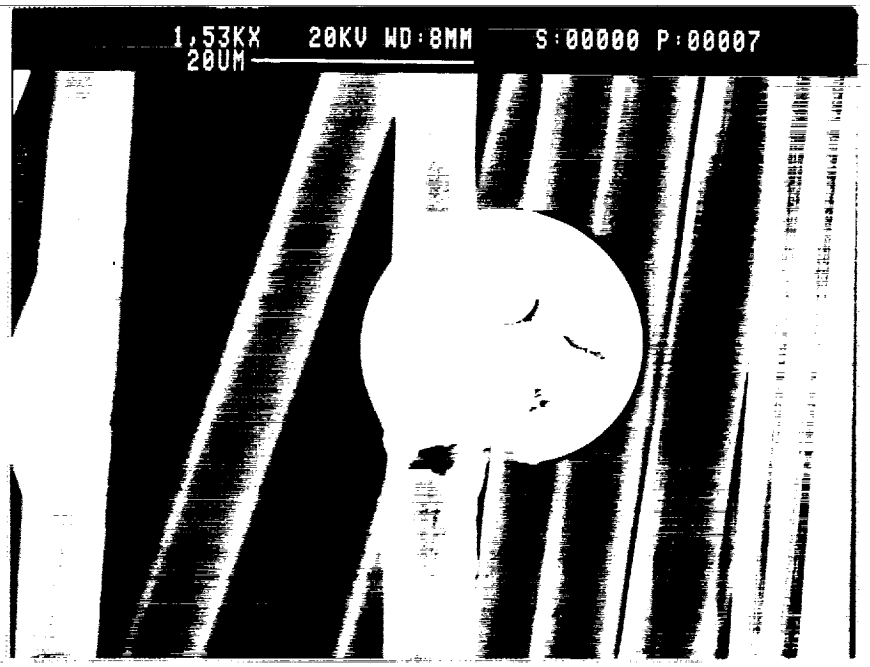

fig. 32. Micrograph of Scraped LaRC-TPI/XAS Prepreg

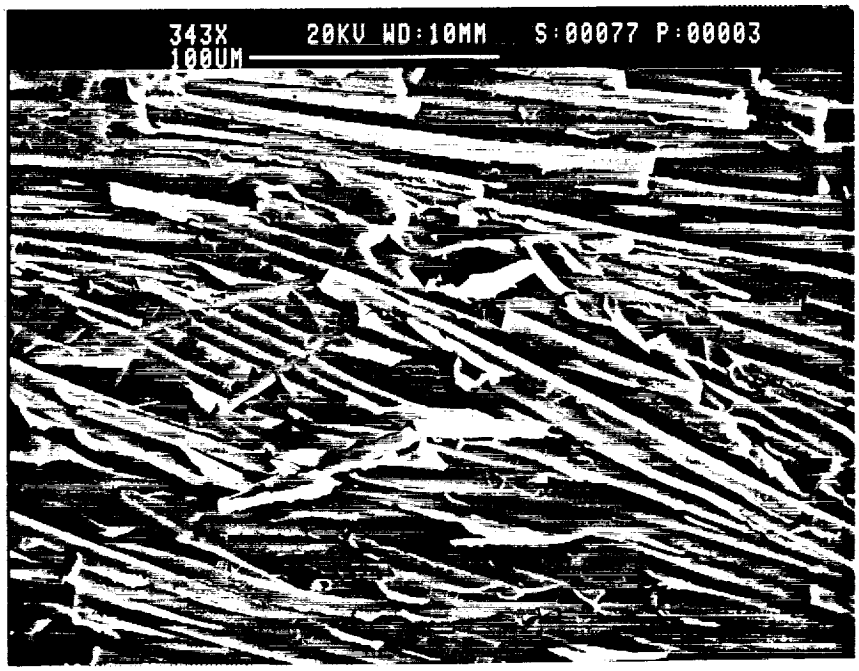

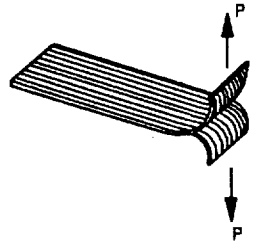

fig. 33. Micrograph of Fractured LaRC-TPI/XAS Coupon

portions of the matrix material retained by the fiber. If the fiber retained the matrix, that would mean that the bond between the two materials was stronger than the matrix itself. Nevertheless from the information gathered on amorphous LaRC-TPI/XAS samples, it appeared that it would make a suitable choice for a comparative adhesion study for LaRC-TPI composites.

5.3.2 Matrix Manipulation

From studies performed by Muellerleile and Wilkes (25), a thermal cycle was developed so that LaRC-TPI could remain semicrystalline. This thermal cycle was developed for the neat resin. Based on the results of their study, their thermal cycle was translated into a composite processing cycle. The semicrystalline thermal cycle was employed specifically to try to improve the adhesion of the LaRC-TPI/AS-4 system. The presence of crystallinity would also improve the mechanical performance at elevated temperatures, i.e., above T_g, and the solvent resistance of the material. In this case, any improvement in adhesion might be attributable to nucleation of crystallinity at the fiber surface, i.e., transcrystallinity.

5.3.2.1 Semicrystalline Thermal Cycle

Muellerleile and Wilkes found that LaRC-TPI lot 58-702 had the maximum amount of crystallinity when it was isothermally annealed at 320°C. As a result, LaRC-TPI crystallization kinetics were extensively characterized at this temperature. The maximum amount of crystallinity was observed when the sample was annealed at 320°C for 180 minutes. Similar observations had been noted in other versions of the LaRC-TPI 1500 series material (22).

The semicrystalline composite thermal cycle consisted of three parts: a pre-treatment, consolidation, and a post-treatment. The pre-treatment occurred when the polymer was melted

onto the fibers during prepregging. Instead of using a one minute residence time in the convection oven, the sample was annealed at 320°C for 180 minutes. Upon removal from the oven, the fibers radiated the heat away extremely rapidly. In essence, the sample was quenched. The post-treatment occurred during the second phase of the lamination cycle. Overall, the semicrystalline lamination cycle was similar to the amorphous cycle with a few notable differences. The altered cycle

- increased the temperature from 22°C to approximately 360°C at 5°C/min
- applied a consolidation pressure of 0.34 MPa at 250°C
- held the temperature at approximately 360°C for 30 minutes
- quenched the sample in water
- cooled the platens to 320°C
- placed the sample back in hot press and applied a consolidation load of 0.34 MPa
- held the temperature at 320°C for 180 minutes
- quenched the sample in water.

The two part thermal treatment was necessary to recrystallize this material. In this cycle, the most crucial step was the first quench or cooling step. During this step, the temperature of the coupon dropped below T_g. As a result, any residual nuclei that survived during consolidation were immobilized. This was a key step because the longer the nuclei remained at temperatures above T_g, the chances for their survival decreased. The residual nuclei that survived were allowed to grow during the post-treatment phase of the lamination cycle.

A sample of the semicrystalline coupon was taken for thermal analysis. At this point, it was observed that the matrix had a melting point of 338°C and a heat of fusion of 5.9 J/g of polymer. Comparing this piece of semicrystalline coupon to the neat resin annealed at 320 °C for the 3 hours, it appeared that a significant portion of the crystallinity had been retained. This was a good indication that it was possible to translate the neat resin thermal cycle into a composite lamination consolidation cycle.

5.3.2.2 Semicrystalline Lamination Procedure

The cycle given in section 5.3.2.1 mimicked the thermal cycle developed by Muellerleile and Wilkes (25). In an attempt to process a composite coupon using the above thermal cycle, a vacuum hotpressing technique was used. The coupons were produced using a vacuum bag in conjunction with a hot press. The cycle listed in section 5.3.2.1 employed a water quench to cool the sample. Normally, steel molds are used to fabricate composites but the previously specified cycle would be too damaging for a steel mold. As a result, the aluminum foil vacuum bag served as the primary molding surface for this coupon. In addition to the vacuum bag, a frame was constructed out of release coated fiberglass fabric to provide some in-plane constraint for the coupon during consolidation. The fiberglass fabric frame was approximately 25.4x25.4 cm square with a 2.5x7.5 cm rectangle cut out to contain the coupon. A 2.5x7.5 cm rectangle of Kapton coated with Frekote 33 release agent was placed on one side of the fabric frame, followed by four layers of unidirectional prepreg. The prepreg was covered with an identical piece of release coated Kapton. The coupon and the frame were vacuum bagged in 0.2 mm aluminum foil and sealed with low temperature vacuum sealant. A schematic of the vacuum bag can be seen in fig. 34. The coupon was processed using with the temperature and pressure cycle given above.

Again, a piece of the composite coupon was analyzed using DSC. Like the prepreg, it was observed that the coupon retained a significant amount of crystallinity.

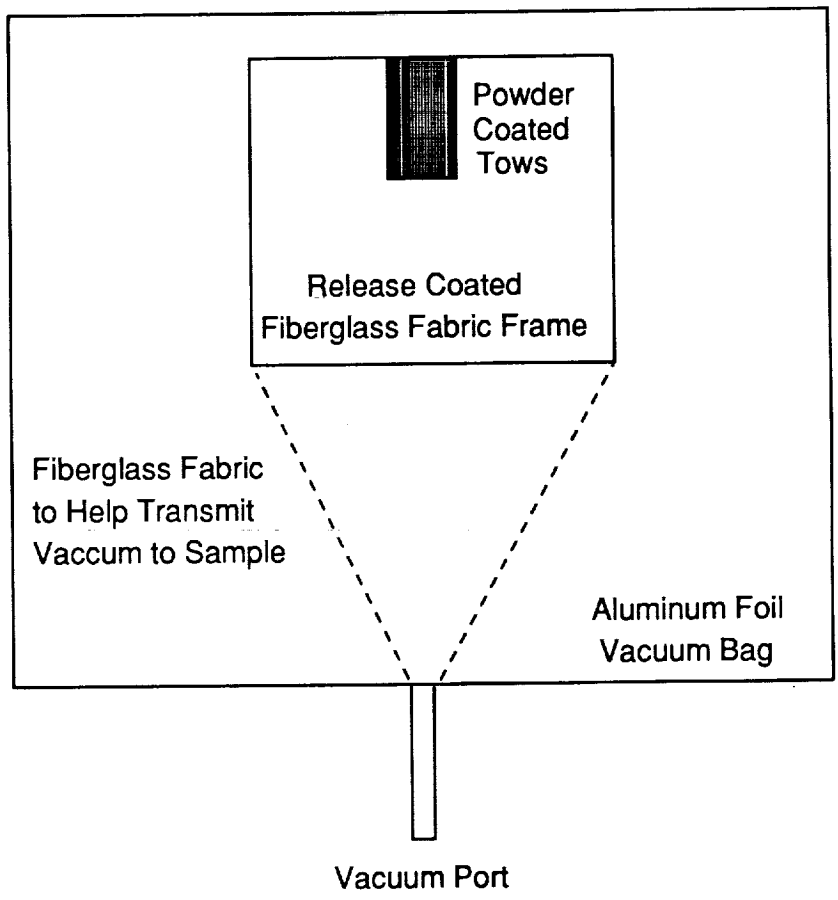

fig. 34. Schematic of Vacuum Bag Layout

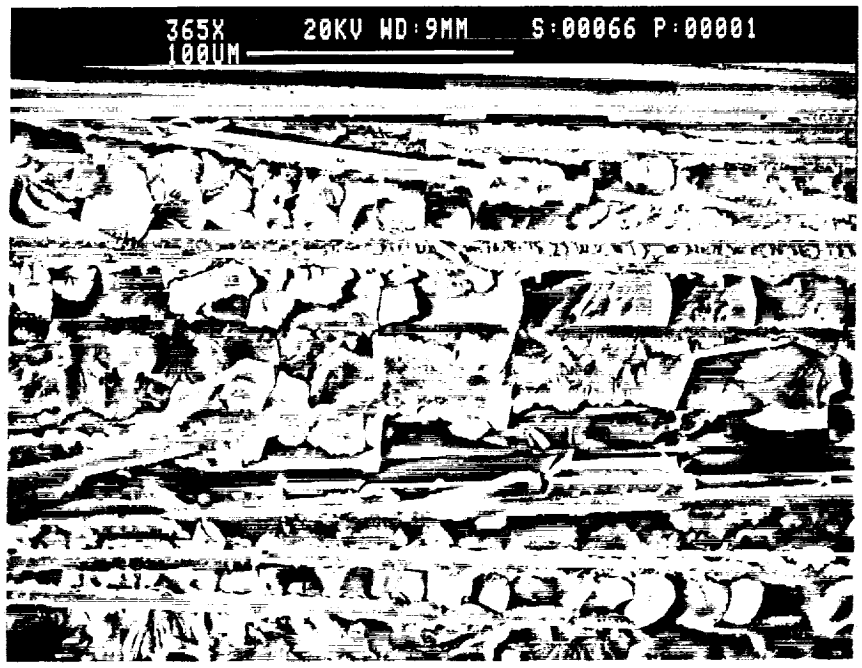

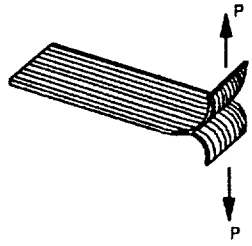

fig. 35. Micrograph of Fractured Semicrystalline LaRC-TPI/AS-4 Coupon

5.3.2.3 *Semicrystalline Coupon Testing and Evaluation*

Like the previous coupons, the semicrystalline LaRC-TPI/AS-4 coupon was fractured in a double cantilever beam-like fashion. The fractured coupon, as seen in fig. 35, was completely different when compared to the amorphous LaRC-TPI/AS-4 coupon, fig. 25. Unlike the amorphous LaRC-TPI/AS-4 coupons, a significant amount of matrix adhered to the fiber. As can be seen especially in the lower portion of fig. 35, the matrix appeared to be very chunky. This could be attributed to the thermally-induced cracking, or to the inherently brittle nature of the semicrystalline material. From these semicrystalline coupons, it appeared that matrix manipulation may offer an improvement in the degree of adhesion in LaRC-TPI/graphite composites.

5.4 *Summary*

Early investigation concentrated on individually pursuing the paths to promote adhesion, namely varying the fiber or the matrix. As a result, no coupons were produced for the semicrystalline LaRC-TPI/XAS combination. Looking at the results for the amorphous LaRC-TPI/XAS coupons and the results for the semicrystalline LaRC-TPI/AS-4 coupons, potentially the most promising coupons could be the semicrystalline LaRC-TPI/XAS coupons.

The next chapter describe efforts to quantify the degree of adhesion for the different treatments. In this phase of the study, both fibers and both structural forms of LaRC-TPI are investigated.

6.0 Mechanical Testing

In the previous chapter, several potential solutions to the interfacial adhesion problem were qualitatively investigated. From that investigation, there were observable differences in adhesion when the fiber and the matrix were altered. The next step focused in quantitatively evaluating the differences in adhesion for the various combinations of fiber and matrix. Since interfacial adhesion appeared to be the key factor observed in the previously described SEM analysis, the goal in this next phase of the study was to measure the strength of the fiber/matrix interface. The transverse tensile test was chosen to accomplish that task. Transverse tensile coupons were fabricated, instrumented, and tested to failure. These steps and the results are discussed below.

6.1 Specimen Fabrication

6.1.1 Prepreg Production

Based on the results of the prepreg evaluation discussed in the last chapter, four types of prepreg were produced. They were: amorphous LaRC-TPI/AS-4, semicrystalline LaRC-TPI/AS-4, amorphous LaRC-TPI/XAS, and semicrystalline LaRC-TPI/XAS. A number of pieces of each type of prepreg were made. Each piece was approximately 2.5 cm wide by 15 cm long. Henceforth, the types of prepreg listed above will be referred to as amorphous/AS-4, semicrystalline/AS-4, amorphous/XAS, and semicrystalline/XAS. These strips, in turn, were used to produce square unidirectional laminates which were then cut into tensile coupons. All strips were prepregged using the process described in ch. 4. The basic experimental parameters for each of the prepreg strips are listed in Appendix A. The parameters in Appendix A include the ambient temperature and relative humidity, moisture deposition rate, oven temperature, oven residence time, and matrix volume fraction of each piece of prepreg.

Relative to the parameters determined in ch. 4, there were slight discrepancies between the original parameters and those used in the production of the prepreg strips. The discrepancies in the prepregging parameters occurred due to seasonal increases in humidity compared to the original ambient conditions in the room where the experiments were calculated, making reproducibility difficult. In an effort to minimize ambient condition variations, the room windows were sealed using polyethylene tarps and duct tape. Once the room was sealed, an air conditioner and a dehumidifier were used to control the ambient environment. Although great care was taken to control the ambient conditions, it was impossible to consistently maintain the ambient conditions originally suggested. The ambient temperature ranged from 22.2 to 24.4°C, and the relative humidity ranged from 58 to 62 percent. Despite these differences

relative to the original conditions, the fibers appeared to have drop sizes and distributions similar to those seen during original moisture characterization tests. As a check, additional moisture deposition studies were performed. In this moisture deposition study, both AS-4 and XAS fibers were studied. The study considered 3 temperature and 3 humidity levels. Measurements were taken at temperatures of 22.2°C, 23.3°C, and 24.4°C, and relative humidity levels of 55%, 58%, and 62%. These ambient parameters covered the spectrum of conditions present.

The moisture accumulation data for AS-4 and XAS fibers at the ambient conditions listed above can be seen in fig. 36. From fig. 36, it can be seen that the ambient temperature and relative humidity do impact the moisture accumulation data for these fibers. With respect to this study, the moisture accumulation behavior in the range around 1.6 cm/s bears the greatest attention, since that was the region chosen for prepregging. At that moisture deposition rate, the moisture accumulation ranged from 40 to 110%, depending on the ambient conditions. Recall, section 4.3.2.2 defined the terminology of the moisture deposition study. Although the range was broad, the average accumulation was approximately 70%. This was true for several variations in the ambient conditions. Comparing this data with fig. 13, the moisture accumulation behavior remained relatively unchanged, given the variations in the fiber surfaces and the ambient conditions used during prepregging.

The other prepregging parameters were fairly consistent from strip to strip, relative to the original conditions. The average moisture deposition rates, plus or minus a standard deviation, were around 1.6 cm/s. The oven temperatures were somewhat low for the amorphous samples. This occurred because it took more than one minute for the oven to stabilize at 330°C. For the semicrystalline samples, the oven temperatures were correct. The oven residence times were consistent with the originally suggested thermal cycles for both the amorphous and the semicrystalline samples. In terms of matrix volume fraction, there were variations among the individual prepreg strips within each laminate. On the average, each laminate had a matrix volume fraction around 40%. It should be noted that the matrix volume

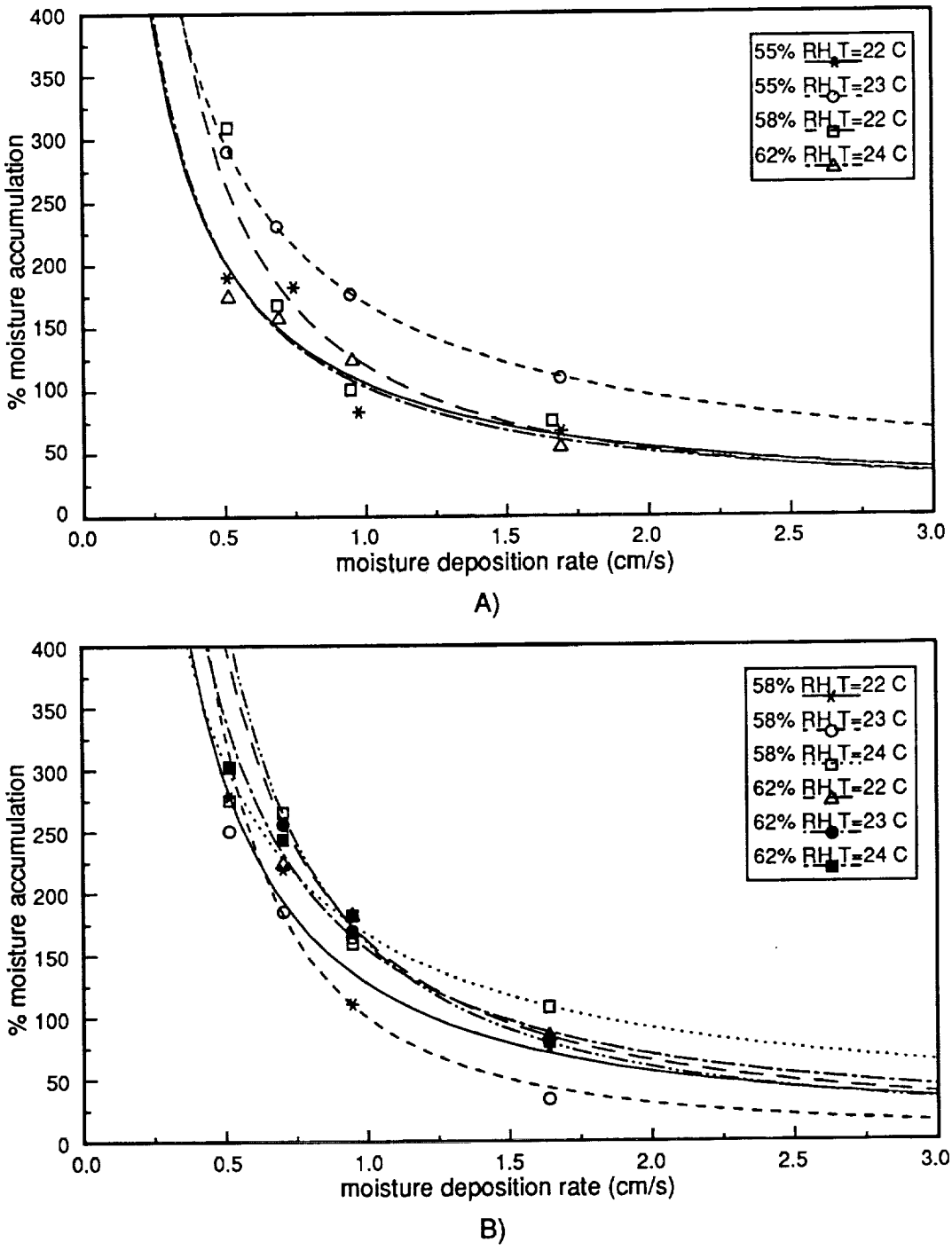

fig. 36. Moisture Accumulation Behavior at Ambient Conditions Ranging from 22.2-24.4°C and 55-62% RH: for A) AS-4 Fibers and B) XAS Fibers

fraction of each strip was lower along the lengthwise edges of each strip and higher along the middle.

6.1.2 Laminate Production

6.1.2.1 Layup

The 2.5x15 cm prepreg strips were sectioned into shorter 2.5x7.5 cm strips. The shorter prepreg strips were arranged in a 7.5x7.5 cm matched metal mold. The strips were arranged so that there were three prepreg strips per layer of the laminate. To compensate for the non-uniformities in the distribution of the matrix across the width of each strip, care was taken to balance the matrix distribution within each layer of the laminate. This was accomplished by slicing the strips lengthwise, i.e., making them 1.25 cm wide, and splicing the strips within each layer, e.g., a strip with a high matrix volume fraction adjacent to a low matrix volume fraction strip which would be adjacent to another high matrix volume fraction strip, etc. In addition to balancing the matrix distribution within a layer, the individual layers were arranged so that the matrix volume fraction was balanced within the laminate. A strip with a low matrix volume fraction in layer 16 being on top of a high matrix volume fraction strip in layer 15, being on top of a strip with a low matrix volume fraction in layer 14, etc. When stacking the prepreg to make a laminate, the edges of the laminate were fused together using a soldering gun every time two new layers were added. The edges were fused to minimize interlayer slippage. The layup for all laminates produced was 0°_{16}. The components of each layer for half of the laminate is given in Appendix B. The components of each layer are given in terms of the sample identification numbers. For specific information, refer to Appendix A. Since the laminate layup is symmetric about the geometric midplane of the laminate, only half of the components are listed, i.e., layer 9 is identical to layer 8, layer 10 is identical to layer 7, etc.

6.1.2.2 *Mold and Vacuum Bag Preparation*

Prior to layup, the mold was treated with Frekote 33 release agent. The unconsolidated 16-layer laminate was separated from each side of the mold by a layer of 0.1 mm Kapton film which was also treated with Frekote 33 release agent.

Chapter 5 described the processing cycles used for both the amorphous and semicrystalline laminates. All laminates were produced using a vacuum hotpressing technique. A schematic of the vacuum bag layout is given in fig. 37.

The construction of the vacuum bag began by cutting a 61x76 cm piece of 0.2 mm aluminum foil. The sheet was creased to produce a 61x38 cm pouch. The pouch was opened and the mold was placed inside. The mold was located at least 2.5 cm from the crease in the vacuum bag and it was centered with respect to the length of the vacuum bag. Once the mold was properly positioned, a 10x10 cm piece of 0.2 mm aluminum (not shown) was placed over the base and the plunger of the mold to help keep the edges from piercing the vacuum bag. A thermocouple was embedded into the mold to monitor the laminate temperature during processing. The entire mold was draped with three layers of fiberglass fabric. The fiberglass fabric provided added protection so that the edges of the mold would not puncture the vacuum bag. The vacuum bag was closed by bringing the upper layer of aluminum foil over the draped mold. At this point, the fold at each end of the bag was spread and a piece of vacuum sealant spanning the width of the bag was placed on the inside bottom surface of the vacuum bag. The piece of sealant overlapped at the fold of the vacuum bag and always ran close to the edge of the vacuum bag. A piece of vacuum sealant was also placed on the inside bottom surface, running along the length of the vacuum bag. The paper backing was removed from the surfaces of the vacuum sealant. After the sealant was exposed, each end of the vacuum bag was grasped and stretched. Once it was stretched, the vacuum bag was sealed by crimping the corners and the midpoint of the sealant seam. The span between the sealed

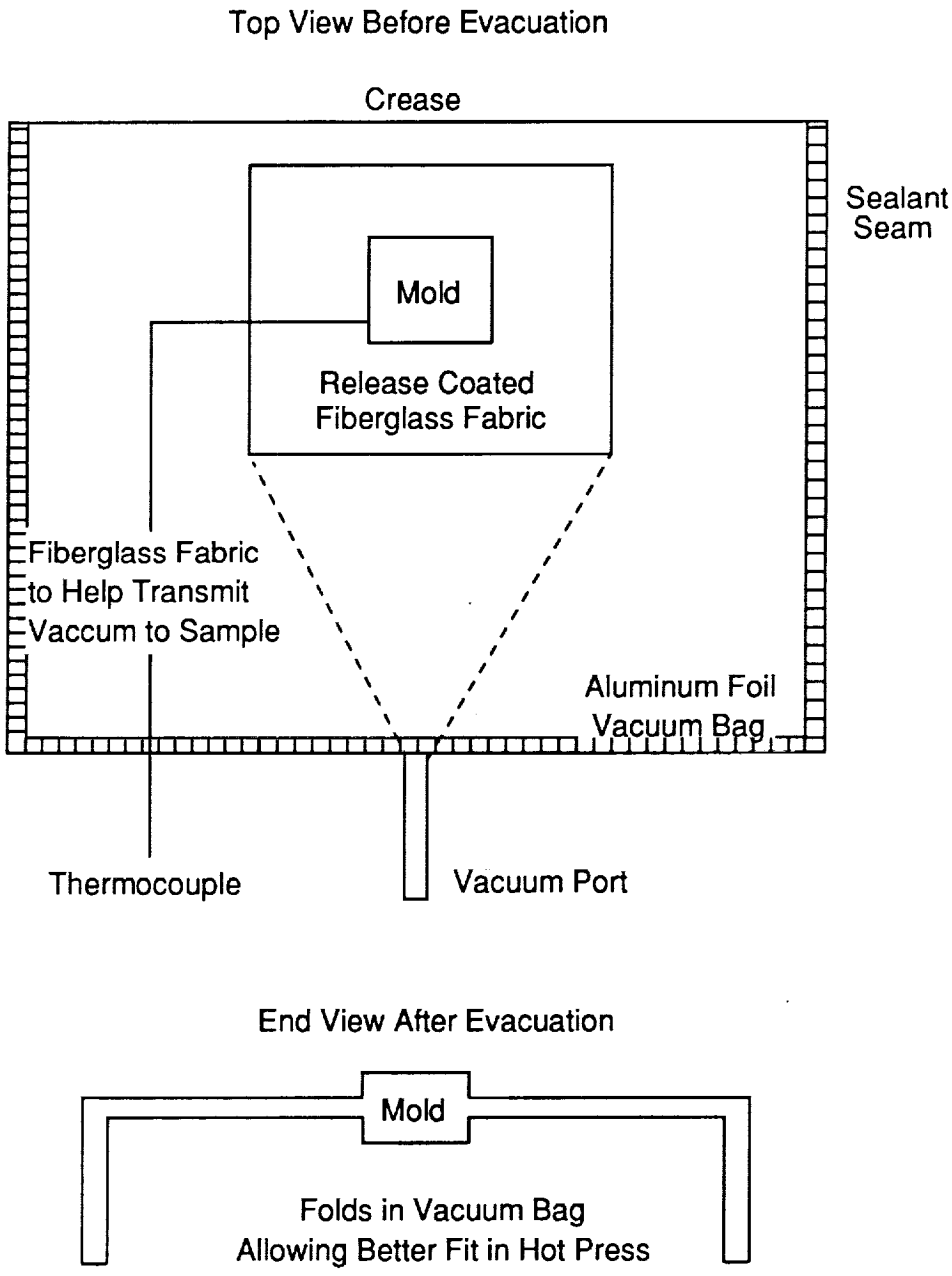

fig. 37. Layout of Vacuum Bag Used in Laminate Production

C-2

points was continually halved so that the seam was sealed with the minimum number of ripples placed in it. This procedure was repeated for the seam on the opposite side of the vacuum bag. Before the end of the vacuum bag could be closed, two steps had to be taken. First, the vacuum port had to be prepared. The vacuum port was a curved tube with a piece of fiberglass fabric taped around one end of the tube. The fiberglass fabric was added to help transmit the vacuum to the laminate. In some cases, it would be possible that the vacuum bag could collapse around the vacuum port, sealing it off from the laminate. If this happened, certain areas could be under adequate vacuum while the remainder of the laminate would only be partially evacuated. The vacuum port preparation began by placing a coil of vacuum sealant around the vacuum port about 4 cm from the end wrapped in fiberglass fabric. That section of the vacuum port was placed at the midpoint of the sealant strip running along the length of the vacuum bag. A short strip of vacuum sealant, around 2.5-4 cm long, was placed on top of the sealant coil surrounding the vacuum port. The other area that needed protection was the point where the thermocouple penetrated the vacuum bag. To minimize vacuum losses, a section of the thermocouple wires, away from the seam, needed to be separated and stripped of their fiberglass insulation. The exposed wires were covered on both sides by a piece of vacuum sealant which was attached to the vacuum bag. A procedure similar to the one utilized for the vacuum port was used to prepare the area where the thermocouple exited the vacuum bag. After the vacuum port and the thermocouple were ready, the vacuum bag was closed. This was accomplished by drawing the top and bottom of the vacuum bag evenly around the vacuum port and crimping the sealant around it. The thermocouple area was closed next using the same procedure. Upon completing the vacuum port and the thermocouple, the seam at the end of the vacuum bag was divided into several smaller sections. Each individual section was stretched and the midpoint of the each seam was sealed. Again, each seam was completed by progressively subdividing the remaining portions. All the seams were hand crimped and visually inspected to ensure that they were sealed. Upon completion, the seams were flattened using a steel roller to maximize the surface area covered by the sealant.

Once the vacuum bag was complete, it was evacuated. At this point, any vacuum leaks were traced and repaired. The vacuum bag was monitored for several minutes to ensure the system was stable. After it stabilized, the sides of the vacuum bag were bent so that the sample could fit into the hot press. The vacuum bag was monitored again to ensure that new leaks were not introduced. The completed form of the vacuum bag remained under vacuum pressure for an additional 30-60 minutes. At the end of that time, the vacuum bag was placed into the hot press and the platens were brought close to the vacuum bag but did not touch it. The mold was aligned with respect to a 7.5x7.5 cm Kapton tape border which was centered on the upper platen. After the mold was aligned, the platens were brought in contact with the vacuum bag. A contact load ranging from 113-227 kilograms was placed on the vacuum bag and the lamination cycle commenced. It should be noted that all laminates were produced in a Tetrahedron Pneumapress P-400 Hotpress.

6.1.2.3 Lamination Cycles

The consolidation cycle for the amorphous and semicrystalline laminates were given in ch. 5. The amorphous cycle was implemented as stated in that chapter with one exception. In the cycle outlined in ch. 5, the laminate was cooled under ambient conditions. The amorphous laminates produced for mechanical testing were cooled at a controlled rate of 2.5°C/min. This was done to maintain consistency with the cooling rates employed for the various laminates produced. Cooling was achieved by using two commercial fans at their highest setting. The fans were always oriented so that the airflow passed from the front to the rear of the hotpress. The semicrystalline cycle was altered in terms of the consolidation pressure and the form of cooling. The consolidation pressure was altered to maintain uniformity between the amorphous and the semicrystalline laminates. The cooling type was changed from a water quench to forced air cooling. This was done to minimize the severity of cooling, since a metal mold

was being used, and to maintain uniformity in laminate production. The revised cycle consisted of

- ramping from ambient temperature to approximately 360°C at 5°C/min.
- applying a consolidation of 2.1 MPa at 250°C
- holding the temperature at approximately 360°C for 30 minutes
- cooling the sample at approximately 2.5°C/min. to 200°C
- ramping from 200°C to 320°C at 5°C/min.
- holding the temperature at 320°C for 180 minutes
- cooling the sample at approximately 2.5°C/min. to 200°C.

The platen pressure was removed once the laminate temperature fell below 200°C. The vacuum bag was removed from the press and it was allowed to equilibrate to ambient pressure. Once at ambient pressure, the vacuum bag was opened and the laminate was removed from the mold.

6.1.2.4 Discussion

One problem arose during lamination: the vacuum bag leaked. This was due to the fact that the vacuum sealant degraded from the prolonged exposure to elevated temperatures during processing. The vacuum bag did not leak during the thermal ramps and isothermal holds but it leaked while the laminate was being cooled. The sealant degradation caused the seam to lose some of its elasticity which in turn allowed the bag to separate in isolated spots. Gen-

erally, the leaks were patched but sometimes several inches of mercury were lost during this period. It should be noted that an external load was always on the laminate when the vacuum failed.

The laminates that lost vacuum were the amorphous/XAS and the semicrystalline/XAS. The vacuum pressure for the amorphous/XAS laminate rose to 3 in. of mercury during its cool down. The semicrystalline laminate suffered the greatest vacuum loss. It rose to 6 in. of mercury during processing. The vacuum was partially regained during the 3 hour anneal at 320°C but it never regained the initial vacuum pressure level. The effect of vacuum loss during the cool down is unknown.

6.1.3 Laminate Evaluation

6.1.3.1 C-scan

All four laminates were examined using an ultrasonic scanning device. The samples were evaluated using a 10 MHz transducer with a S-80 reflectoscope and US 450 laboratory scanner made by Automation Industries. For comparative purposes, the laminates were evaluated using identical scanning parameters.

It should be noted that the amorphous laminates were fabricated and evaluated first. When these laminates were ultrasonically evaluated, the issue of incomplete consolidation arose. In an attempt to improve the C-scan results, both amorphous laminates were reprocessed under the same conditions used previously. The laminates were re-evaluated. The results remained unchanged. Given that reprocessing did not alter the C-scan results, the semi-crystalline laminates were only processed once. The primary reason for not reprocessing the semicrystalline laminates was to avoid altering their level of crystallinity.

The results of the ultrasonic evaluation for all the laminates are given in fig. 38. From fig. 38, it is seen that all of the laminates appeared to be poorly consolidated. Of the four laminates, laminates C and D appear to show the lowest amounts of consolidation. The C-scan indicated that there were isolated regions that were well consolidated, while the rest of the laminate was virtually unconsolidated. For this to be the case, there should have been a drastic difference in the thickness of the laminate from location to location. However, there were only slight thickness gradients, i.e., 0.03 to 0.05 mm, in all the laminates but nothing that indicated the differences observed in the C-scans. In addition to the slight thickness gradient, a slight warp was detected in the laminates. It was possible that the warp altered the C-scan results. To understand the C-scan results to a greater extent, it would have been necessary to dissect the laminates. This step was not completed until all the laminates were fabricated.

6.2 *Transverse Tensile Testing*

6.2.1 Tensile Coupon Preparation

The tensile coupons were cut from the four laminates. The four laminates were stacked together, clamped to a plate, and cut all at once. A diamond saw was used to cut the stack of laminates. The laminates were cut by starting at the right side of the laminate. From each laminate, three 1.9 cm wide and 7.5 cm long transverse tensile coupons were produced. A total of twelve tensile coupons were cut from the stack of laminates. The scheme used to identify the coupons was based on the first letter of the form of the matrix, the first letter of the fiber used and the coupon number, in that order. For example, AA1 was an amorphous/AS-4 tensile coupon which was the first sample from the right side of the 7.5x7.5 cm laminate.

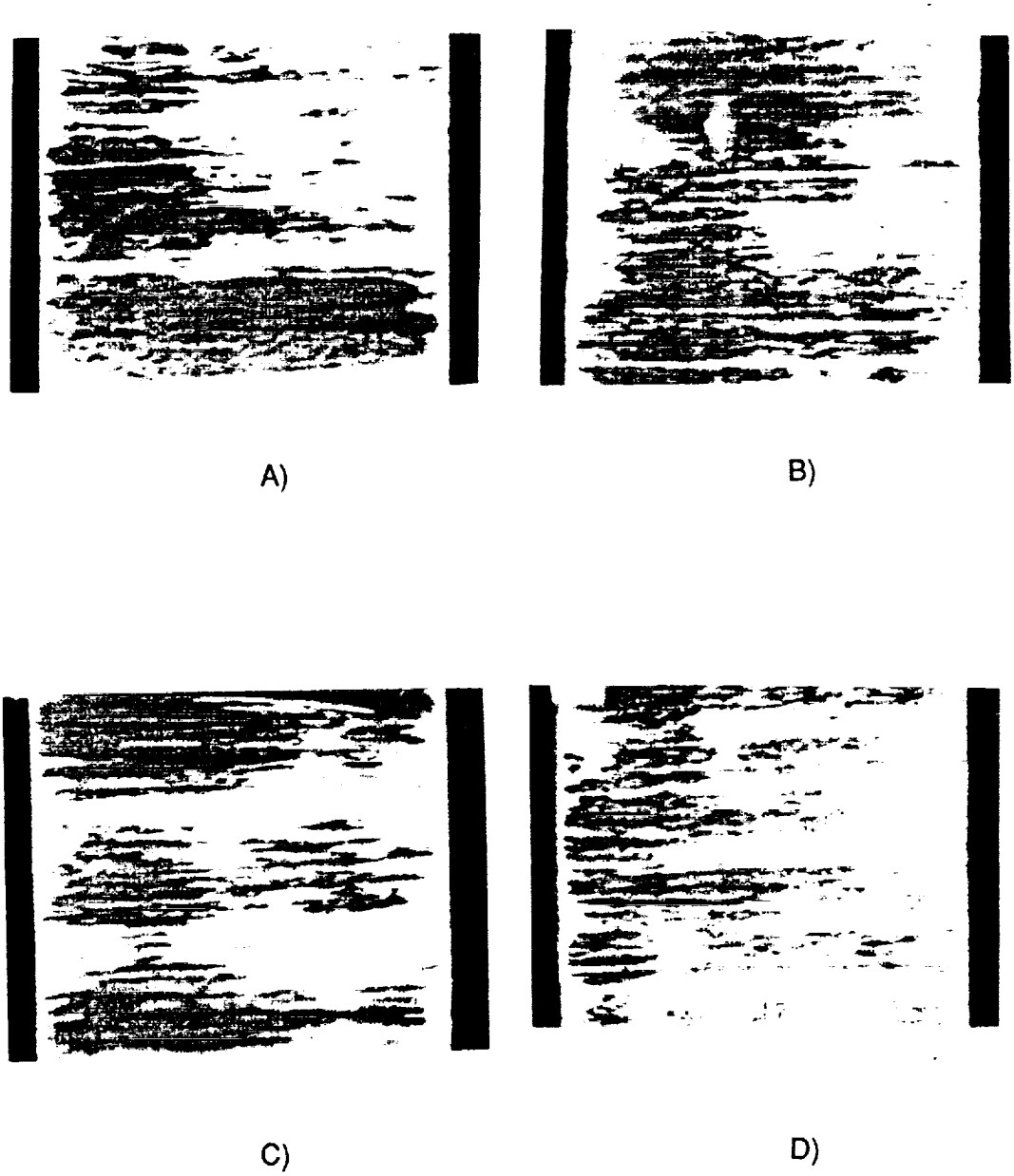

fig. 38. C-scans of LaRC-TPI Composites: A) Amorphous/AS-4, B) Amorphous/XAS, C) Semicrystalline/AS-4, and D) Semicrystalline/XAS

Prior to cutting into tensile coupons, the laminates were dried in a vacuum oven at 90°C for at least 6 hours. The dried laminates were weighed on an analytical balance. After cutting, the coupons were dried in a vacuum oven at 90°C for another 6 hours. The individual coupons were weighed using the balance mentioned previously. The dimensions of each sample were measured and are given in Table 2. The thickness reported in Table 2 was an average of five measurements taken along the length of a coupon. For all samples, the standard deviation in the thickness of the tensile coupon was less than 0.03 mm. Since the length of fiber used in each tensile coupon was known, the mass of the fiber could be calculated. Subtracting this from the total weight of the specimen, it was possible to find the mass of the matrix in each coupon. After calculating each of these quantities, the volume of the fiber and the matrix were determined, since the densities of each were known. From this, the matrix volume fraction was calculated for each coupon and is listed in Table 2.

Visually inspecting the coupons after sectioning, it appeared that the samples were consolidated to a greater extent than the C-scans revealed. Some surface flaws were noted in the samples. It was felt that this could have been the cause of the poor C-scan results. A post failure study will address this in greater detail later.

The tensile coupons were prepared for strain gauging according to the recommendations given with Micro-Measurements M-Bond 200 Adhesive Kit. The strain gauges used were FCA-2-11 0°/90° rosettes from Texas Measurements Incorporated. The gauges were placed back to back in the center of each transverse tensile coupon. After the gauges were attached, the wires from the gauges were arched back over the gauge area and were soldered to one-half of the terminal tabs. The lead wires which connected the gauges to the data acquisition system were soldered to the remaining terminal tabs. Once this was completed, the tensile coupons were kept in a desiccator prior to testing.

Table 2. **Physical Properties of LaRC-TPI Composite Coupons**

Sample ID	Length (cm)	Width (cm)	Thickness (mm)	v_m (%)
AA1	7.5	1.9	0.541	42.6
AA2	7.5	1.9	0.536	42.2
AX1	7.6	1.9	0.518	42.4
AX2	7.6	1.9	0.526	43.6
CA1	7.6	1.9	0.521	41.3
CA2	7.6	1.9	0.511	40.9
CX1	7.6	1.9	0.536	43.6
CX2	7.6	1.9	0.526	43.4

6.2.2 Testing Procedure

The transverse tensile testing was performed on an Instron 4202 Universal Testing Machine. All samples with the exception of AA1 were tested using a 454.5 kg load cell on the 227.3 kg range. Sample AA1 was tested first and it was tested using a 45.4 kg load cell. The lower range load cell was used because of the poor transverse tension properties observed for the amorphous/AS-4 in previous portions of the study. The load cell was calibrated before each run. Strain and load data were acquired during the test using a 3530 Orion Data Logger from Solatron Instruments coupled with an IBM AT personal computer. During each test, the four gauges and the load were monitored every two seconds. The loading rate was 0.05 cm/min.

Prior to each testing session, an aluminum coupon of similar dimensions to the composite coupons was placed in the machine to make certain that the data acquisition system and the testing setup were in order. After this was assured, the composite coupons were tested.

None of the coupons used bonded tabs, rather strips of 320 grit sandpaper were used to minimize slippage in the grips. Testing began by placing the coupons into the upper grip. Each coupon was then aligned by squaring the coupons with respect to the the flat faces of the

upper grips. Once aligned, the grips were tightened so that the coupon position remained fixed. This procedure was repeated for the lower grip. Additional tightening of the grips was completed once the coupon was oriented properly in the testing machine. The gauge length for each coupon was approximately 5 cm. The strain gauge lead wires and the connection from the load cell were then attached to the Orion data logger. Once everything was in order, the data acquisition package was activated and the strain gauge values were checked for consistency. The coupon was ready for testing.

6.2.3 Testing Results

After testing, the raw voltage data acquired by the data acquisition system were translated into load and strains using a previously written software package. The translated data were imported into Lotus 1-2-3 where the strains from the front and back gauges in the 1 and the 2 direction were averaged and, using the load, the transverse stresses were determined. Recall, the 1-direction is oriented parallel to the fibers and the 2-direction is oriented perpendicular to the fibers. The equation used to calculate the transverse stress, or the stress in the 2-direction, was

$$\sigma_2 = \frac{P}{w\bar{t}}$$

where P was the experimentally observed load, w was the width of the tensile coupon, and $\bar{t}$ was the average thickness of the coupon reported in Table 2. From the stress-strain relations, the transverse modulus was determined by using the slope of the relation. In addition to determining the stress-strain behavior of the coupons, the relation between the strain in the 1-direction, ε_1, and the strain in the 2-direction, ε_2, was graphed. The transverse Poisson's ratio, or ν_{21}, was determined using the negative of the slope of the relationship.

6.2.3.1 *Amorphous/AS-4 Coupons*

Coupon AA1 was tested four times. The first test was stopped due to slippage of the coupon in the grips. The second test was stopped at a load of 25 kg to obtain a rough idea of the modulus for this amorphous sample. The third test was terminated prior to failure because the limit of the load cell was almost exceeded. The range on the load cell was increased and on the fourth test, the sample failed at a stress just under 37.6 MPa. The data acquired during these four tests was extremely consistent, uniform, and linear.

Coupon AA2 was tested three times. The first test was terminated due to slippage in the grips. The second test ended when the sample failed in the grips at a stress approximately 24.2 MPa. Since the majority of the test section was still in one piece, the sample was repositioned in the grips to account for the lost portion of the coupon. The gauge length remained unchanged and the sample was retested. On the third test, sample AA2 failed in the gauge length at a stress just under 28.9 MPa. The stress-strain relations for samples AA1 and AA2 are given in fig. 39. The relation between ε_1 and ε_2 for coupons AA1 and AA2 are given in fig. 40. As can be seen in fig. 39 and fig. 40, the data are of high quality. The failure stress, transverse tensile modulus, percent strain to failure and Poisson's ratio, ν_{21}, for these samples are given in Table 3.

6.2.3.2 *Amorphous/XAS Coupons*

Both AX1 and AX2 were each loaded twice. During the first test for each coupon, the coupon slipped in the grips. Coupon AX1 and coupon AX2 failed on the second test around 31.0 MPa and 30.1 MPa respectively. The relation between σ_2 and ε_2 can be found in fig. 41. The relation between ε_1 and ε_2 can be found in fig. 42. As one can see in fig. 41, the data for the three tests were linear but the slopes differed, indicating that there was a difference in

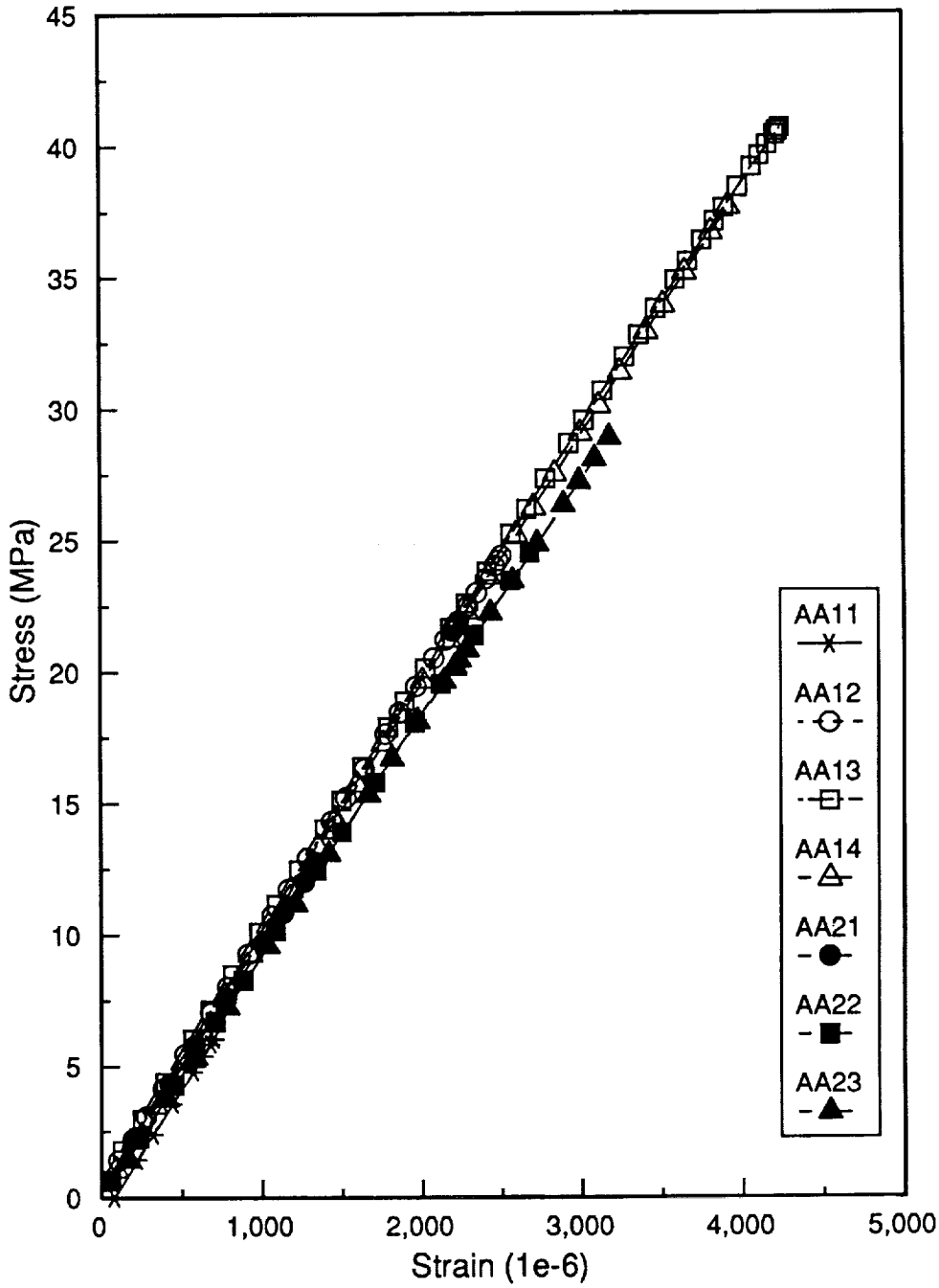

fig. 39. Relationship between σ_2 and ε_2 for coupons AA1 and AA2

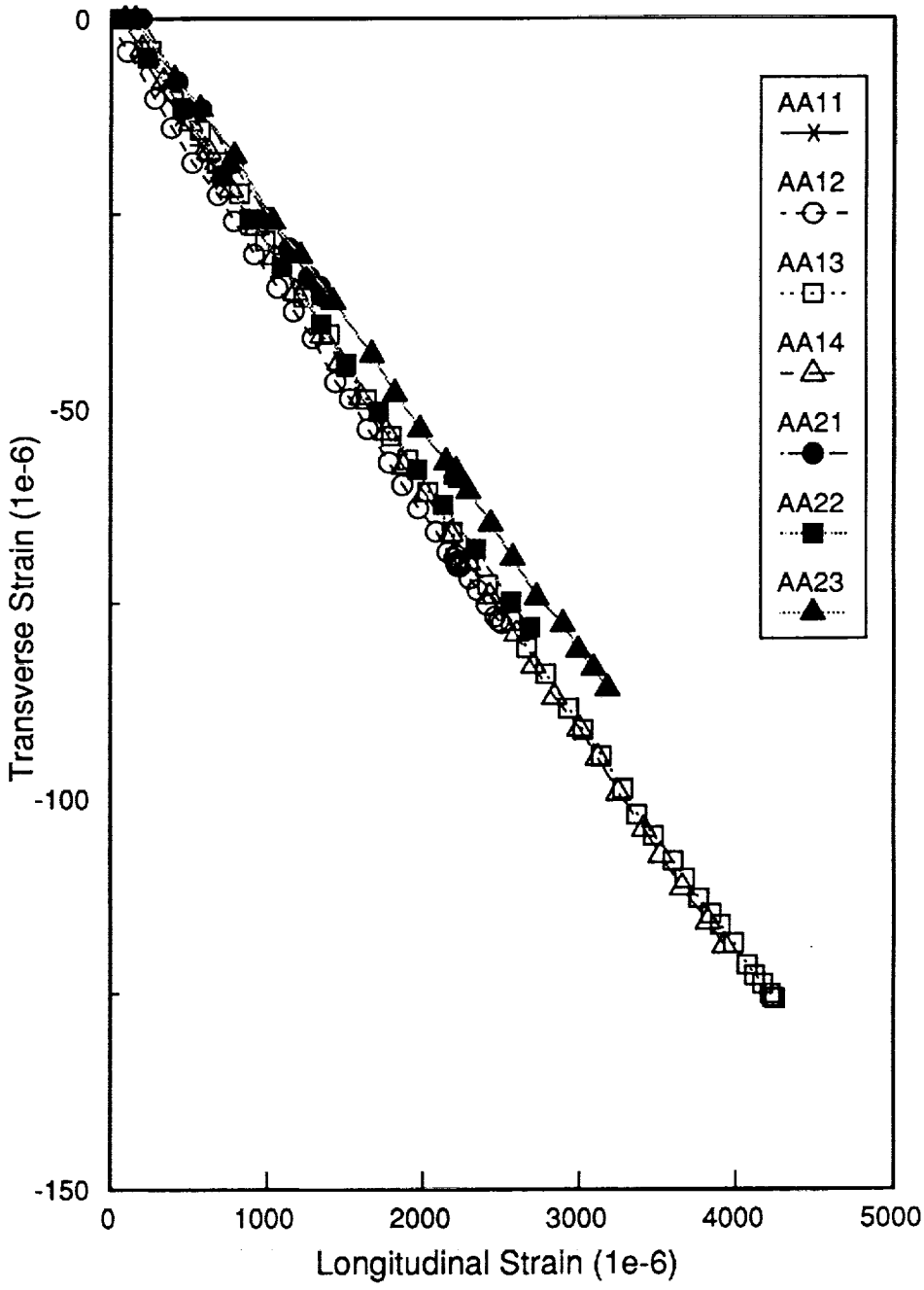

fig. 40. Relationship between ε_1 and ε_2 for coupons AA1 and AA2

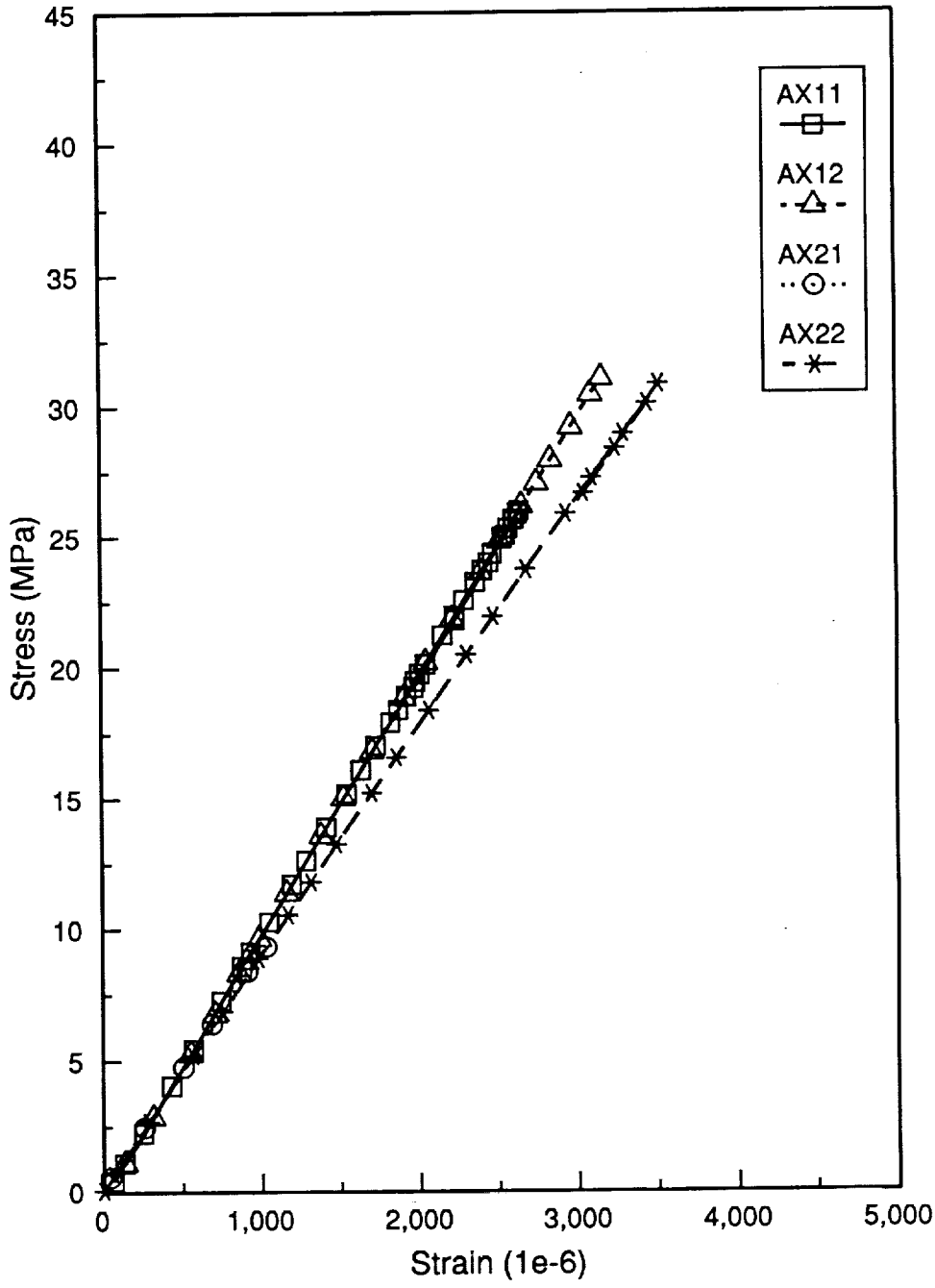

fig. 41. Relationship between σ_2 and ε_2 for coupons AX1 and AX2

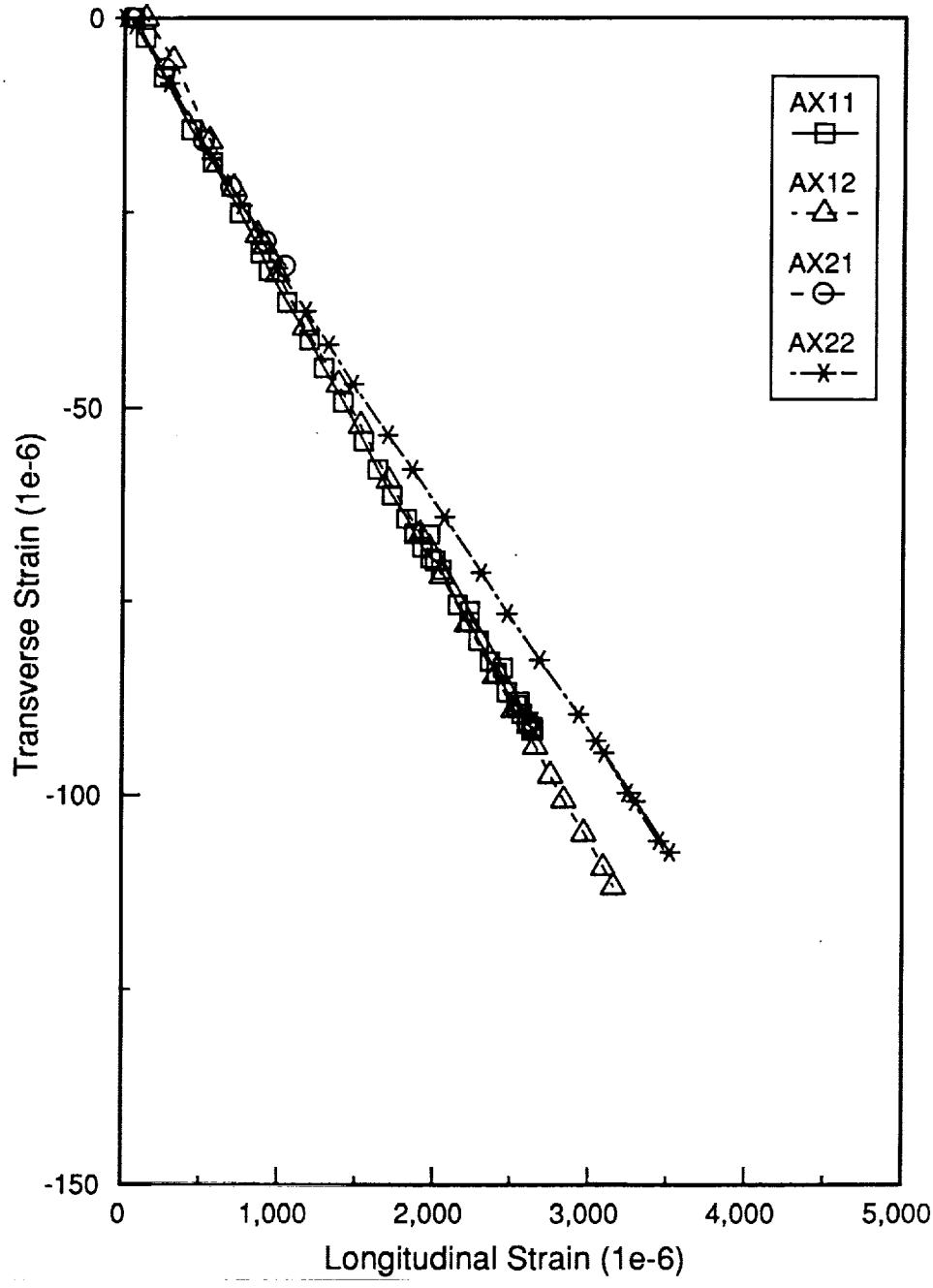

fig. 42. Relationship between ε_1 and ε_2 for coupons AX1 and AX2

modulus between the coupons. This behavior was also reflected in fig. 42. In this case, the data were close to being linear, but there was a slight non-linearity in the relationship for the AX2 coupons. The specific mechanical properties for coupons AX1 and AX2 can be found in Table 3.

6.2.3.3 *Semicrystalline/AS-4 Coupons*

Coupon CA1 was successfully loaded to failure on the first attempt and it failed at a stress of 12.0 MPa. Coupon CA2 was tested twice. During the first test, the coupon slipped in the grips. After readjusting the grips, CA2 failed during the second test at a stress of approximately 12.9 MPa. The data were consistent and linear for the three tests. The stress-strain behavior for these coupons are given in fig. 43. For purposes of comparison, the data from the various laminates are all plotted using the same scale. The relationship for determining Poisson's ratio is shown in fig. 44. The mechanical properties for the CA coupons can be found in Table 3.

6.2.3.4 *Semicrystalline/XAS Coupons*

The CX1 and CX2 coupons both failed on the first test. Coupon CX1 failed at approximately 8.6 MPa and coupon CX2 failed around 11.3 MPa. The stress-strain relations for these coupons are given in fig. 45. The relation between ε_1 and ε_2 is given in fig. 46. In fig. 45, there is a difference in the slopes of the data. This reflects a difference in the modulus between the two coupons. Like the other coupons, the mechanical properties for these coupons are given in Table 3.

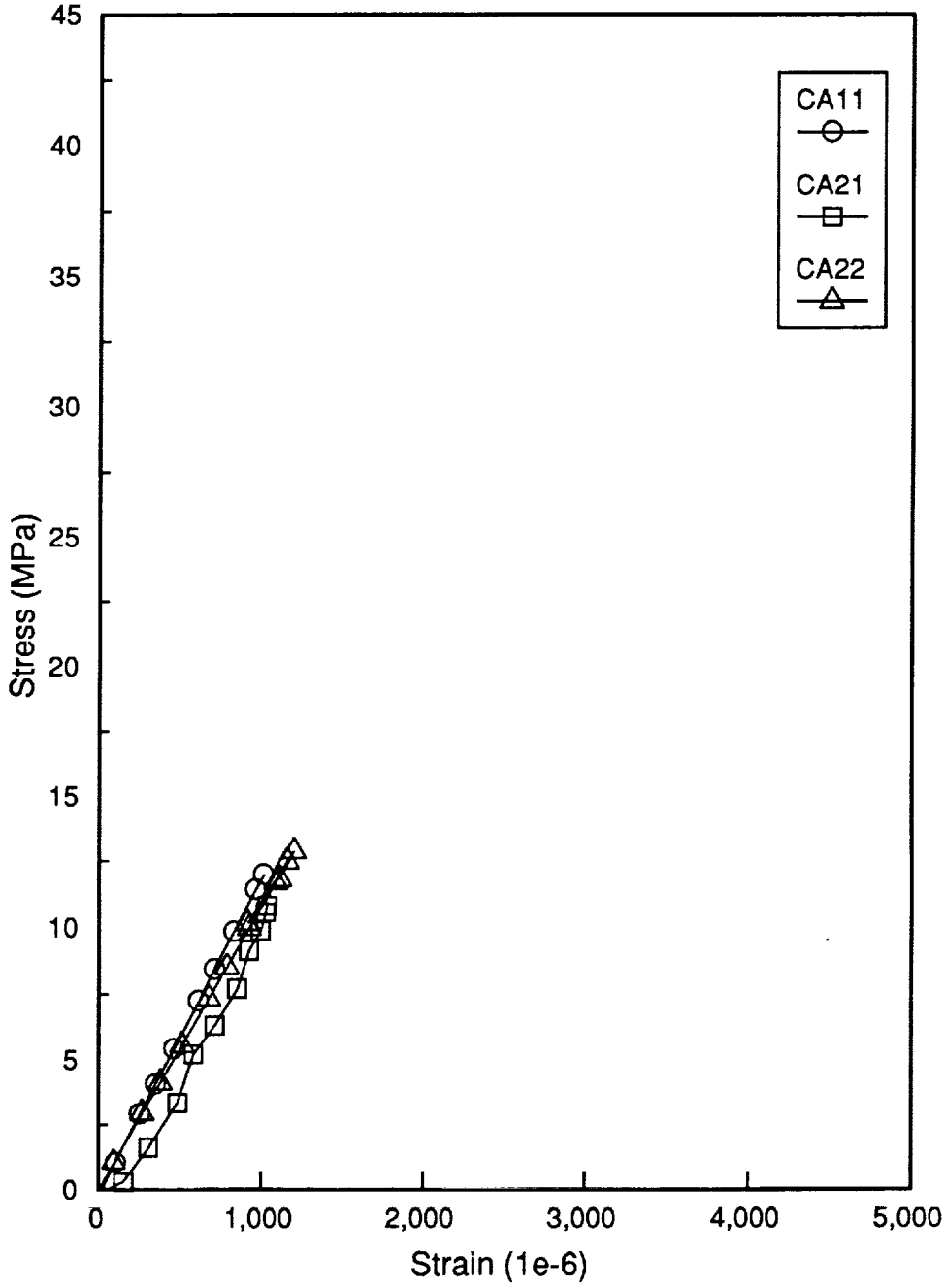

fig. 43. Relationship between σ_2 and ε_2 for coupons CA1 and CA2

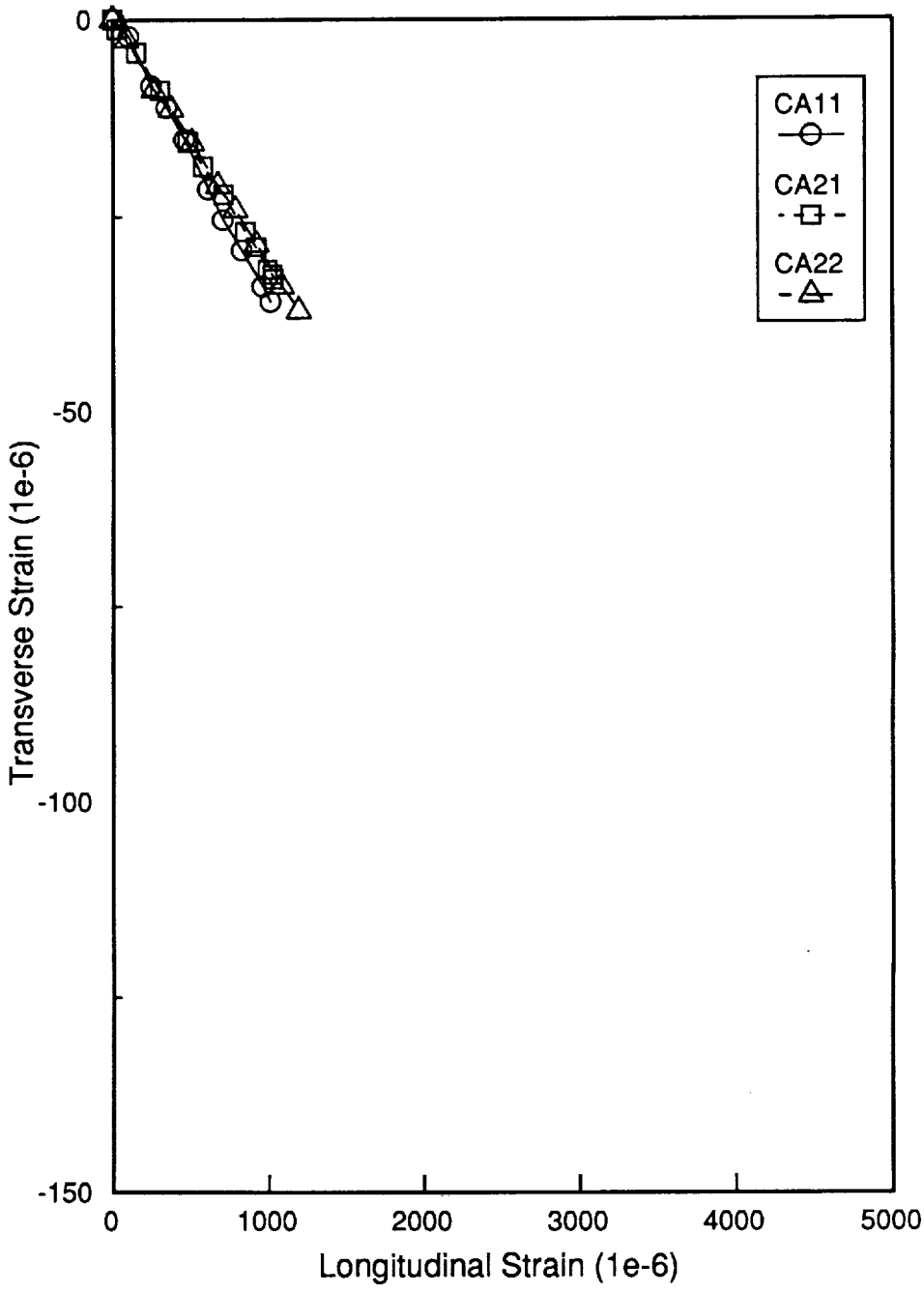

fig. 44. Relationship between ε_1 and ε_2 for coupons CA1 and CA2

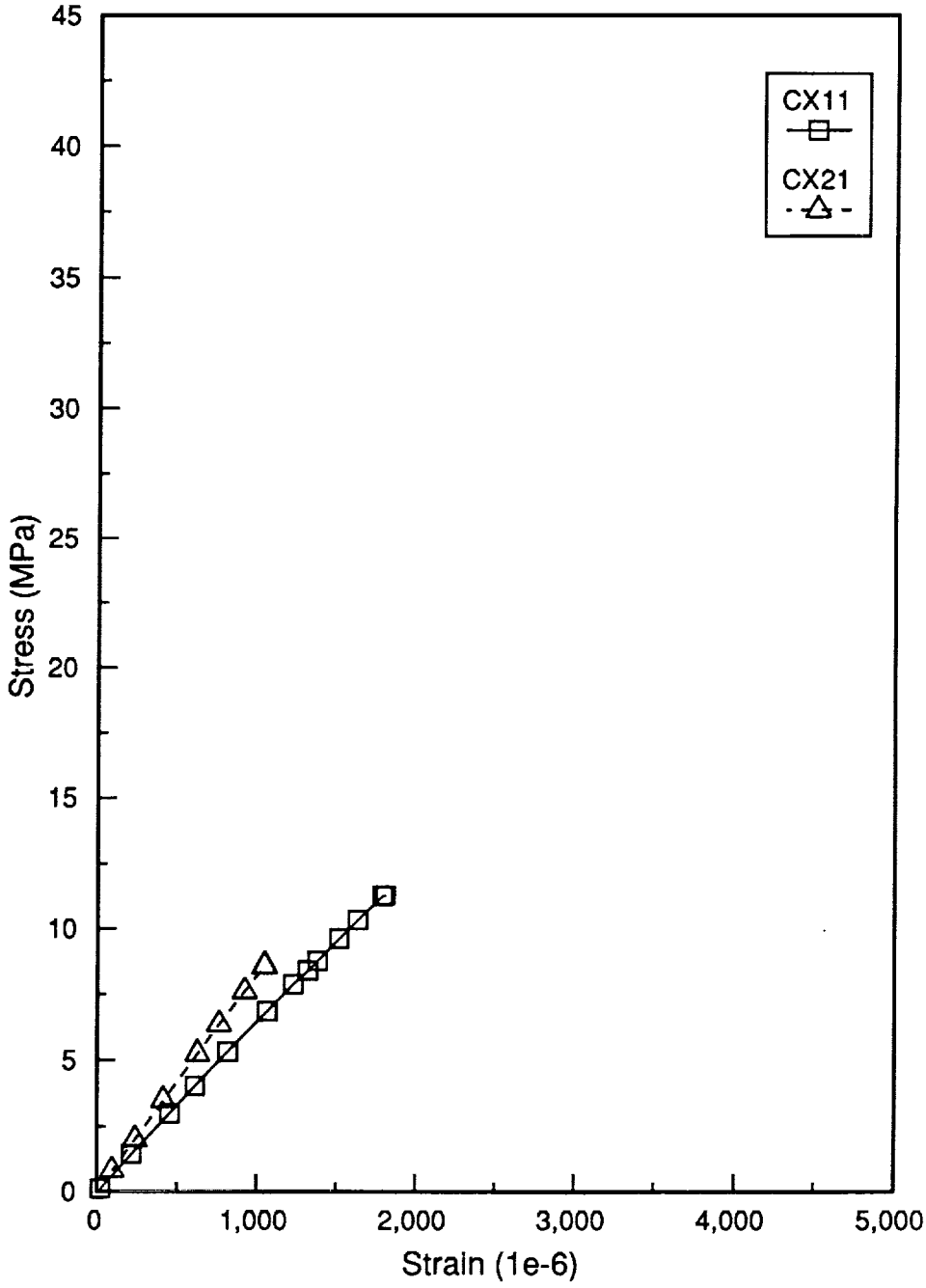

fig. 45. Relationship between σ_2 and ε_2 for coupons CX1 and CX2

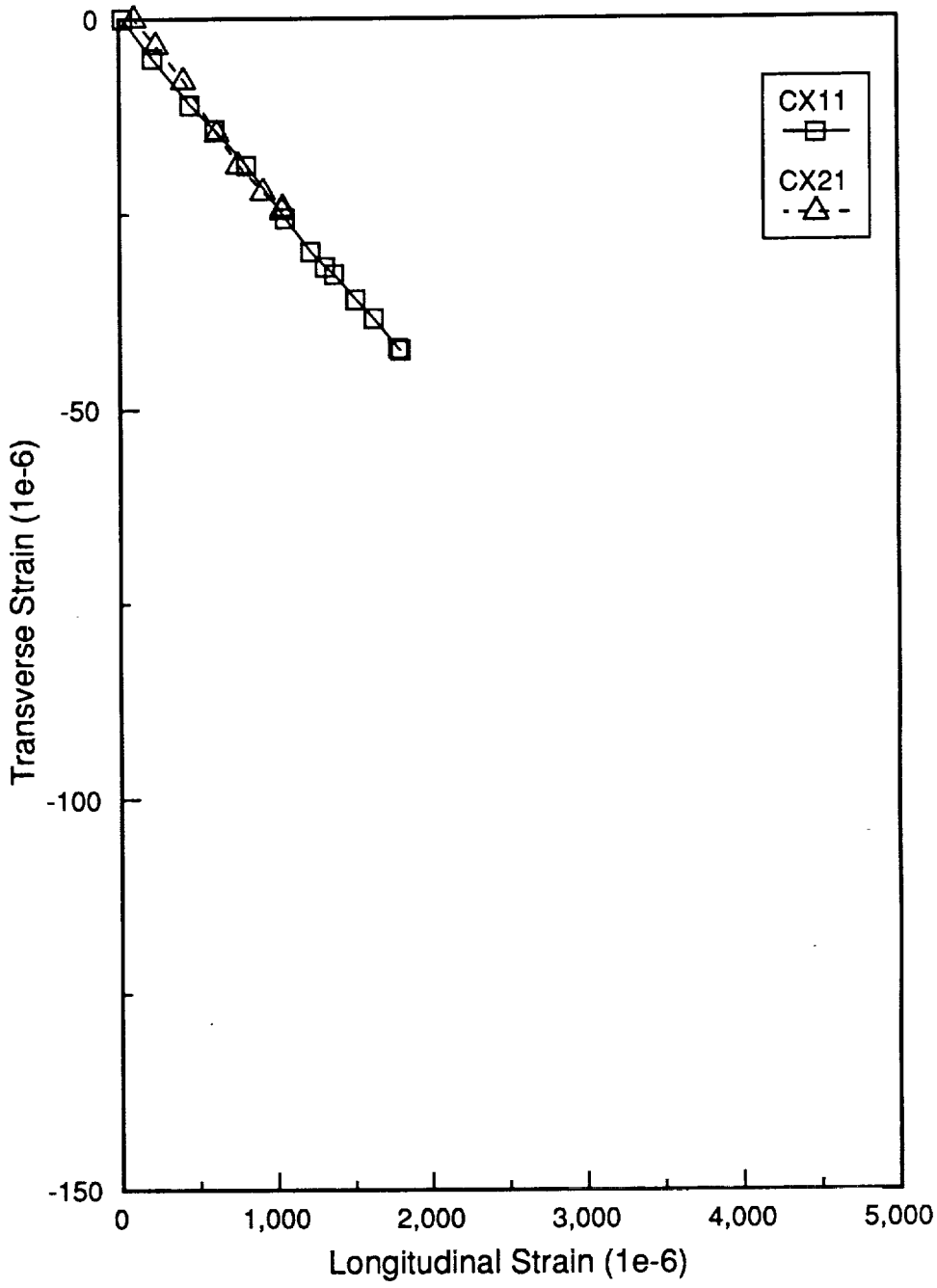

fig. 46. Relationship between ε_1 and ε_2 for coupons CX1 and CX2

Table 3. Mechanical Properties of LaRC-TPI Composite Coupons

Sample ID	Failure Stress (MPa)	Strain to Failure (%)	Average Modulus (GPa)	Average ν_{21}
AA1	37.6	0.393	9.58	0.032
AA2	28.9	0.318	9.17	0.030
AA average	**33.3**	**0.356**	**9.38**	**0.031**
AX1	31.0	0.316	9.90	0.036
AX2	30.1	0.345	8.82	0.032
AX average	**30.6**	**0.331**	**9.36**	**0.034**
CA1	12.0	0.101	12.1	0.037
CA2	12.9	0.120	10.8	0.032
CA average	**12.4**	**0.110**	**11.4**	**0.034**
CX1	11.3	0.181	6.27	0.024
CX2	8.61	0.105	8.13	0.026
CX average	**9.94**	**0.143**	**7.24**	**0.025**

6.2.4 Discussion of Test Results

The duplicate results for the each type of coupon were consistent. Overall, for all coupons, the failure strengths were lower than expected. Surprisingly, the amorphous matrix coupons had failure strengths about 2.5 times higher than those measured for the semicrystalline matrix coupons. Looking at the effect due to the fiber alone, the AS-4 coupons were higher in all cases. However, the strengths were only 10 to 20% higher than strengths for the counterpart XAS coupons. Similar behavior was noted in the trends of percent strain to failure. It was believed that the strengths were lower in the semicrystalline samples because in comparison to the amorphous matrix, the matrix was more brittle. There was also the possibility that the semicrystalline samples suffered from microcracking due to fabrication, thus weakening the matrix. Since the crystallinity in the coupons was maximized with the consolidation cycle used, the matrix may have been brittle resulting in reduced strength and increased likelihood of microcracking. However, since the cooling rates were rather slow, i.e.,

the laminate were not thermally shocked, microcracking seems to be less of a possibility. One note of curiosity, all transverse tensile coupons failed in the lower half of the coupon, between the terminal tabs and the portion in the grips.

Among the four amorphous coupons, the transverse modulus was fairly consistent. The average transverse modulus for the amorphous coupons was approximately 9.37 GPa. The modulus of the four semicrystalline coupons had some variability. For the semicrystalline/AS-4 coupons, the average modulus was around 11.4 GPa. This translated into a 15% increase in modulus over the amorphous/AS-4 samples. This could be expected based on the mechanical behavior of neat semicrystalline polymers. The disappointment occurred in the semicrystalline/XAS samples. The average modulus was around 7.24 GPa. This represented a 35% drop from the values reported for the semicrystalline/AS-4 coupons and 23% drop from the amorphous coupons. The modulus of the semicrystalline/XAS coupons should not have been lower than their amorphous counterparts. At this point, the cause for such a reduction in modulus can not be explained.

The literature offers very little comparative transverse tensile data for LaRC-TPI composites. The information that is available comes from samples generally made using other manufacturing techniques. Table 4 provides transverse tensile strength and modulus for several thermoplastic/graphite composites. Only one LaRC-TPI data point actually uses powder prepreg. None of the data points listed actually use the same form of LaRC-TPI presented in this study. The samples that were listed represent variations of LaRC-TPI. These data are of some comparative value because they provide a rough scale to measure the performance of the composites fabricated in this study. From Table 4, one can note that the transverse tensile data of the two entries for TPI varies widely. In comparison to these data points, the transverse tensile data for amorphous LaRC-TPI composites from this study is substantially closer to the data obtained by Johnston, et al (18). The modulus reported by both Johnston, et al. and Olson (26) was lower than that observed for the amorphous LaRC-TPI composites investigated in the present study. No semicrystalline LaRC-TPI data was available in the lit-

erature for comparison since this study produced the first semicrystalline LaRC-TPI composites. Instead, transverse tensile data is reported for PEEK composites produced using BASF powder prepregging (27). The two types of PEEK/G30-500 composites listed in Table 4 have transverse tensile strengths that are roughly 5 times the value seen for the semicrystalline LaRC-TPI composites studied here. Interestingly, the transverse modulus for these composites is around 9.6 GPa whereas the semicrystalline LaRC-TPI/AS-4 composites studied here have a transverse modulus around 11.4 GPa. In addition, in comparing the strain-to-failure for the PEEK/composites to either semicrystalline LaRC-TPI laminate, it can be noted that the strain-to-failure for the semicrystalline LaRC composites is 7 times smaller than that reported for the PEEK composites, indicating that semicrystalline LaRC-TPI is substantially more brittle than PEEK.

Table 4. Transverse Mechanical Properties for Other Thermoplastic/Graphite Composites

Type of Composite	Process	σ_2 (MPa)	E_2 (GPa)	Strain to Failure (%)
LaRC-TPI(1:1)/2.5%PISO$_2$ AS-4 (18)	Slurry	33.1	8.2	0.48
New TPI/IM8 (26)	Powder	61.4	7.6	----
150 PEEK/G30-500 (27)	Powder	63.4	9.6	0.70
450 PEEK/G30-500 (27)	Powder	69.6	9.9	0.71

The next chapter focuses on the results of a microstructural investigation of the failed transverse tensile coupons.

7.0 Microscopic Evaluation

As was discussed in the last chapter, all the samples had low transverse tensile strengths compared to other thermoplastic/graphite composites. Given the observed mechanical properties, this chapter correlates the microstructural characteristics with the macroscopic behavior. The microstructural analysis used both optical and scanning electron microscopy.

7.1 Scanning Electron Microscopy

7.1.1 Sample Preparation

A fracture surface from each transverse tensile coupon was mounted onto an aluminum SEM stub. Each stub was coated with a 140Å layer of gold. All stubs were analyzed u ıg a Cambridge Stereoscan 200 Scanning Electron Microscope.

7.1.2 Results

7.1.2.1 Amorphous/AS-4 Coupons

In ch. 5, the amorphous form of the matrix was observed to adhere poorly to the AS-4 fibers. Yet from ch. 6, it was seen that the transverse tensile results for the amorphous/AS-4 coupons had the highest transverse strengths observed in this study. An electron micrograph of a fractured transverse tensile coupon can be seen in fig. 47. From the micrograph, it appears that the fiber/matrix adhesion was still rather poor. Comparing fig. 47 to fig. 25, one can see that the fracture surface of the transverse tensile coupon exhibits a greater amount of adhesion than its predecessor. However, the adhesion in either sample is poorer than desired.

7.1.2.2 Amorphous/XAS Coupons

Based on the micrographs seen in ch. 5, the amorphous/XAS coupons were expected to have improved mechanical properties since they appeared to have a greater amount of fiber/matrix adhesion relative to the amorphous/AS-4 coupons. The transverse tensile data indicated that the properties of the amorphous/XAS coupons were roughly equivalent to the properties observed with the amorphous/AS-4 coupons. The fractured surfaces of the amorphous/XAS coupons can be seen in fig. 48. These coupons appeared to exhibit greater amounts of fiber/matrix adhesion than the amorphous/AS-4 coupons seen in fig. 47. Relative to the fractured surfaces seen in fig. 33, the amorphous/XAS transverse tensile coupons exhibited roughly the same amount fiber/matrix adhesion.

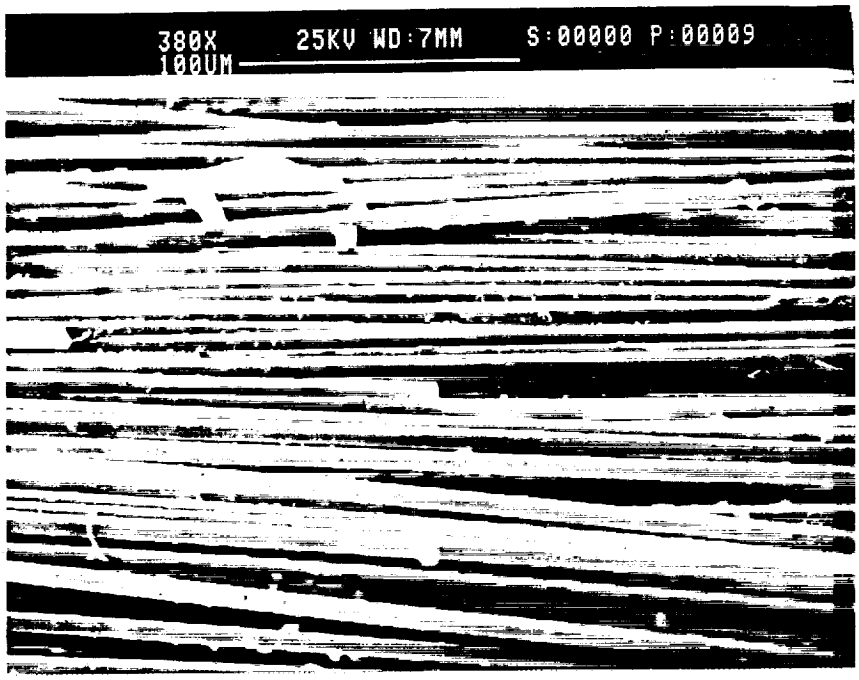

A)

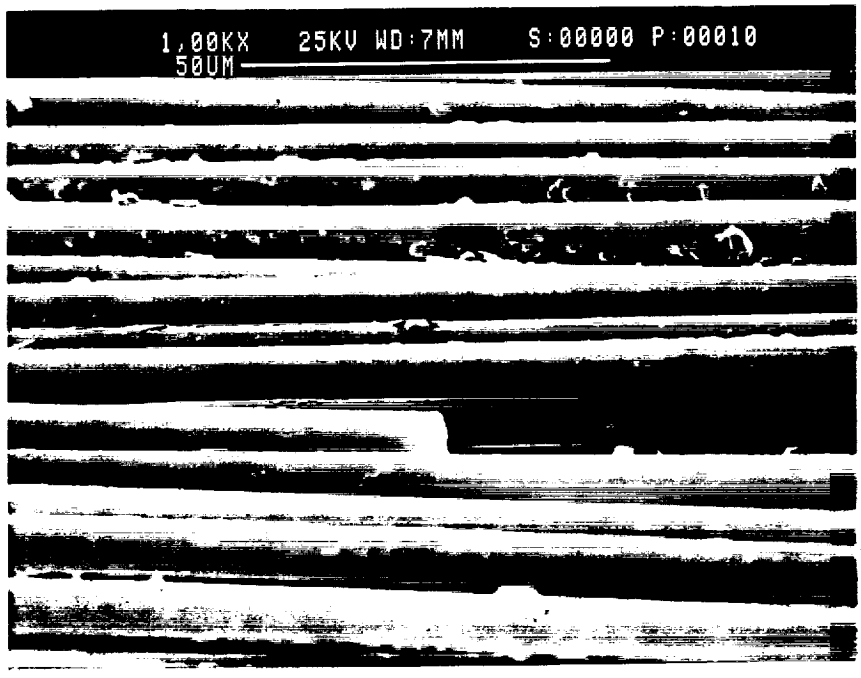

B)

fig. 47. **Micrographs of an Amorphous/AS-4 Transverse Tensile Coupon Tested to Failure:** A) Low and B) High Magnification

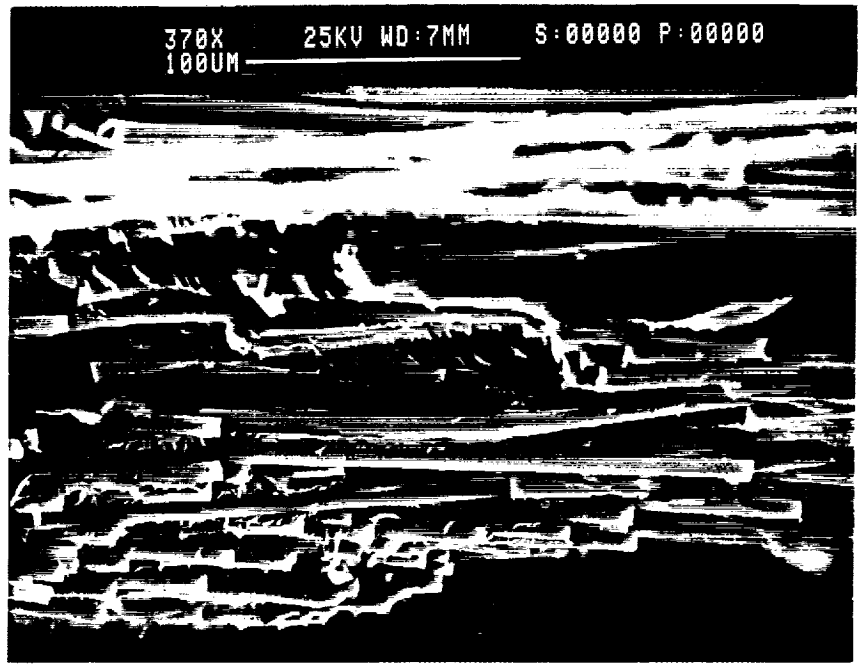

A)

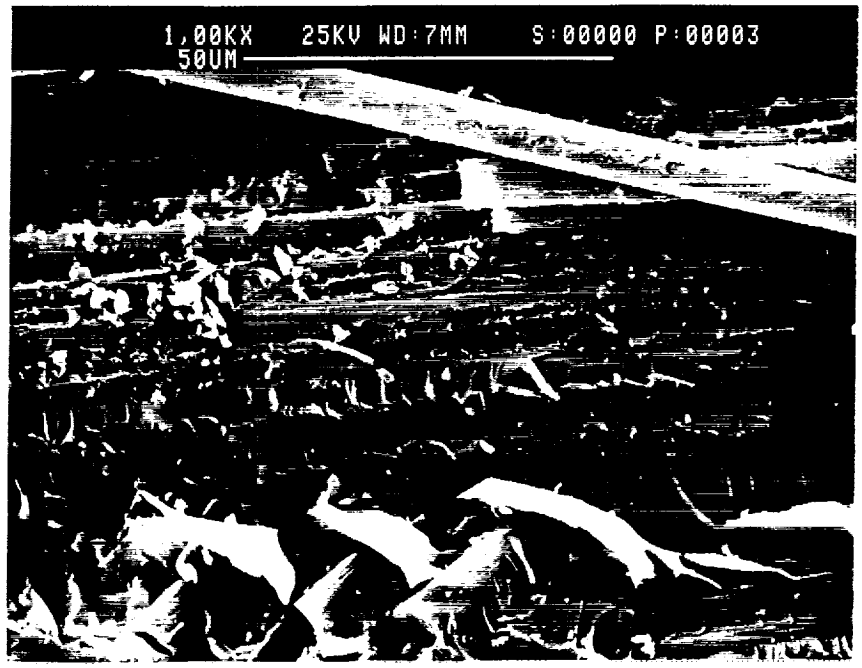

B)

fig. 48. **Micrographs of an Amorphous/XAS Transverse Tensile Coupon Tested to Failure:** A) Low and B) High Magnification

7.1.2.3 *Semicrystalline/AS-4 Coupons*

From the micrographs in ch. 5, the semicrystalline/AS-4 composites appeared to have greatly improved adhesion. However, the transverse tensile data for this sample set showed a marked decrease in the transverse tensile strength and a modest improvement in transverse modulus. An example of a low and a high magnification electron micrograph from a semicrystalline/AS-4 coupon is given in fig. 49. In both micrographs, a significant amount of the matrix appeared to adhere to the fibers. Comparing fig. 49 to fig. 35, two samples seem to be similar in terms of the amount of fiber/matrix adhesion present. The major difference was that fig. 35 illustrated a coarser texture to the failed matrix than did fig. 49. The coarser texture may be attributed to microcracking, due to the severity of the cooling phase in the earlier version of the semicrystalline lamination cycle.

7.1.2.4 *Semicrystalline/XAS Coupons*

Of all the transverse tensile coupons tested, the semicrystalline/XAS coupons had the poorest mechanical properties. There are no previous micrographs to compare with this sample. Extrapolating on the changes in the fiber/matrix adhesion caused by altering the fiber alone and the matrix alone, it was hoped that this combination would prove to have the best properties. It was a great surprise when this did not occur. Using electron microscopy, it was hoped that this mystery could be explained. Two electron micrographs of the fractured semicrystalline/XAS transverse tensile coupons can be seen in fig. 50. As one can note in both micrographs, the fiber/matrix adhesion is very poor. The fiber/matrix adhesion is almost as poor as the adhesion observed in the early amorphous/AS-4 small unidirectional laminates. In addition to extremely poor adhesion, these samples appeared to be deficient in terms of matrix. This was evidenced by areas where the fibers were partially coated. If the fibers were not completely wetted out during consolidation, that could partially explain the

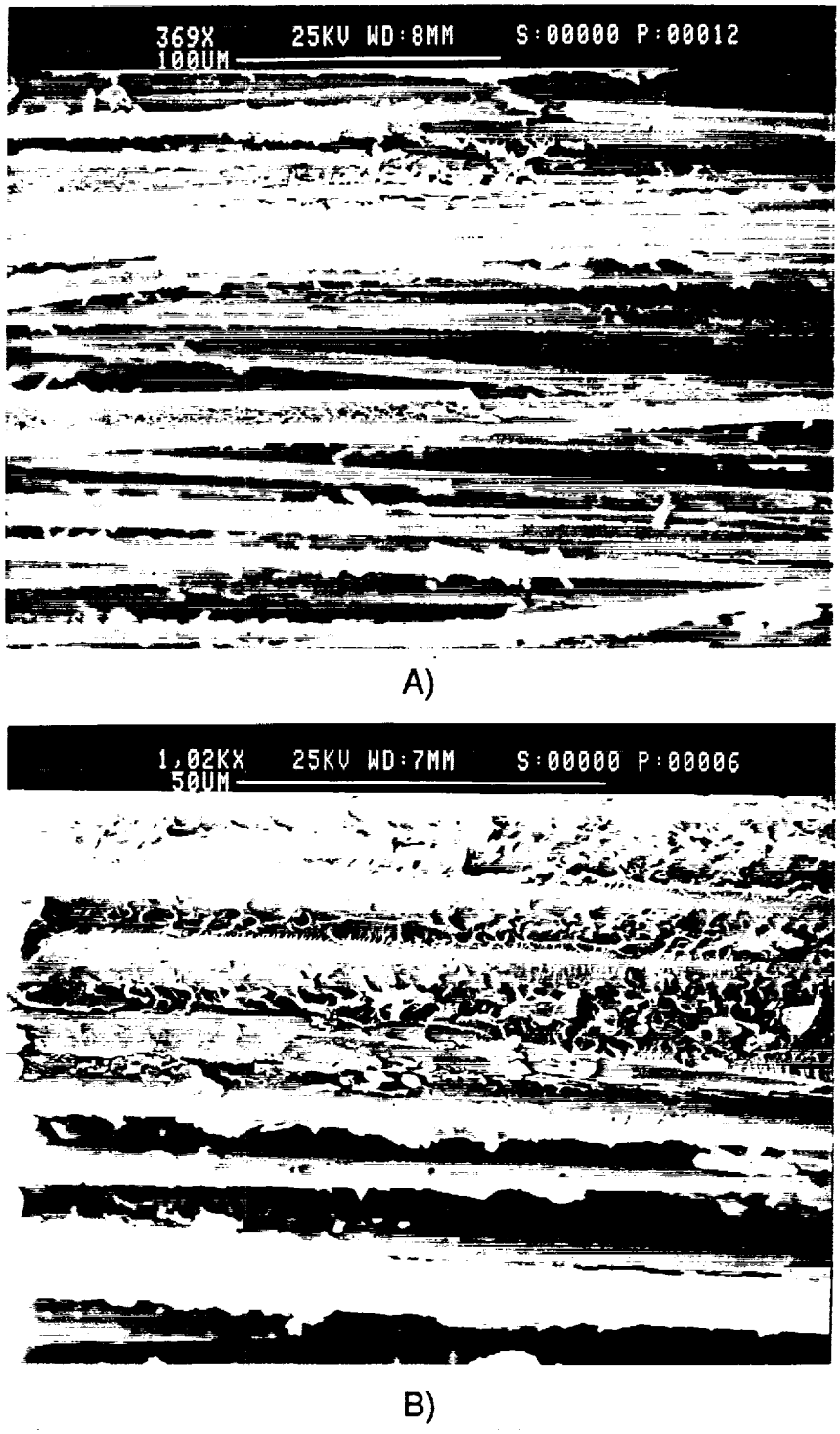

fig. 49. Micrographs of a Semicrystalline/AS-4 Transverse Tensile Coupon Tested to Failure: A) Low and B) High Magnification

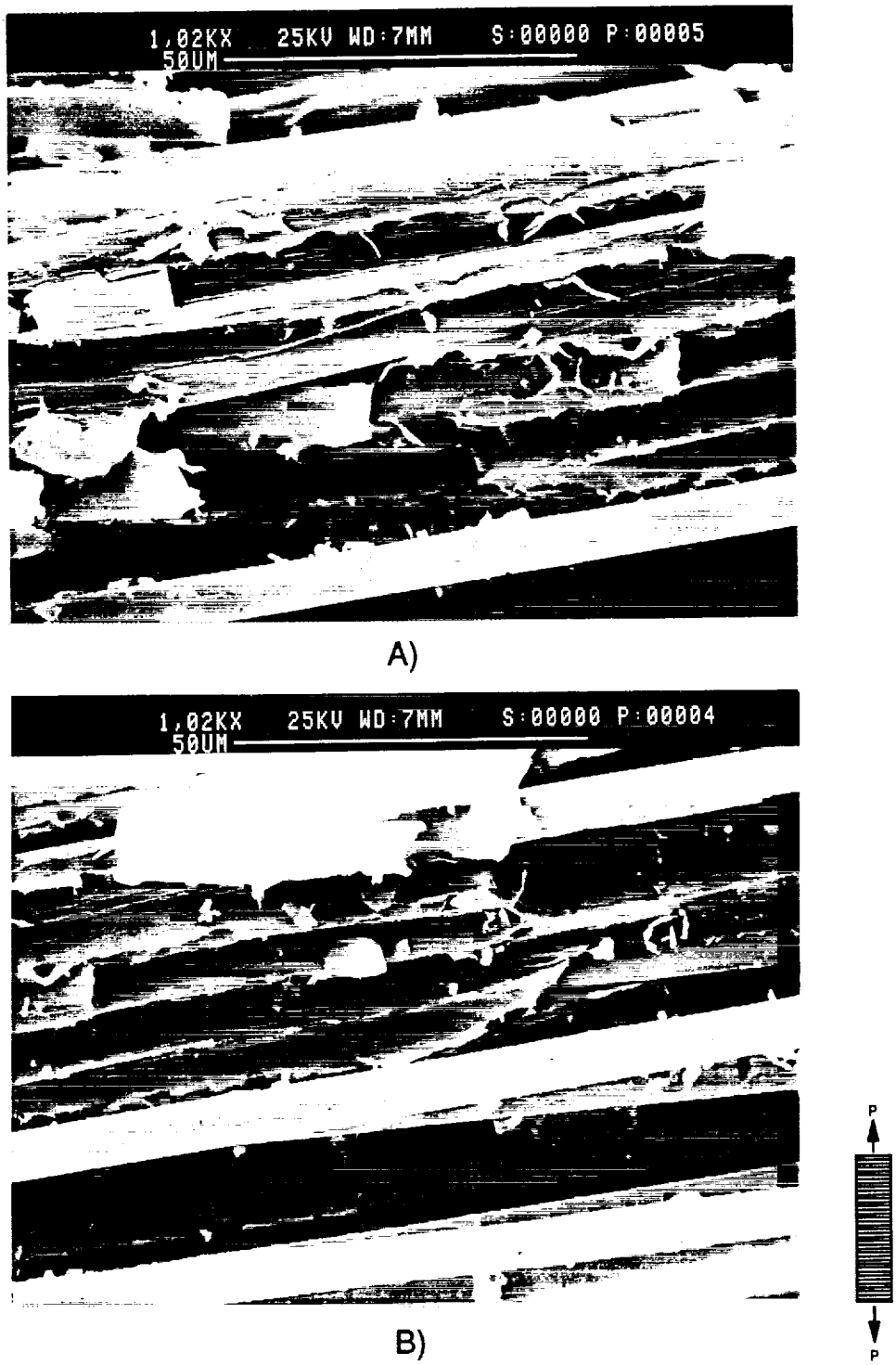

fig. 50. Micrographs of a Semicrystalline/XAS Transverse Tensile Coupon Tested to Failure: A) Showing Poor Adhesion and B) Poor Wetting

poor properties as well as the poor fiber/matrix bonding. This will be investigated further during the optical microscopy phase of the investigation.

7.2 Optical Microscopy

Optical microscopy has a dual purpose in this study. First, by using optical microscopy, it is possible to assess the degree of consolidation of the laminates. Recalling from ch. 6, the ultrasonic evaluation of the laminates revealed that the laminates might have been poorly consolidated. Second, in addition to determining the degree of consolidation, optical microscopy will hopefully answer the questions raised by the poor mechanical properties observed in the semicrystalline composite coupons.

7.2.1 Sample Preparation

The samples used in optical microscopy consisted of tested and untested pieces from each laminate. These samples were embedded in epoxy. After embedding, the samples were rough polished using 240, 320, 400, and 600 grit silicon carbide disks on an Ecomet 3 grinder/polisher by Buehler. Final polishing was completed progressively using 3μm, 1μm, and 0.3μm alumina suspensions with Buehler Texmet polishing cloths on the grinder/polisher. At each step in the polishing process, the samples were polished with the smallest number of cycles so that polish induced pullout could be minimized. Each sample was ultrasonically cleaned in tap water before proceeding to the next polishing grit. All samples were examined and photographed on a Nikon Epiphot Optical Microscope. All photographs shown were taken at a magnification of 200X.

7.2.2 Results

7.2.2.1 *Amorphous/AS-4 Coupons*

Optical micrographs from various portions of the amorphous/AS-4 laminate are given in fig. 51. Part A of fig. 51 comes from an untested section of one the laminates, while part B is a representative section from a test coupon near the failure zone. In part A, it can be seen that the sample is consolidated fairly well. There are isolated matrix-rich pockets distributed throughout the coupon. In the middle right-hand portion of the micrograph, one can see that there are matrix-poorer regions. Part B is taken from sample AA1. Like the untested piece, this coupon also appears to be well consolidated. This micrograph shows very small pores widely scattered throughout the coupon. Many of the pores appear to be smaller than the fiber diameter. At the top center of the micrograph, one can note the matrix rich vein running across the laminate. This vein appears to marked by matrix pullout, perhaps induced by polishing, or by cracking. These micrographs are representative sampling of the microstructural behavior noted for the amorphous/AS-4 family.

7.2.2.2 *Amorphous/XAS Coupons*

As in the previous cases, part A of fig. 52 refers to an untested section of the laminate and part B comes from coupon AX1. Like the amorphous/AS-4 laminate, the amorphous/XAS laminate appears to be well consolidated. Again there are small areas where the matrix appears to be missing. A few of these areas, namely the vertical streak at the right hand of the picture of part A, appear to be devoid of matrix. In reality, these regions are areas that have not been completely polished. The dark regions that appear between fibers are actually matrix-poor or matrix-devoid regions. A good example of this occurs in the upper central

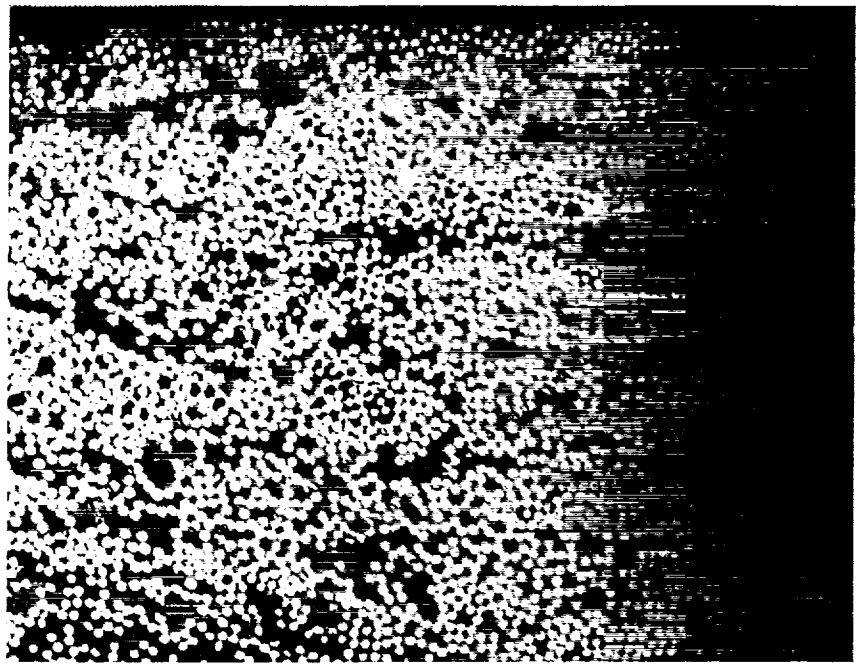

A)

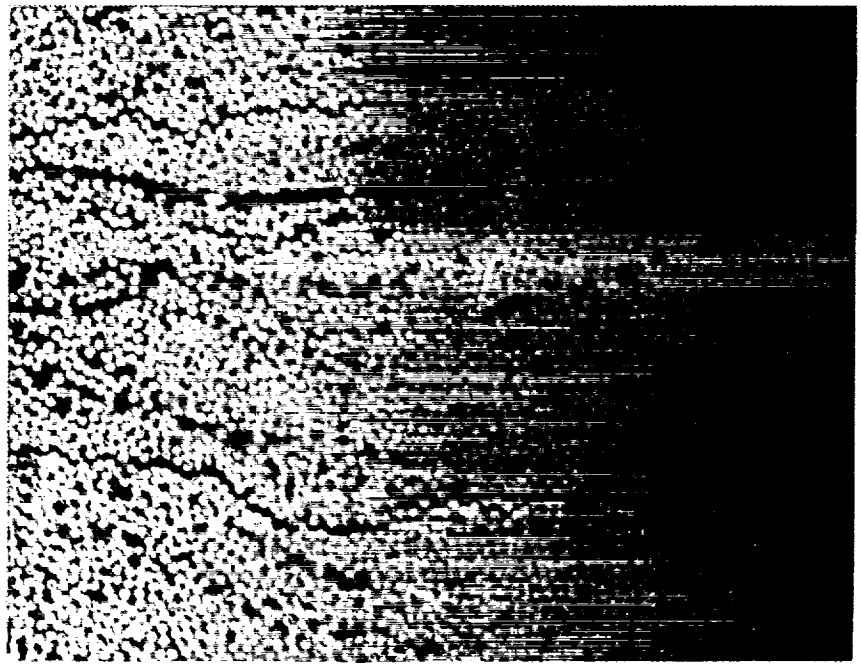

B)

fig. 51. Optical Micrographs of the Amorphous/AS-4 Laminate: Taken from A) an Undeformed Coupon and B) Failed Coupon AA1

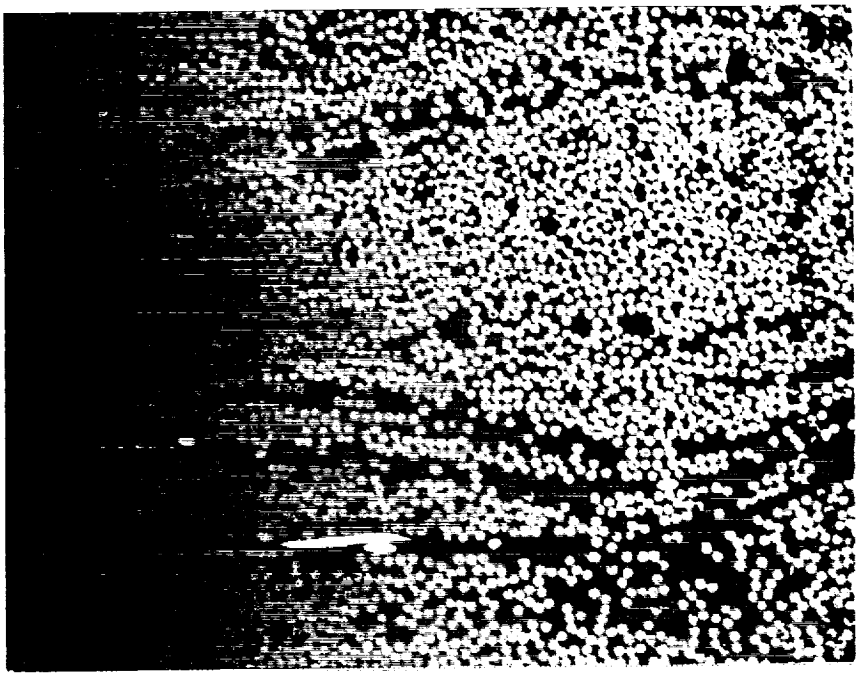

A)

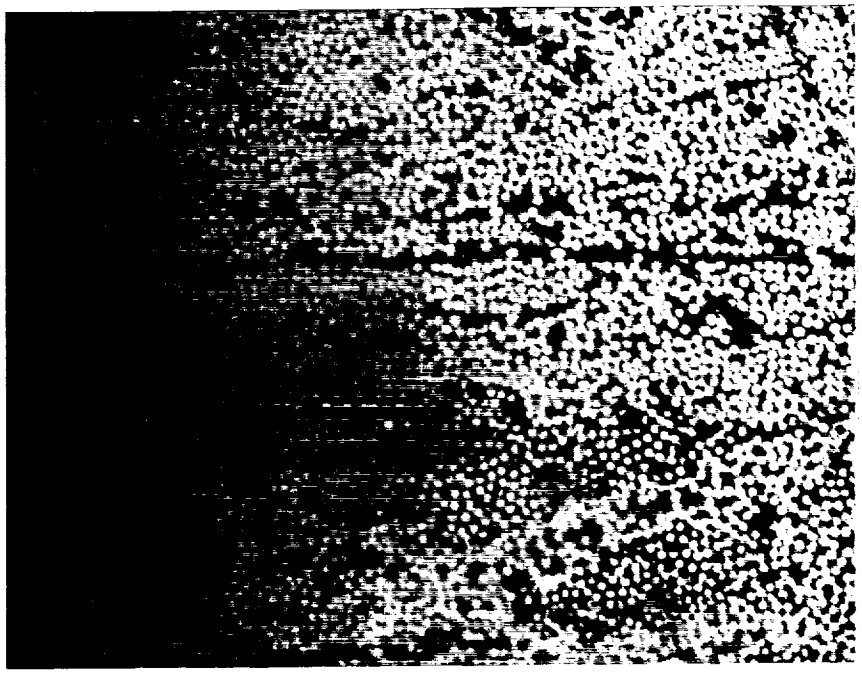

B)

fig. 52. Optical Micrographs of the Amorphous/XAS Laminate: Taken from A) an Undeformed Coupon and B) Failed Coupon AX1

portion of the picture. In addition, one should note the horizontal veins at the lower central portion of the micrograph. These veins are matrix-rich regions. The veins seem to denote the remnants of the individual layers in the laminate. In part B of fig. 52, the presence of matrix-poor regions dotted with matrix-devoid regions in the lower central portion of the micrograph can be noted. Again, the section taken from coupon AX1 appears to be fairly well consolidated.

7.2.2.3 Semicrystalline/AS-4 Coupon

Unlike the amorphous coupons, the semicrystalline/AS-4 coupons appear to be consolidated to a lesser extent. Part A of fig. 53 comes from an untested section of the semicrystalline laminate and part B is a section from coupon CA1. Not only does part A appear to be consolidated to a lesser extent, it also has large regions that are matrix-poor. These areas appear to be large voids. Apparently, these matrix-poor regions turn into voids due to matrix pullout during polishing. The matrix poor regions, prior to pullout, appeared as the regions seen in the lower and center sections of part B.

7.2.2.4 Semicrystalline/XAS Coupons

The semicrystalline/XAS coupons had the poorest mechanical properties of all the coupons tested. Recalling fig. 50, these samples also had extremely poor fiber/matrix adhesion. From fig. 50, it appeared that matrix did not completely wet out the fibers. Optical microscopy revealed that there were numerous matrix poor areas present in several pieces of the CX coupons that were examined. Examples of representative areas of the microstructure for the semicrystalline/XAS laminate are given in fig. 54. Part A of fig. 54 shows an untested section of the laminate and part B shows at a piece taken from coupon CX2 near the failure zone. The untested sample appears to be poorly consolidated. There are intermittent area where

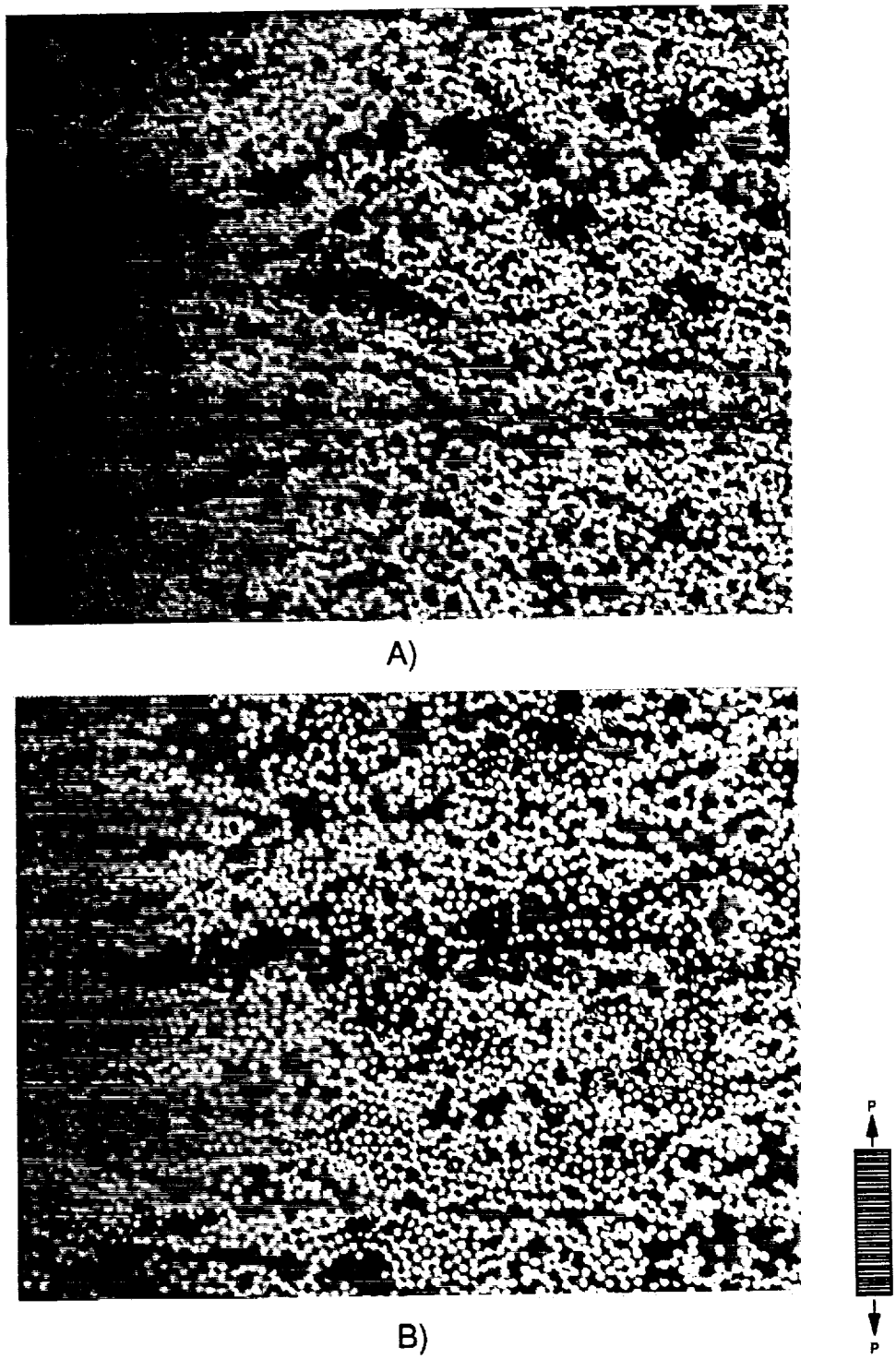

fig. 53. **Optical Micrographs of the Semicrystalline/AS-4 Laminate:** Taken from A) an Undeformed Coupon and B) Failed Coupon CA1

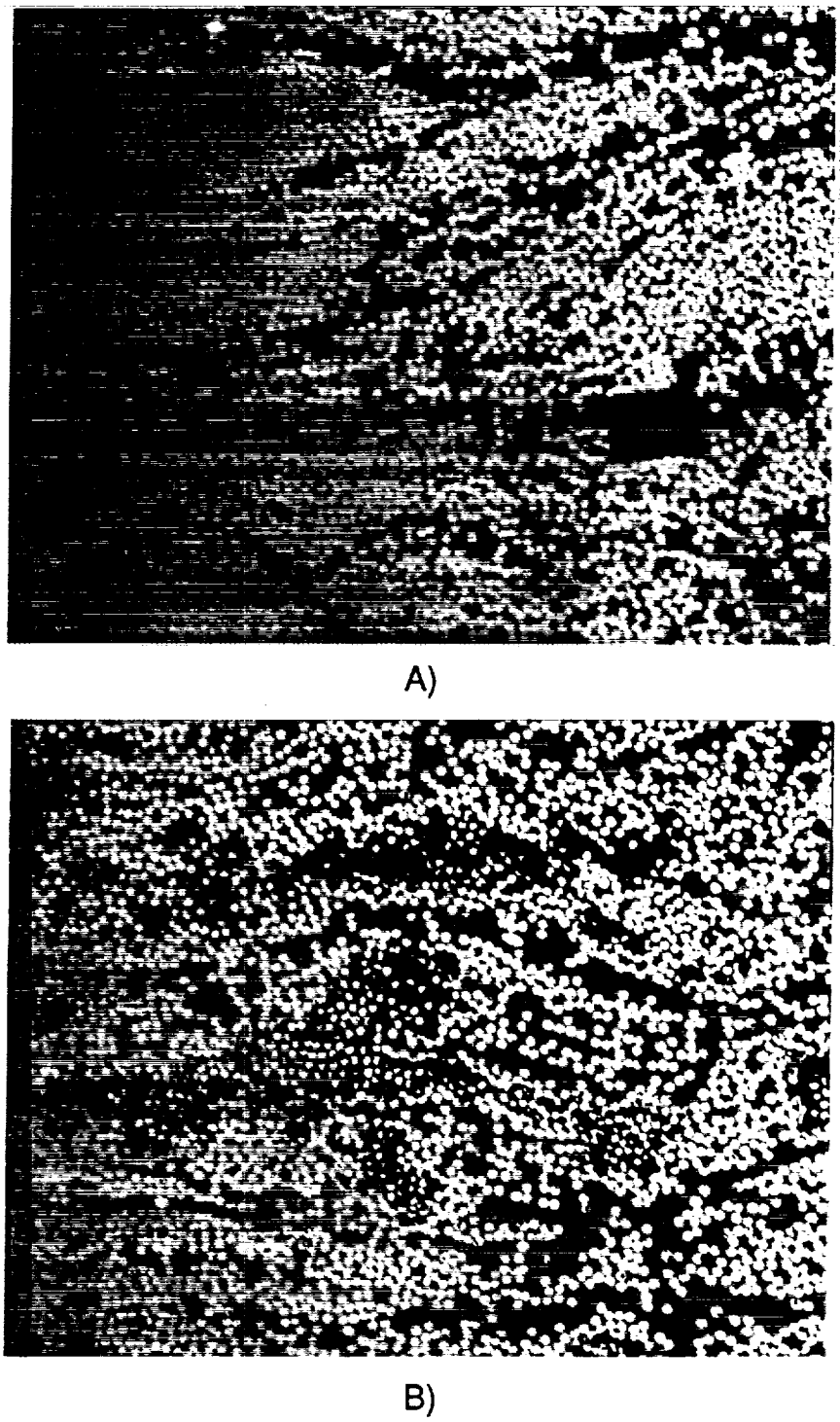

fig. 54. Optical Micrographs of the Semicrystalline/XAS Laminate: Taken from A) an Undeformed Coupon and B) Failed Coupon CX2

the matrix is absent or less abundant. An example of a matrix-poor area can be seen in the upper left hand corner of part B. This matrix-poor region is associated with a region of densely packed fibers. Previous matrix-poor areas have not always been associated with regions of densely packed fibers, although such an area would appear to be a likely candidate for this to occur. The micrograph in part B illustrates the widespread problem of poor matrix infiltration apparent in the semicrystalline/XAS samples. The microscopic behavior observed here and in fig. 50 seems to correlate well with the poor mechanical performance of these samples seen in ch. 6.

7.2.3 Discussion

The degree of adhesion observed from the micrographs for the amorphous/AS-4, amorphous/XAS, and semicrystalline/AS-4 coupons were consistent with the corresponding electron micrographs seen in ch. 5. The microstructure from optical microscopy of both amorphous behavior was consistent with the observed macroscopic behavior from the transverse tensile testing. The microstructure of the semicrystalline/AS-4 composites had scattered areas that were matrix poor or matrix devoid. This did not appear to impact the interfacial adhesion but that may partially account for the poor transverse strengths observed. For the case of the semicrystalline/XAS coupons, the same phenomena was observed but to a greater extent than the semicrystalline/AS-4 case. The greater degree of matrix poor regions did correlate well with the mechanical properties observed for this family of samples.

In terms of consolidation, it appears that the amorphous laminates were fairly well consolidated, contrary to the C-scan information. For the semicrystalline laminates, the laminates were not as well consolidated. Matrix-poor regions existed in both types laminates.

8.0 Semicrystalline to Amorphous Transformation

From ch. 6, it was observed that the amorphous composites had the best mechanical performance. In ch. 7, the semicrystalline/AS-4 composites appeared to have better adhesion compared to its amorphous counterpart whereas the semicrystalline/XAS composites appeared to have the poorer adhesion compared to its amorphous counterpart. From the optical micrographs in ch. 7, it appeared that the fibers were incompletely wetted out in the semicrystalline/XAS composites, thus at least partially accounting for the poor adhesion and the poor mechanical response observed previously. Since this laminate was poorer in quality than other laminates, a fair assessment of the influence of crystallinity on the fiber/matrix adhesion in LaRC-TPI composites could not be made. In an attempt to gain more information on the influence of the form of the matrix on adhesion, the remaining semicrystalline transverse tensile coupons were transformed to amorphous transverse tensile coupons. This experiment was performed to see how the fiber/matrix adhesion and the mechanical properties changed as a result of the transformation. It was anticipated that the mechanical response and adhesion would return to the values previously observed for the amorphous composites.

8.1 Sample Preparation

In an attempt to note the changes in the fiber/matrix adhesion due to altering the form of the matrix, the remaining transverse tensile coupons were only given a thermal treatment during the transformation. No consolidation pressure was applied during the transformation. This was done to minimize the differences between the semicrystalline coupons tested previously and the transformed semicrystalline to amorphous coupons. Based on fig. 50, it appeared that the wetting may improve if a coupon was reconsolidated during the transformation, thus altering the comparison.

8.1.1 Sample Geometry

One 1.9x7.5 cm coupon remained from each semicrystalline laminate. To preserve the number of specimens, each coupon was cut in half. The average dimensions of each half coupon is given in Table 5.

Table 5. Physical Properties of Transformed Composite Coupons

Sample ID	Length (cm)	Width (cm)	Thickness (mm)
CAT1	3.8	1.9	0.476
CAT2	3.8	1.9	0.490
CXT1	3.8	1.9	0.507
CXT2	3.8	1.9	0.513

8.1.2 Mold Preparation

Although an additional consolidation pressure was not to be applied to the coupons, the samples needed to be constrained to maintain an even cross sectional area. The coupons were restrained using a 7.5x7.5 cm matched metal mold. The interior of the mold was shimmed to fit the coupon dimensions using 18 layers of 0.03 mm Upilex film. The 18 layer shim was cut in the shape of a T, as seen in fig. 55. The mold and two 7.5x7.5 cm pieces of Upilex film were coated with Frekote 33 release agent. The mold was assembled by

- laying a sheet of release coated Upilex film over the base of the mold
- placing the T-shaped shim on top of the release coated Upilex film
- fitting a piece of the semicrystalline/AS-4 and XAS coupon into the mold and
- covering the components with the second layer of release coated Upilex film.

The plunger was laid into the well of the mold. It was then placed into an Instron 3116 Environmental Chamber. Two 11 kg weights were placed on top of the plunger to constrain geometric variations through-the-thickness.

8.1.3 Thermal Treatment

The semicrystalline composite samples were transformed using the amorphous thermal treatment used in laminate production. Specifically, the thermal treatment consisted of

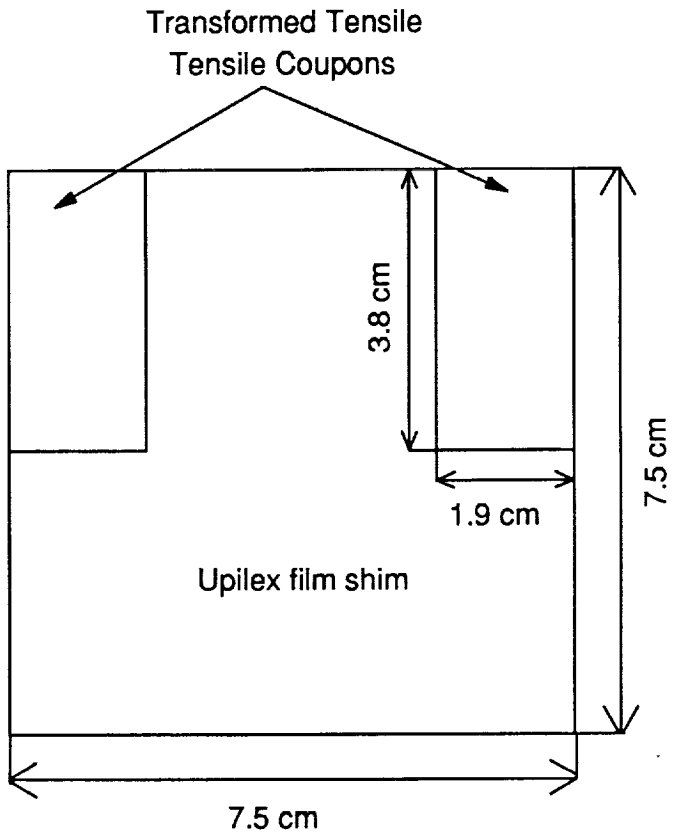

fig. 55. Schematic of Mold Setup used for the Transformed Coupons

- ramping the temperature from 22.2°C to 371°C at at rate of 7.5°C/min.
- holding the temperature at 371°C for an hour
- cooling the samples to 200°C at a rate of 2.5°C/min.

Once the samples were below 200°C, the samples were removed from the mold.

8.1.4 Strain Gauging

Each half coupon was prepared for strain gauging based on the recommendations that accompanied the Micro-Measurements M-Bond 200 Adhesive Kit. The strain gauges used in these tests were CEA-06-062WT-120 0°/90° rosettes from Micro-Measurements. Like the early test coupons, the gauges were placed back to back in the center of each half coupon. Once the gauges were bonded to the half coupon, the lead wires were soldered to the terminal tabs. Upon completion, the samples were kept in a desiccator prior to testing.

8.2 Mechanical Testing

8.2.1 Procedure

The testing procedure listed in section 6.2.2 was employed for the semicrystalline half coupons. The procedure deviated in only one area, namely the geometry of the sample in the testing machine. In this case, the gauge length was approximately 1.9 cm.

8.2.2 Results

8.2.2.1 Transformed/AS-4

Three tests were performed on the two transformed tensile coupons. The first transformed coupon, CAT1, was tested twice. The first test was halted because of slippage in the grips. After adjusting the grips, the coupon was tested again. The second tested ended when the coupon failed at 21.4 MPa. The second transformed coupon, or CAT2, was only tested once and it failed at a stress of 29.9 MPa. The relation of σ_2 vs. ε_2 for CAT1 and CAT2 can be seen in fig. 56. From the slope of this relation, the transverse modulus for CAT1 and CAT2 were 8.60 and 9.45 GPa, respectively. By plotting the relation of ε_1 vs. ε_2, the transverse Poisson's relation, ν_{21}, was obtained. The relation between ε_1 and ε_2 for CAT1 and CAT2 can be seen in fig. 57. The transverse Poisson's ratio for CAT1 and CAT2 are given in Table 6.

8.2.2.2 Transformed/XAS

Again, three tests were performed on the two transformed coupon. The first transformed XAS coupon, or CXT1, was tested once. The first test was halted due to slippage in the grips. While the grips were being tightened, the grip assemblage twisted causing the coupon to fail prematurely. The second transformed XAS coupon, or CXT2, was tested once and it failed at a stress of 43.5 MPa. The relation of σ_2 vs. ε_2 for CXT2 can be seen in fig. 58. The transverse modulus for this sample was 10.0 GPa. The relation of ε_1 vs. ε_2 is given in fig. 59. From this relation, the transverse Poisson's ratio for CXT2 coupon is given in Table 6.

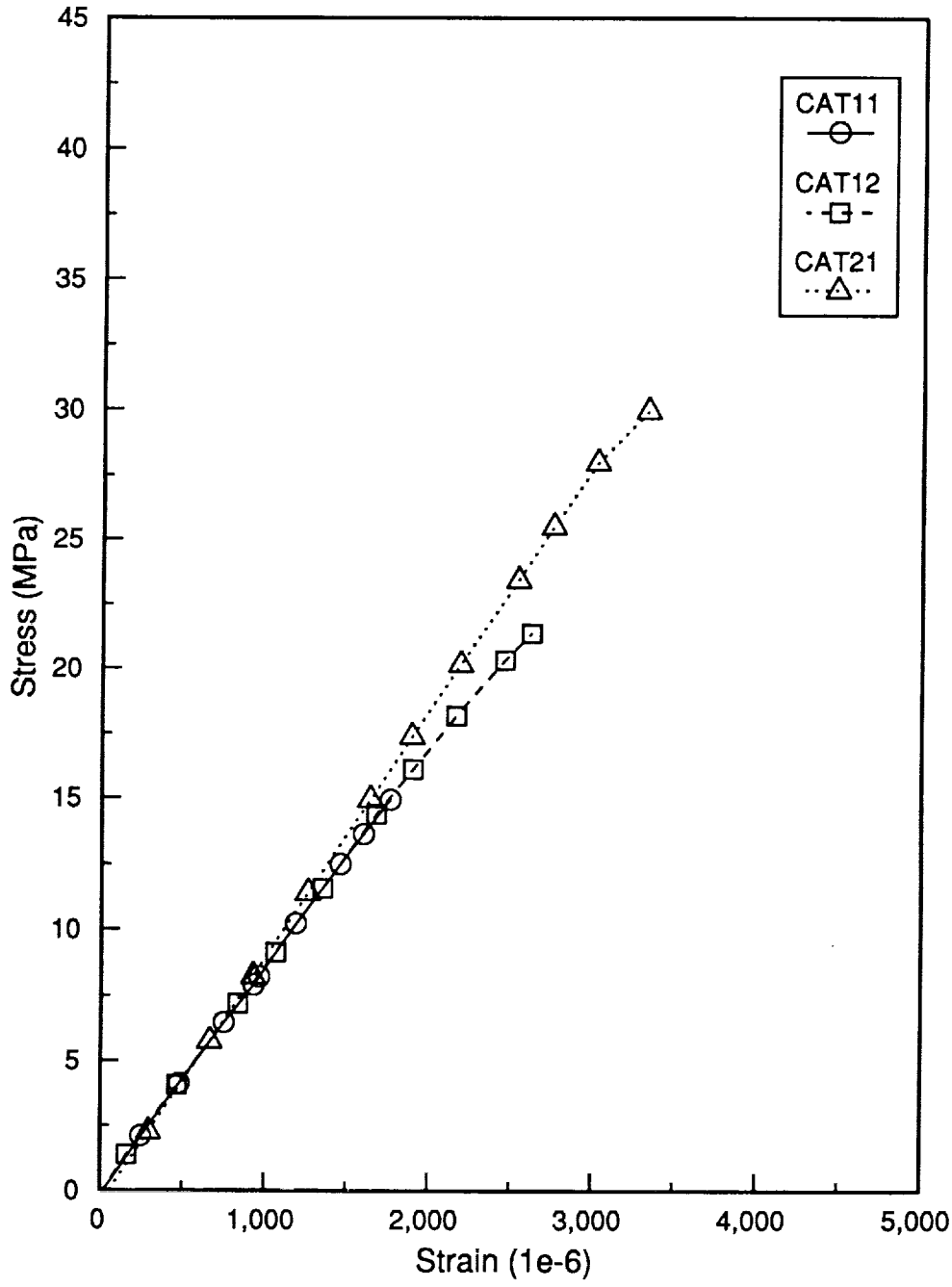

fig. 56. Relationship between σ_2 and ε_2 for coupons CAT1 and CAT2

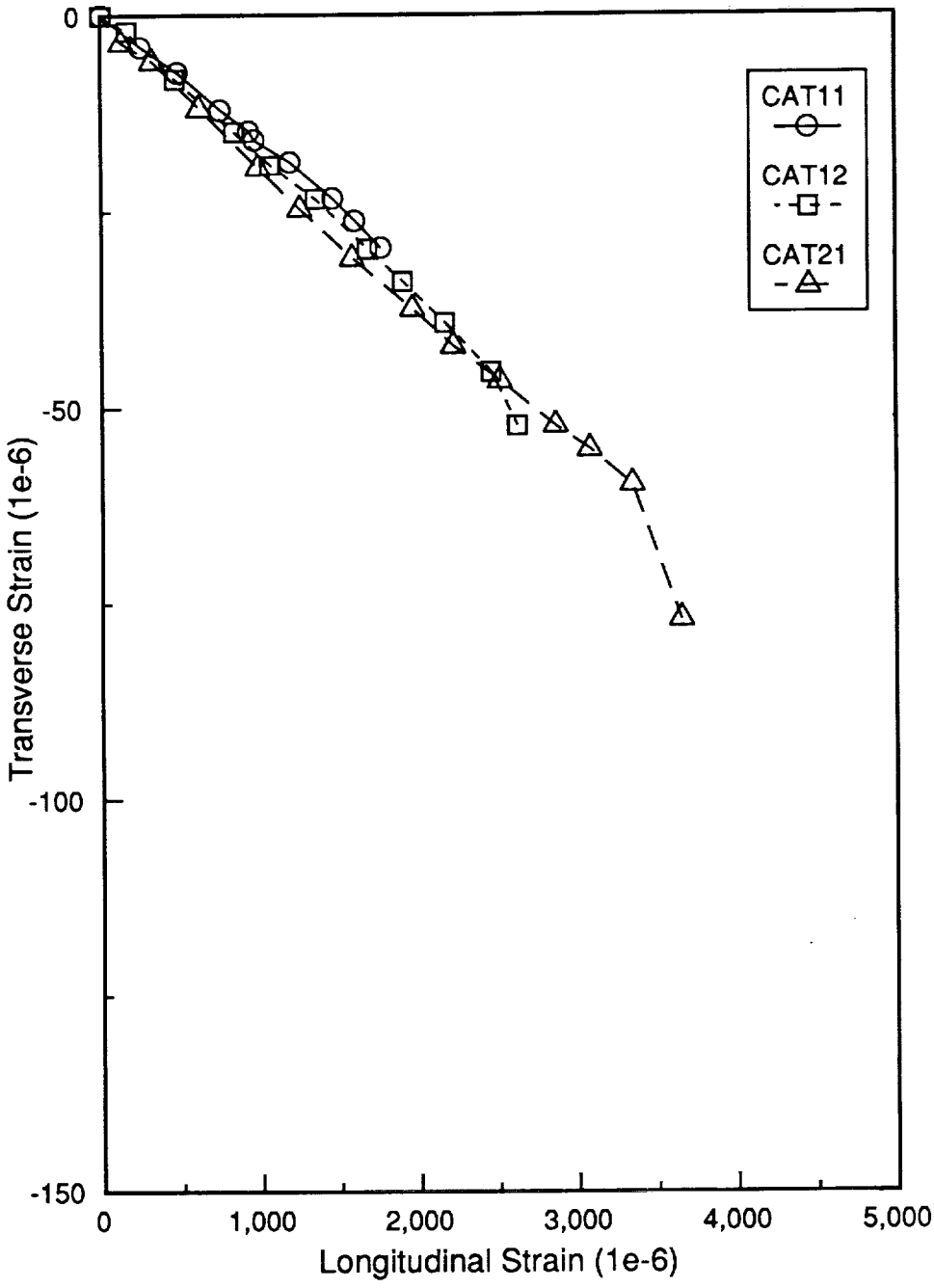

fig. 57. Relationship between ε_1 and ε_2 for coupons CAT1 and CAT2

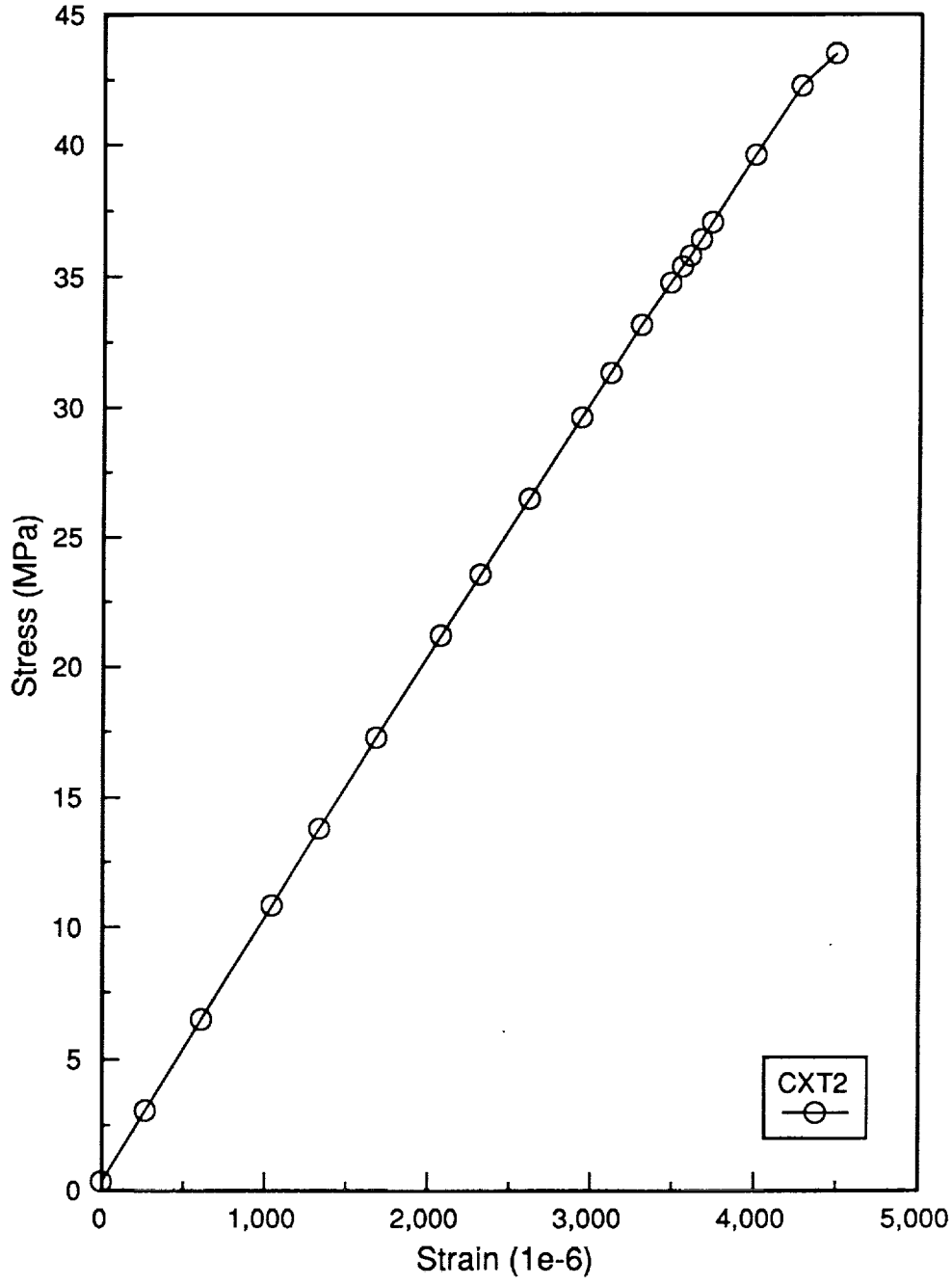

fig. 58. Relationship between σ_2 and ε_2 for coupon CXT2

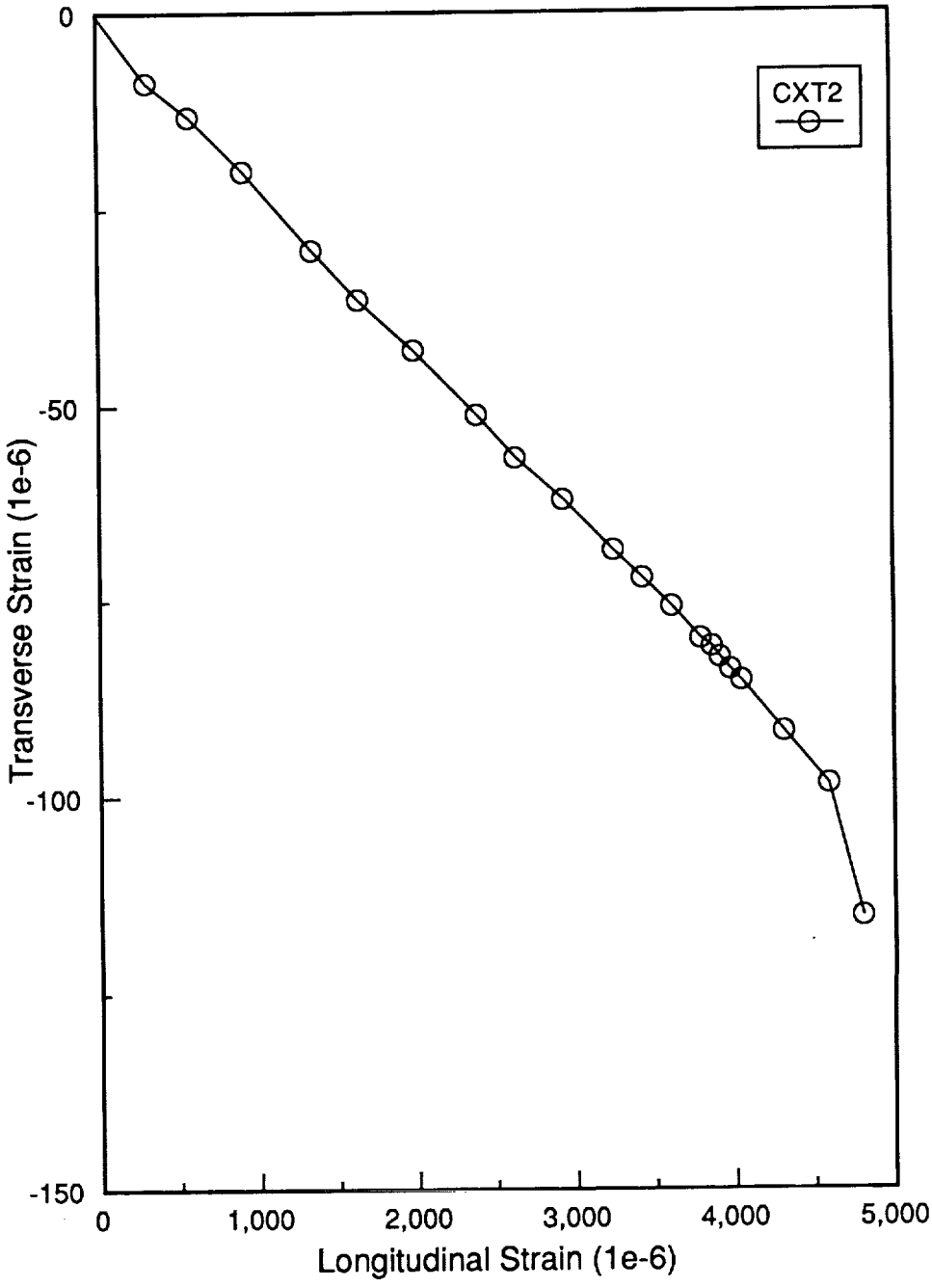

fig. 59. Relationship between ε_1 and ε_2 for coupons CXT2

8.2.3 Discussion of Mechanical Test Results

The mechanical results for the transformed/AS-4 and XAS transverse tensile coupons are summarized in Table 6. Comparing the results seen in Table 6 to the results seen in Table 3, differences are observed. The transformed/AS-4 coupons, namely CAT1 and CAT2 coupons, had average transverse failure strengths that were approximately 2 times greater than those observed for the semicrystalline/AS-4, or CA, coupons. Compared to the amorphous/AS-4, or AA, coupons, the transformed/AS-4 coupons had transverse failure strengths that were about 1.3 times lower than the amorphous/AS-4 average. In terms of the transverse modulus, the average for the transformed coupons was lower than the average transverse modulus of the semicrystalline and amorphous/AS-4 coupons. Compared to the two original AS-4 groups, the transformed/AS-4 coupons more closely resembled the results obtained for the amorphous/AS-4 coupons. Looking at the results for the transformed/XAS, or CXT, coupon, the strength showed considerable improvement when compared to the semicrystalline/XAS, or CX, and the amorphous/XAS, or AX, coupons. The transformed/XAS coupon had a failure strength about 1.4 times larger than the average amorphous/XAS failure strength and about 4.3 times larger than the average semicrystalline/XAS failure strength. The transverse modulus for the transformed/XAS coupon was higher than the modulus observed for the semicrystalline/XAS and for the amorphous/XAS coupons. Since only one transformed/XAS coupons was evaluated, the absolute magnitude of the data can not be relied upon, thus making the results from the transformed/XAS coupon less dramatic.

Table 6. Mechanical Properties of Transformed Composite Coupons

Sample ID	Failure Stress (MPa)	Strain to Failure (%)	Average Modulus (GPa)	Average ν_{21}
CAT1	21.4	0.262	8.60	0.017
CAT2	29.9	0.365	9.45	0.019
CAT average	**25.7**	**0.314**	**9.02**	**0.018**
CXT2	**43.5**	**0.479**	**10.0**	**0.021**

It is interesting to note the trend in the data obtained for the transformed/AS-4 and transformed/XAS coupons. First, recall that all the original samples failed in the lower half of the specimen, usually below the externally bonded terminal tabs. The first transformed coupons, CAT1 and CXT1, came from the lower half of each coupon. This was the desired comparison, given that all the samples failed in that half of the coupon. Unfortunately, the CXT1 coupon prematurely failed. In an attempt to obtain some data on the effect of the transformation, the upper half of each coupon was tested, namely CAT2 and CXT2. As one can see from Table 6, the results for CAT2 and were higher than those obtained for CAT1. This seems to further indicate that there was a gradient in the degree of consolidation in the laminates.

8.3 *Microscopic Analysis*

To complete the comparison between the original and the transformed samples, it was necessary to evaluate the microstructure of the transformed coupons. Like the original samples, the transformed coupons were evaluated in terms of scanning electron and optical microscopy.

8.3.1 Scanning Electron Microscopy

Samples for SEM analysis were taken from the lower half of each failure surface and mounted onto aluminum stubs. The stubs were prepared as outlined previously in ch. 7.

As an initial comment, it can be noted that a significant amount of voids exist in the CAT and the CXT coupons. This may be attributed to the fact that the consolidation pressure used during the transformation was very low and did not inhibit void growth.

8.3.1.1 Results for Transformed/AS-4

Aside from the presence of voids, the failure surfaces seen in fig. 60 were vastly different than those seen in fig. 47 and fig. 49. The adhesion observed in the transformed/AS-4 coupons appeared to be dramatically better than either the amorphous/AS-4 or semicrystalline/AS-4 coupons. In fig. 60, the coupons appeared to have a significant amount of cohesive failure in the matrix. This type of failure is quite surprising and no substantiated reason for this behavior can be offered at this time.

8.3.1.2 Results for Transformed/XAS

The micrographs of the transformed/XAS samples, seen in fig. 61, also showed an improvement in improvement in the adhesion with respect to the micrographs of the amorphous/XAS coupons and semicrystalline/XAS coupons seen in fig. 48 and fig. 50. Like the transformed/AS-4 coupons, the failure surface appeared to exhibit greater amounts of cohesive failure in the matrix. The failure surfaces of the transformed/XAS coupon more closely resembled the behavior observed for the amorphous/XAS samples. Compared to the semicrystalline/XAS coupons, there was a dramatic improvement in the fiber/matrix adhesion. As mentioned in ch. 7, the matrix appeared to poorly wet the fibers in the semicrystalline/XAS laminate which may explain the poor performance observed for this laminate.

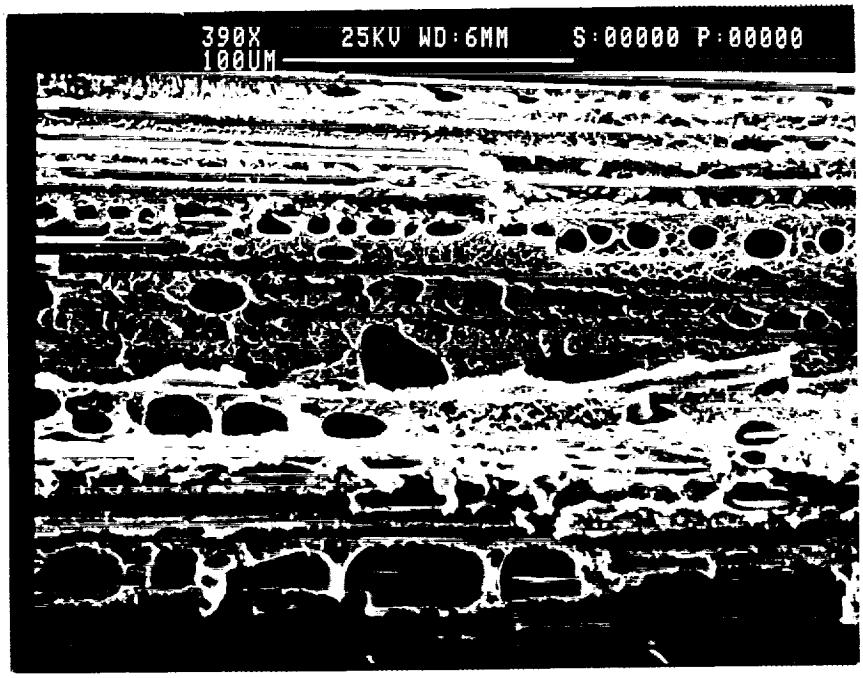

A)

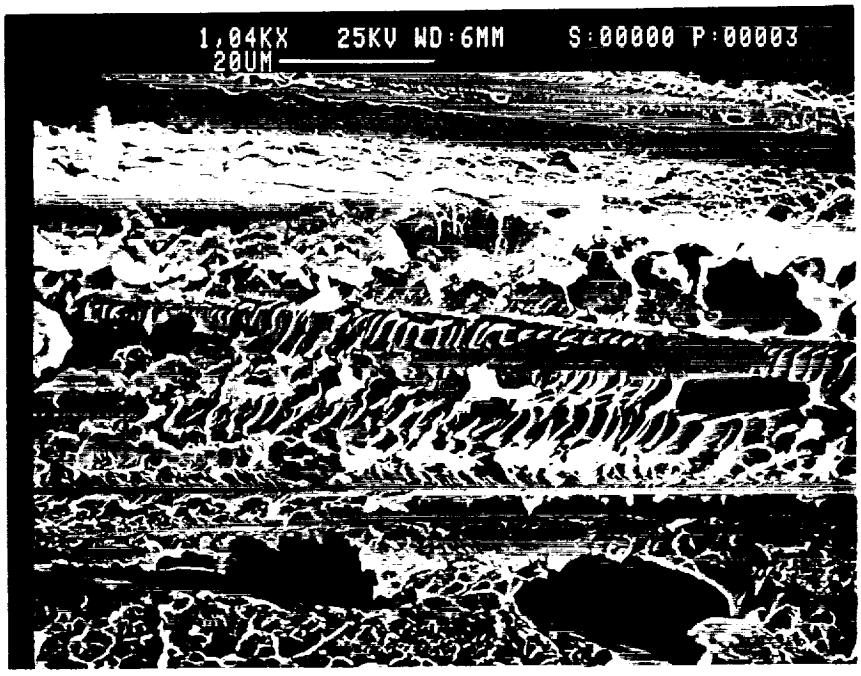

B)

fig. 60. Micrographs of a Transformed/AS-4 Transverse Tensile Coupon Tested to Failure: A) Low and B) High Magnification

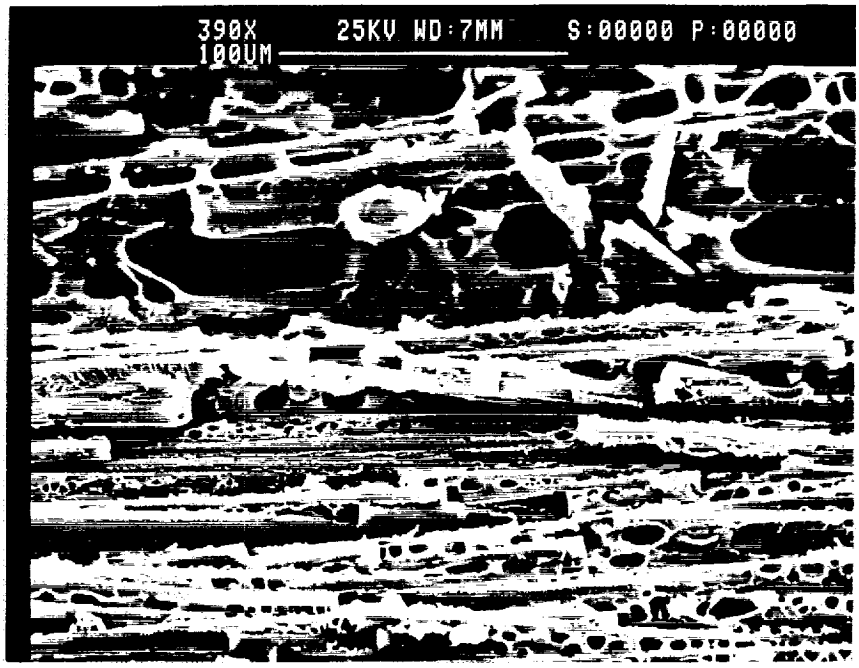

A)

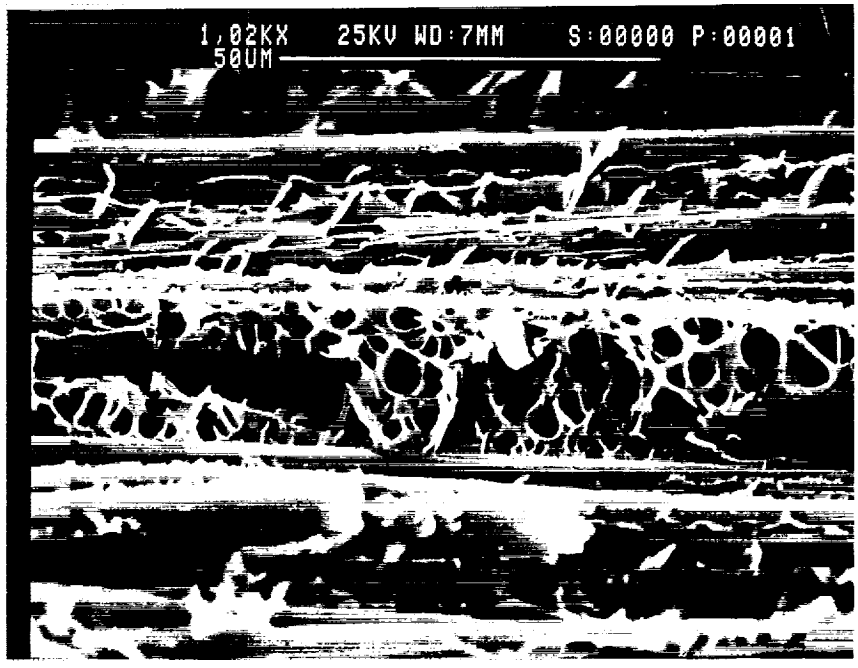

B)

fig. 61. Micrographs of a Transformed/XAS Transverse Tensile Coupon Tested to Failure: A) Low and B) High Magnification

8.3.2 Optical Microscopy

Samples for optical microscopy were prepared in as previously described in ch. 7. It is anticipated that optical microscopy will confirm the presence of void formation seen during the SEM evaluation.

8.3.2.1 Results for Transformed/AS-4

As it can be seen in fig. 62, there appears to be extensive void formation and fiber pullout in both of the transformed/AS-4 coupons tested to failure. In fig. 62A), there also appears to be broad bands of poorly infiltrated areas. This is not surprising when compared to the original semicrystalline/AS-4 coupons, as seen in fig. 53.

8.3.2.2 Results for Transformed/XAS

Like their AS-4 counterparts, the transformed/XAS coupons, seen in fig. 63, are also plagued with voids and fiber pull out. There are also a few areas of where the poorly infiltrated fibers can be seen. Compared to the semicrystalline/XAS coupons seen in fig. 54, the amount of area containing defects appears to be slightly higher in the transformed/XAS coupons.

8.4 Summary of Transformed Samples

By transforming the semicrystalline coupons, it was expected that the mechanical properties would return to the levels observed in the initial testing. Similar results were anticipated with

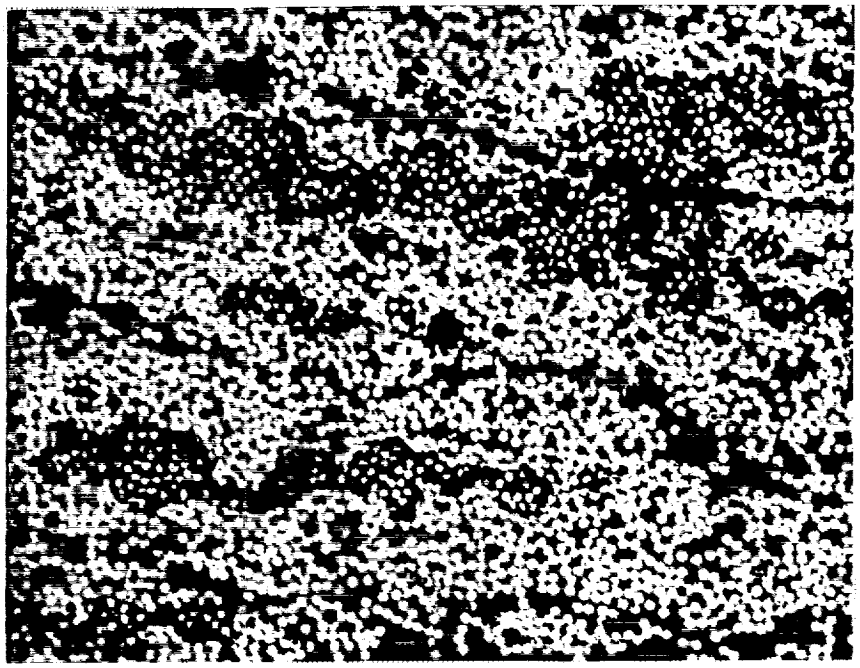

A)

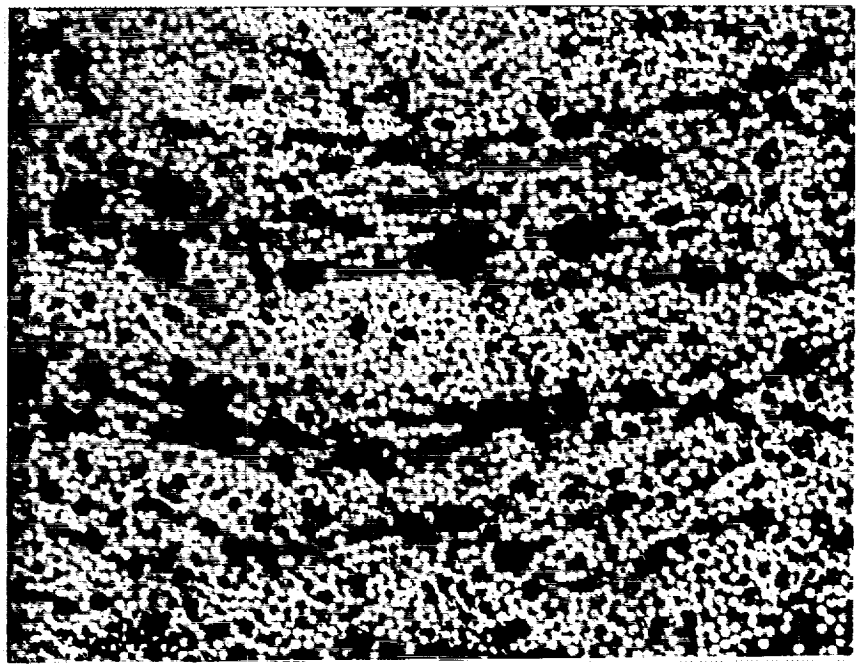

B)

fig. 62. Optical Micrographs of Transformed/AS-4 Coupons: A) Coupon CAT1 and B) Coupon CAT2

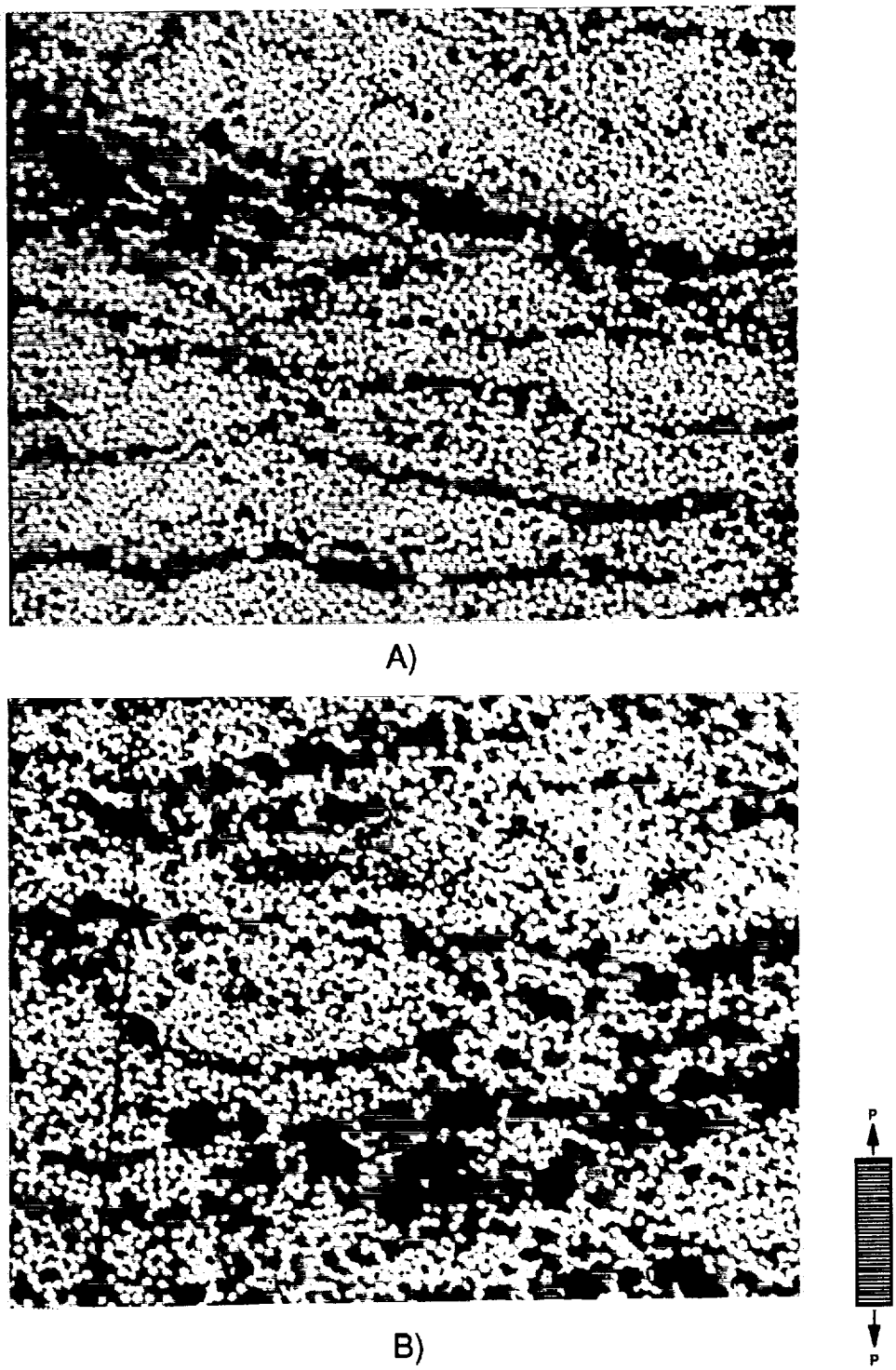

fig. 63. **Optical Micrographs of Transformed/XAS Coupons:** A) Coupon CXT1 and B) Coupon CXT2

regard to fiber/matrix adhesion. The mechanical response of the transformed coupons, for both AS-4 and XAS, was comparable to the mechanical response of the original amorphous coupons. Interestingly enough, the fiber/matrix adhesion for both types of transformed coupons surpassed the observed results for all previous coupons, despite the extensive amount of void and pullout area. The fiber/matrix adhesion results were rather surprising. Unfortunately, a sound explanation does not exist at this time. One potential reason for this behavior could be linked to the fact that the transformed samples had a greater total time at the processing temperature compared to the original semicrystalline coupons. Recall, the original amorphous laminates were processed twice based on the results of the ultrasonic evaluation. Comparing the transformed laminates to the original amorphous laminates, the total time at the processing temperature was roughly the same. This could indicate that the length of the isothermal hold was too short in the original amorphous and semicrystalline cycles to adequately consolidate the laminates. There is no additional experimental data to confirm that explanation at this time. It should also be noted that the extensive amount of defects in both samples is linked to the fact that no significant consolidation pressure was applied to the samples during the transformation.

9.0 Conclusions

9.1 Process

The moistened-fiber method for producing powder prepreg appeared to be successful. This technique produced prepreg with powder uniformly distributed onto the fibers and a 40% matrix volume fraction was consistently attained. In addition, the method was successful in removing the water introduced into the prepreg system, as evidenced by the lack of significant void formation in the early test coupons and the laminates produced for mechanical testing. Although the process appears to be successful, due to a number of problems, the evaluation of the process, or the prepreg from it, were not evaluated as extensively as desired. Of these problems, the most severe was the poor fiber/matrix adhesion.

9.2 *Fiber/Matrix Adhesion and Mechanical Properties*

In ch. 5, the issue of fiber/matrix adhesion was discussed. As a solution to the problem, an alternative fiber and an alternative form of the matrix were investigated. Transverse tensile testing coupled with a microstructural analysis of the failed samples was performed. A summary of all the data from the mechanical testing plus the limited comparative data from other investigators is given in Table 7. From this table, it can be noted that the amorphous coupons equalled or outperformed their semicrystalline counterparts for both fiber systems. This was true for all cases except for the modulus of the semicrystalline/AS-4 coupons. This material had the greatest modulus reported despite its extremely poor transverse tensile strength. When looking at one form of the matrix while varying the fiber, it appeared there was a very slight increase in the mechanical properties for the AS-4 coupons compared to the XAS coupons. The variation was slight enough it could be said there was no major difference between the two fibers.

From the SEM microscopic analysis, the fiber/matrix adhesion for the AS-4 coupons appeared to be greater for the semicrystalline form of the matrix. In comparison, the opposite was true for the XAS coupons. The fiber/matrix adhesion exhibited by the semicrystalline/XAS coupons was the worst observed in the study. The observed adhesive and mechanical behavior was contrary to the expectations for semicrystalline/XAS composites. The high expectations for this system were based on the improved wetting characteristics observed of LaRC-TPI on XAS fibers, and the microscopic evaluation of the fractured amorphous/XAS and the semicrystalline/AS-4 coupons. Optical microscopy revealed that this sample appeared to be incompletely infiltrated compared to the other coupons produced. In addition, the semicrystalline composite coupons seemed plagued by fiber pullout. It is believed that the fiber pullout induced by polishing was promoted by the brittleness of the matrix and weakness of the partially infiltrated structure.

Table 7. Summary of Thermoplastic/graphite Composite Transverse Mechanical Properties

Type of Composite	Failure Stress (MPa)	Strain to Failure (%)	Average Modulus (GPa)
AA average	33.3	0.356	9.38
AX average	30.6	0.331	9.36
CA average	12.4	0.110	11.4
CX average	9.94	0.143	7.24
CAT average	25.7	0.314	9.02
CXT2	43.5	0.479	10.0
LaRC-TPI(1:1)/2.5%PISO$_2$ AS-4 (18)	33.1	0.48	8.2
New TPI/IM8 (26)	61.4	----	7.6
150 PEEK/G30-500 (27)	63.4	0.70	9.6
450 PEEK/G30-500 (27)	69.6	0.71	9.9

In an effort to understand the effect of the matrix had on the performance of these composites, the remaining semicrystalline coupons were transformed to amorphous coupons. The properties of these coupons were roughly equal to or slightly lower than corresponding properties observed for the original amorphous coupons. In terms of fiber/matrix adhesion, both the transformed AS-4 and XAS coupons appeared to have greater adhesion compared to the all samples previously evaluated. It is believed that the additional time at the processing temperatures may have improved the fiber/matrix wetting which could explain the improved interfacial adhesion.

Overall, none of the mechanical test results, particularly the transverse tensile strengths, can be considered to be acceptable for contemporary composite materials. The results from the mechanical testing and microscopic examination were fairly consistent throughout the study and confirm this statement. It is apparent that more questions have been raised than answered. As for future work, the following areas need attention

- Neat resin properties - This study has measured the failure strengths of the various composites. To obtain an exact degree of adhesion in the composites, the failure

strengths of the two forms of the neat resin must be determined so that the composite data may be gauged relative to its respective neat resin sample.

- Fibers - The wetting characteristics of additional fiber systems needs to be investigated. By looking at the wetting characteristics of other fibers, the adhesion potential of these systems can be gauged with respect to LaRC-TPI.

- Consolidation - From the ultrasonic and optical microscopic evaluations, it can be observed that neither the semicrystalline nor the amorphous laminates were well fabricated. As a result, both lamination cycles need to be optimized to ensure greater reproducibility between the laminates.

- Process - Once suitable fibers are chosen, resume the verification of the process to measure its success.

- Varying the crystalline content in a laminate - After the fabrication aspects of LaRC-TPI/graphite composites are resolved, it will be possible to investigate the effect of amount of crystallinity on the adhesive and mechanical performance. Perhaps by investigating different levels of crystallinity, it will be possible to find an optimal amount where both the mechanical properties and the fiber/matrix adhesion will improve.

This list is rather extensive and offers considerable potential for future studies. Of that list, the important areas for making progress with LaRC-TPI composites would be the second and the third entry. With regard to investigating other fibers, additional wetting studies should be performed. While investigating other fiber systems, the lamination cycles, both amorphous and semicrystalline, need to be optimized. This will ensure a greater level of quality and continuity in the laminates produced. Once these two aspects have been resolved, small amounts of material can be prepregged and evaluated for their mechanical and microscopic

performance relative to the current LaRC-TPI and other high performance thermoplastic/graphite composites.

10.0 Additional Observations

This thesis has looked at two structural forms of the matrix, eg., amorphous and semicrystalline. As one may recall from ch. 5, Muellerleile and Wilkes (25) generated a thermal cycle to maintain crystallinity in the neat polymer. That cycle was incorporated into a lamination cycle. An example of such a laminate can also be seen in ch. 5. That coupon was evaluated using a DSC to determine the degree of crystallinity relative to the neat polymer. The evaluation revealed that a significant amount of crystallinity was retained in the coupon relative to the neat polymer. Given the successful early results, this cycle was presumed to generate crystallinity consistently. No intermediate evaluation was deemed necessary prior to mechanical testing. For completeness in characterization, a postmortem thermal evaluation was performed at the end of this entire study. The evaluation revealed no unexpected results in the amorphous/AS-4, amorphous/XAS, and semicrystalline/AS-4 laminates. It was noted that semicrystalline/AS-4 laminate did appear to have less crystallinity relative to the coupon produced in ch. 5 and relative to the neat polymer. The reduction observed was not proportional to the difference in the matrix content of the laminates. However, there was a surprise in the results from the semicrystalline/XAS laminate. According to the DSC analysis, there were no detectable signs of crystallinity present. Samples of the semicrystalline/XAS prepreg were tested. The results showed that the prepreg was definitely semicrystalline. Once this

was confirmed, the thermal history generated while processing this laminate was rechecked for differences relative to the semicrystalline/AS-4 thermal history. This recheck revealed no significant differences between the two semicrystalline thermal histories. There were no other apparent processing differences between the laminates. Thus assuming the laminate was actually amorphous rather than semicrystalline, the observed behavior, both mechanical and microscopic, did not correspond with the results obtained for the amorphous/XAS laminate. This is quite a mystery and no logical answer can be offered at this time. This important piece of information does not alter the observed results but it certainly compounds the mystery of the poor behavior of this laminate. It also raises an interesting question, namely if this sample was amorphous, why did the mechanical and interfacial behavior improve so drastically? No valid answer exists for that observation either.

11.0 References

1. Lee, W.J., J.C. Seferis, and D.C. Bonner. "Prepreg Processing Science," *SAMPE Quarterly,* 17(2):58-68 (1986).

2. Cattanach, J.B., G. Guff, and F.N. Cogswell. "The Processing of Thermoplastics Containing High Loadings of Long and Continuous Reinforcing Fibers," *Journal of Polymer Engineering,* 6:345-361 (1986).

3. Muzzy, J.D. "Processing of Advanced Thermoplastic Composites," *ASME Symposium on Manufacturing Science of Composites,* pp. 27-39 (1988).

4. Rosen, S.L. *Fundamental Principles of Polymeric Materials.* New York: Wiley and Sons, pp.37-46 (1982).

5. Throne, J.L. and M.S. Sohn. "Electrostatic Dry Powder Prepregging of Carbon Fiber," *Proceedings of the 35th International SAMPE Symposium,* pp. 2086-2101 (1990).

6. Muzzy, J., B. Varughese, V. Thammongkol, and W. Tincher. "Electrostatic Prepregging of Thermoplastic Matrices," *SAMPE Journal,* 25(5):15-21 (1989).

7. Edie, D.D., G.C. Lickfield, M.J. Drews, M.S. Ellison, L.E. Allen, J.R. McCollum, and H.L. Thomas. "Thermoplastic Coating of Carbon Fibers: Annual Report 1987-1988," NASA Research Grant NAS-1-680 (1988).

8. Baucom, R.A. and J.M Marchello. "LaRC Powder Prepreg System," *Proceedings of the 35th International SAMPE Symposium*, pp.175-187 (1990).

9. Baucom, R., J. Marchello, and J. Throne. "Recent Developments in Dry Powder Processing," *Fiber-Tex*, NASA CP 3082, pp. 235-245 (1989).

10. Iyer, S.R. and L.T. Drzal, "Dry Powder Processing of Thermoplastic Composites," *Proceedings of the American Society for Composites Fifth Technical Conference: Composite Materials in Transition*, pp. 259-266 (1990).

11. Kim, C. and R.A. Gray. "Development of Fiber Spreading Technique for Metal Matrix Composites," NRL Memorandum Report 5831 (1986).

12. Thiede-Smet, M., M. Liu, and V. Ho. "Study of Processing Parameters of PEEK/Graphite Composites Fabricated with FIT Prepreg," *Proceedings of the 34th International SAMPE Symposium*, pp. 1223-1234 (1989).

13. Moore, C.R., J.M. McCollum, and G.C. Lickfield. "Thermoplastic Coating of Carbon Fibers - Effect of Melting Technique on Prepreg Shear Strength," *Fiber-Tex*, NASA CP 3082, pp. 247-251 (1989).

14. Muzzy, J., B. Varughese, and P.H. Yang. "Flexible Towpreg by Powder Fusion Coating of Filaments," *Proceedings of the 48th Annual Technical Conference of the Society of Plastics Engineers*, pp. 1385-1389 (1990).

15. Throne, J.L. and A.L. Ogden. "Polymer Powder Prepregging - A Status Report," ASEE Final Report, NASA-Langley Research Center (1988).

16. Ogden, A.L., M.W. Hyer, J.T. Muellerleile, G.L. Wilkes, and A.C. Loos. "The Development of an Alternative Thermoplastic Powder Prepregging Technique," *Proceedings of the American Society for Composites Fifth Technical Conference: Composite Materials in Transition*, pp.249-259 (1990).

17. St. Clair, A.K. and T.L. St. Clair. "A Multi-Purpose Thermoplastic Polyimide," *SAMPE Quarterly*, 13(1):20-25 (1981).

18. Johnston, N.J., T.L. St. Clair, R.M. Baucom, and T.W. Towell. "Polyimide Matrix Composites: Polyimidesulfone/LaRC-TPI (1:1) Blend," *Proceedings of the 34th International SAMPE Symposium*, pp. 976-987 (1989).

19. Burks, H.D., T.L. St. Clair, and T.H. Hou. "Characterization of Crystalline LaRC-TPI Powder," *SAMPE Quarterly* 18(1):1-8 (1986).

20. Hou, T.H., J.M. Bai, and T.L. St. Clair. "A DSC Study on Crystalline LaRC-TPI Powder - A New Version with Higher Initial Molecular Weight," *SAMPE Quarterly*, 18(4):20-24 (1987).

21. Ohta, M., S. Tamai, T.W. Towell, N.J. Johnston, and T.L. St. Clair. "Improved Melt Flow and Physical Properties of Mitsui Toatsu's LaRC-TPI #1500 Series Polyimide," *Proceedings of the 35th International SAMPE Symposium*, pp. 1030-1044 (1990).

22. Hou, T.H. and J.M. Bai. "Characterization of LaRC-TPI 1500 Powders - A New Version with Controlled Molecular Weight," *Proceedings of the 35th International SAMPE Symposium*, pp. 1594-1608 (1990).

23. Hou, T.H., N.T. Wakelyn, and T.L. St. Clair. "Investigation of Crystalline Changes in LaRC-TPI Powders," *Journal of Applied Polymer Science,* 36:1731-1739 (1988).

24. Bascom, W.D. "Interfacial Adhesion of Carbon Fibers," NASA CR 178306 (1987).

25. Muellerleile, J.T. and G.L. Wilkes. "Preliminary Results for Crystallization Behavior of LaRC-TPI and CPI Thermoplastic Polyimides as Induced from the Glassy State," *Polymer Preprints,* 31(2):637 (1990).

26. Olson, S.H. "Manufacturing with Comingled Yarns, Fabrics, and Powder Prepreg Thermoplastic Composite Materials," *Proceedings of the 35th International SAMPE Symposium,* pp. 1306-1320 (1990).

27. Clemans, S. and T. Hartness. "Thermoplastic Prepreg Technology for High Performance Composites," *SAMPE Quarterly,* 20(4):38-42 (1989).

Appendix A. Experimental Prepreg Parameters

A number of small unidirectional samples of prepreg were made to eventually be used to make 16 layer unidirectional laminates. In all, 96 samples were made for the four combinations of matrix and fiber. These combinations were:

1. Amorphous LaRC-TPI/AS-4
2. Semicrystalline LaRC-TPI/AS-4
3. Amorphous LaRC-TPI/XAS
4. Semicrystalline LaRC-TPI/XAS

The data for each sample are tabulated below. Sample ID corresponds to the date when the prepreg was produced.

Amorphous LaRC-TPI/AS-4 Laminate						
ID number	T (°C)	RH (%)	moisture dep. rate (cm/s)	oven temp. (°C)	oven time (min.)	v_m (%)
5/30 04	22.8	57	1.65	317	1	41.1
5/30 05	22.8	57	1.64	318	1	37.1
5/30 06	22.8	58	1.76	317	1	42.6
5/30 07	22.2	58	1.72	317	1	44.5
5/30 08	22.8	58	1.72	317	1	36.8
5/30 09	22.2	59	1.78	317	1	42.1
5/30 10	22.2	60	1.68	317	1	43.5
5/31 01	23.8	61	1.68	316	1	44.4
5/31 02	24.4	60	1.74	316	1	44.0
5/31 03	24.4	59	1.64	315	1	43.5
5/31 04	24.4	59	1.64	315	1	40.2
8/30 01	24.4	61	1.72	319	1	43.4
8/30 02	24.4	60	1.68	319	1	38.2
8/30 03	24.4	60	1.65	319	1	42.4
8/30 04	24.4	59	1.62	320	1	39.1
8/30 05	24.4	61	1.65	317	1	40.2
8/30 06	24.4	62	1.67	---	1	44.0
8/31 01	23.8	60	1.64	318	1	39.7
8/31 02	24.4	60	1.62	316	1	45.6
8/31 03	24.4	61	1.65	316	1	42.2
8/31 04	24.4	60	1.65	318	1	38.3
8/31 05	24.4	60	1.62	319	1	42.1
8/31 06	24.4	60	1.78	319	1	38.6
8/31 07	24.4	62	1.64	---	1	40.7

Semicrystalline LaRC-TPI/AS-4 Laminate						
ID number	T (°C)	RH (%)	moisture dep. rate (cm/s)	oven temp. (°C)	oven time (min.)	v_m (%)
6/4 01	23.3	62	1.67	319	184	48.8
6/5 01	23.3	59	1.68	319	183	47.5
6/5 02	23.8	56	1.76	319	180	41.4
6/6 02	22.8	60	1.70	319	180	33.2
6/19 01	23.8	60	1.78	319	180	39.2
6/20 01	23.3	60	1.76	319	180	36.7
6/20 02	24.4	55	1.70	319	180	35.9
6/20 03	23.3	63	1.70	319	180	37.6
6/21 01	23.8	62	1.68	319	180	36.7
6/21 02	23.8	57	1.67	319	182	38.0
6/23 01	23.8	59	1.72	319	183	40.8
6/23 02	23.8	59	1.70	319	183	39.0
6/23 03	23.3	60	1.65	319	182	41.6
6/24 01	22.8	60	1.72	319	180	41.6
6/24 02	23.3	60	1.78	319	182	41.2
6/24 03	23.3	60	1.65	319	180	41.4
6/25 01	22.8	60	1.65	319	180	40.8
6/25 02	23.8	58	1.74	319	190	36.3
6/25 03	23.8	60	1.76	319	183	39.0
6/26 01	22.8	62	1.74	319	182	39.0
6/26 02	23.3	59	1.67	319	190	38.9
6/26 03	22.8	60	1.67	319	180	38.5
6/27 01	23.3	61	1.68	319	180	40.8
6/27 02	23.8	58	1.76	319	180	36.7

Amorphous LaRC-TPI/XAS Laminate						
ID number	T (°C)	RH (%)	moisture dep. rate (cm/s)	oven temp. (°C)	oven time (min.)	v_m (%)
7/12 01	23.3	62	1.70	317	1	41.1
7/12 02	23.8	62	1.64	---	1	39.7
7/15 02	23.8	63	1.62	317	1	42.9
7/16 01	23.3	61	1.74	319	1	47.0
7/16 03	23.8	60	1.74	---	1	44.9
7/16 05	23.8	60	1.76	311	1	47.2
7/16 07	23.8	62	1.74	319	1	48.3
7/16 09	23.3	62	1.76	320	1	43.9
7/17 02	23.3	62	1.68	319	1	43.7
7/17 03	23.3	62	1.65	317	1	36.0
7/17 04	23.3	63	1.74	316	1	37.6
7/17 05	23.8	63	1.64	317	1	37.2
7/18 01	23.3	61	1.70	317	1	36.4
7/18 02	23.3	61	1.60	316	1	38.3
7/18 03	23.3	61	1.70	318	1	31.6
7/18 04	23.8	62	1.58	316	1	32.7
7/18 05	23.8	62	1.67	316	1	34.9
7/19 02	23.3	62	1.68	317	1	40.0
7/19 04	24.4	60	1.74	317	1	38.3
7/19 05	24.4	59	1.58	316	1	37.7
7/20 02	23.8	62	1.72	315	1	39.1
7/20 04	23.3	61	1.72	318	1	41.2
7/20 06	23.3	62	1.70	319	1	40.6
7/20 08	23.3	63	1.68	320	1	41.7

Semicrystalline LaRC-TPI/XAS Laminate						
ID number	T (°C)	RH (%)	moisture dep. rate (cm/s)	oven temp. (°C)	oven time (min.)	v_m (%)
7/23 02	24.4	61	1.72	320	180	39.1
7/26 01	23.3	62	1.62	320	182	46.1
7/26 02	23.3	60	1.74	320	180	44.5
7/26 03	23.8	63	1.67	320	180	42.3
7/27 01	23.3	60	1.70	319	181	39.2
7/27 02	24.4	61	1.68	320	183	35.5
7/30 01	23.3	61	1.74	320	180	41.8
7/30 02	23.3	62	1.68	320	180	42.2
7/31 01	23.3	63	1.58	320	182	37.9
7/31 02	23.3	62	1.67	320	180	44.4
7/31 03	23.3	62	1.60	320	180	40.9
8/1 01	22.8	61	1.72	319	180	42.6
8/1 02	23.3	61	1.67	320	180	37.6
8/1 03	23.3	60	1.72	320	184	43.6
8/2 01	22.8	60	1.58	320	187	38.6
8/2 02	23.3	62	1.70	320	183	38.6
8/4 01	22.8	63	1.67	320	187	40.3
8/6 01	23.3	62	1.68	320	180	42.8
8/6 02	23.8	63	1.64	320	182	36.6
8/7 01	22.8	62	1.60	320	180	39.1
8/7 02	23.3	59	1.64	320	180	41.7
8/7 03	23.3	61	1.65	320	180	39.7
8/8 01	23.3	63	1.68	320	191	36.4
8/8 02	23.3	63	1.65	320	180	40.9

Appendix B. Stacking Sequence of Laminates

Layer no.	ID Number		
Amorphous LaRC-TPI/AS-4 Laminate			
layer 1	5/30 06	8/31 05	5/30 05
layer 2	5/31 01	5/31 04	5/30 10
layer 3	8/30 02	5/30 05	5/30 08
layer 4	5/30 04	5/30 07	5/31 02
layer 5	8/30 03	8/30 01	8/30 05
layer 6	8/30 04	8/31 04	8/31 01
layer 7	8/31 03	8/31 07	8/31 05
layer 8	8/31 06	8/30 06	8/31 02
Semicrystalline LaRC-TPI/AS-4 Laminate			
layer 1	6/23 03	6/23 02	6/19 01
layer 2	6/20 03	6/24 03	6/23 01
layer 3	6/20 01	6/25 02	6/24 02
layer 4	6/25 03	6/27 01	6/5 02
layer 5	6/27 02	6/21 02	6/26 02
layer 6	6/25 01	6/24 01	6/23 01
layer 7	6/21 01	6/26 03	6/6 02
layer 8	6/20 02	6/4 01	6/5 01
Amorphous LaRC-TPI/XAS Laminate			
layer 1	7/12 01	7/12 02	7/20 06
layer 2	7/19 04	7/15 02	7/19 05
layer 3	7/17 04	7/17 03	7/17 05
layer 4	7/20 04	7/19 02	7/20 02
layer 5	7/16 05	7/16 09	7/16 01
layer 6	7/18 04	7/18 01	7/18 03
layer 7	7/20 08	7/18 05	7/18 02
layer 8	7/17 02	7/16 07	7/16 03

Semicrystalline LaRC-TPI/XAS Laminate			
layer 1	7/27 01	7/30 01	8/2 01
layer 2	7/23 02	7/31 03	8/7 02
layer 3	7/26 03	8/7 01	8/1 01
layer 4	7/30 02	8/1 02	8/2 02
layer 5	8/6 01	8/7 03	8/4 01
layer 6	7/27 02	8/8 01	7/31 01
layer 7	7/26 01	8/1 03	7/31 02
layer 8	8/6 02	7/26 02	8/8 02

BIBLIOGRAPHIC DATA SHEET	1. Report No. VPI-E-91-07; CCMS-91-08	2.	3. Recipient's Accession No.

4. Title and Subtitle

The Development and Evaluation of an Alternative Powder Prepregging Technique for Use with LaRC-TPI/Graphite Composites

5. Report Date

April 1991

6.

7. Author(s)

Andrea L. Ogden, Michael W. Hyer, Garth L. Wilkes
Alfred C. Loos, Terry L. St. Clair

8. Performing Organization Rept. No.

VPI-E-91-07

9. Performing Organization Name and Address

Virginia Polytechnic Institute and State University
Department of Engineering Science and Mechanics
Blacksburg, VA 24061-0219

10. Project/Task/Work Unit No.

11. Contract/Grant No.

NAG-1-343 NASA-Va. Tech Composites Pro.

12. Sponsoring Organization Name and Address

Polymeric Materials Branch
National Aeronautics and Space Administration
Langley Research Center
Hampton, VA 23665-5225

13. Type of Report & Period Covered

Interim Report 85
6/88-12/90

14.

15. Supplementary Notes

16. Abstract

This study investigates an alternative powder prepregging method for use with LaRC-TPI/graphite composites. The alternative method incorporates the idea of moistening the fiber prior to powder coating. Details of the processing parameters are given and discussed. Processing efforts initially concentrated on producing amorphous LaRC-TPI/AS-4 prepreg. The material was subsequently laminated into small coupons which were evaluated for processing defects using electron microscopy. After the initial evaluation of the material, no major processing defects were encountered but there appeared to be an interfacial adhesion problem. As a result, prepregging efforts were extended to include an additional fiber system, XAS, and an semicrystalline form of the matrix. The semicrystalline form of the matrix was the result of a complex heat treating cycle. Using SEM, the fiber/matrix adhesion was evaluated in these systems relative to the amorphous/AS-4 coupons. Of the samples evaluated, the semicrystalline/AS-4 and amorphous/XAS showed improvements relative to the amorphous/AS-4 coupons. Based on these results, amorphous and semicrystalline/AS-4 and XAS materials were prepregged and laminated for transverse tensile testing. Of the samples tested, the amorphous/AS-4 and XAS coupons had average transverse tensile strengths around 33 MPa, and average transverse tensile moduli around 9.3 GPa. The semicrystalline/AS-4 and XAS had a poorer mechanical performance. The average transverse strengths for these samples was approximately 11 MPa. There was a slight improvement in the transverse modulus for the semicrystalline/AS-4 sample but there was no improvement in the modulus for the XAS counterpart. In terms of adhesion, the interfacial adhesion was comparable with previous results. The notable exception was the semicrystalline/XAS coupons. These coupons exhibited extremely poor interfacial adhesion. Optical micrographs revealed that both semicrystalline samples showed poorer infiltration than the amorphous counterparts, thus offering a partial explanation for the poor mechanical and interfacial response. In an effort to obtain more information on the effect of the matrix, remaining semicrystalline transverse tensile coupons were transformed back to the amorphous state, through heat treatment, and tested. The mechanical properties of the transformed coupons returned to the values observed for the original amorphous coupons and the interfacial adhesion, as observed by scanning electron microscopy, was better than in any previous sample.

17. Key Words and Document Analysis. 17a. Descriptors

powder prepregging, fiber/matrix adhesion, interfacial adhesion, thermoplastic composites, polyimides, amorphous matrix, semi-crystalline matrix

17b. Identifiers/Open-Ended Terms

17c. COSATI Field/Group

18. Availability Statement	19. Security Class (This Report) UNCLASSIFIED	21. No. of Pages 174
	20. Security Class (This Page UNCLASSIFIED	22. Price

VIRGINIA TECH CENTER FOR COMPOSITE MATERIALS AND STRUCTURES

The Center for Composite Materials and Structures is a coordinating organization for research and educational activity at Virginia Tech. The Center was formed in 1982 to encourage and promote continued advances in composite materials and composite structures. Those advances will be made from the base of individual accomplishments of the sixty-five full and associate members who represent eleven different departments in three colleges.

The Center functions through an Administrative Board which is elected yearly and a Director who is elected for a three-year term. The general purposes of the Center include:

- collection and dissemination of information about composites activities at Virginia Tech,
- contact point for other organizations and individuals,
- mechanism for collective educational and research pursuits,
- forum and agency for internal interactions at Virginia Tech.

The Center for Composite Materials and Structures is supported by a vigorous program of activity at Virginia Tech that has developed since 1963. During 1988-89 and 1989-90 fiscal years sponsored research project expenditures for investigation of composite materials and structures have totalled approximately five million dollars annually.

Various Center faculty are internationally recognized for their leadership in composite materials and composite structures through books, lectures, workshops, professional society activities, and research papers.

Research is conducted in a wide variety of areas including design and analysis of composite materials and composite structures, chemistry of materials and surfaces, characterization of material properties, development of new material systems, and relations between damage and response of composites. Extensive laboratories are available for mechanical testing, nondestructive testing and evaluation, stress analysis, polymer synthesis and characterization, material surface characterization, component fabrication, and other specialties.

Educational activities include ten formal courses offered at the undergraduate and graduate levels dealing with the physics, chemistry, mechanics, and design of composite materials and structures. As of 1990, over 150 Doctoral and 175 Master's students have completed graduate programs and are now active in industry, government, and education in the United States and abroad. The Center averaged 125 active student members during 1989-90 and 1990-91. Many Bachelor-level students have been trained in various aspects of composite materials and structures.

The Center has invested in the development of an administrative database (now fully operational for Center members) and a composite material properties database (now ready for data entry).

In addition to the CCMS Report Series, the Center sponsers a bi-monthly Seminar Series attended by faculty, staff, and students and the Center jointly sponsors a sesqui-annual Technical Review with the Center for Adhesive and Sealant Science which is well attended by government and corporate contacts.

MEMBERS OF THE CENTER

Aerospace and Ocean Engineering

Raphael T. Haftka
Eric R. Johnson
Rakesh K. Kapania

Chemical Engineering

Donald G. Baird
Garth L. Wilkes

Chemistry

John G. Dillard
Harry W. Gibson
James E. McGrath
Thomas C. Ward
James P. Wightman

Civil Engineering

Richard M. Barker
Richard E. Weyers

Clothing and Textiles

Jeanette M. Cardamone

Electrical Engineering

Ioannis M. Besieris
Richard O. Claus
Douglas K. Lindner

Engineering Science and Mechanics

Robert Czarnek
David A. Dillard
Normal E. Dowling
John C. Duke, Jr.
Daniel Frederick
O. Hayden Griffin, Jr.
Zafer Gurdal
Robert A. Heller
Edmund G. Henneke, II
Michael W. Hyer
Robert M. Jones
Ronald D. Kriz
Liviu Librescu
Alfred C. Loos
Don H. Morris
John Morton
Ali H. Nayfeh
Daniel Post
J. N. Reddy
Kenneth L. Reifsnider
C. W. Smith
Wayne W. Stinchcomb
Surot Thangjitham

Industrial and Systems Engineering

Joel A. Nachlas

Materials Engineering

Jesse J. Brown, Jr.
Seshu B. Desu
Ronald S. Gordon
D. P. H. Hasselman
Robert W. Hendricks
Ronald G. Kander

Mathematics

Werner E. Kohler

Mechanical Engineering

Charles E. Knight
Craig A. Rogers
Curtis H. Stern

Inquiries should be directed to:
Center for Composite Materials and Structures
Virginia Tech
Blacksburg, VA 24061-0257
Phone: (703) 231-4969
Fax: (703) 231-9452

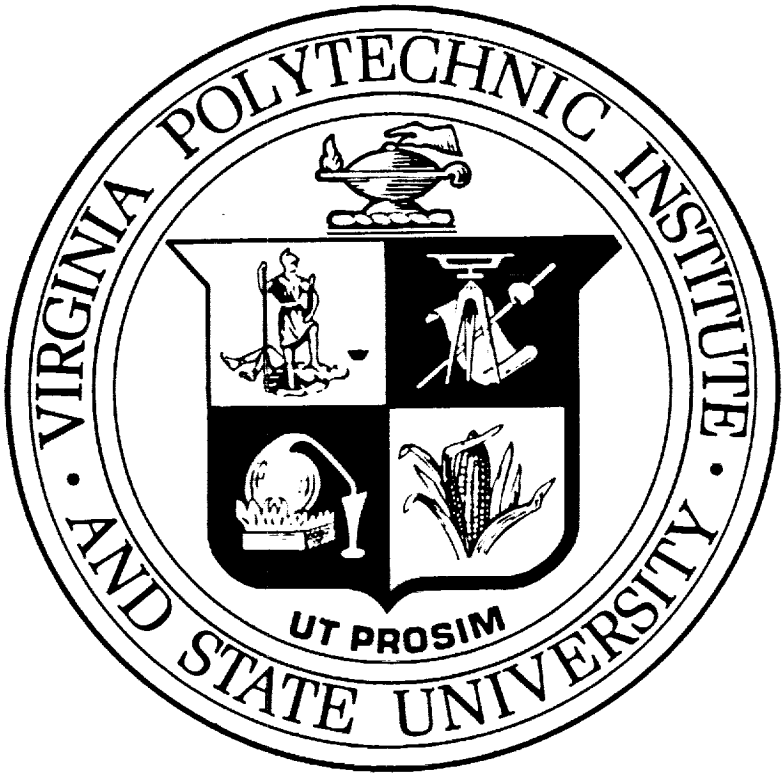
VIRGINIA POLYTECHNIC INSTITUTE
AND STATE UNIVERSITY
UT PROSIM